REPORT SD-TR-81-53

# LEVEL

## Helium Purge Flow Prevention of Atmospheric Contamination of the Cryogenically Cooled Optics of Orbiting Infrared Telescopes: Calculation of He-O Differential Cross Section

NANCY M. HARVEY and RONALD R. HERM
Chemistry and Physics Laboratory
Laboratory Operations
The Aerospace Corporation
El Segundo, Calif. 90245

5 June 81

88

DTIC
JUL 9 1981

C

TR-0081 (6430-03)-1

F04701-80-C-0081

Prepared for

SPACE DIVISION
AIR FORCE SYSTEMS COMMAND
Los Angeles Air Force Station
P.O. Box 92960, Worldway Postal Center
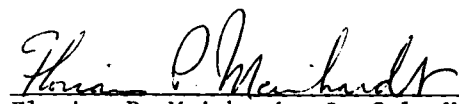Los Angeles, Calif. 90009

AD A101152

DTIC FILE COPY

This report was submitted by The Aerospace Corporation, El Segundo, CA 90245, under Contract No. F04701-80-C-0081 with the Space Division, Deputy for Technology, P.O. Box 92960, Worldway Postal Center, Los Angeles, CA 90009. It was reviewed and approved for The Aerospace Corporation by M. T. Weiss, Acting Director, Chemistry Physics Laboratory and J. L. Lemay, Principal Director, Surveillance, Command, and Control, Defense Development Division. Lt Robert C. Kline, SD/YLVM, was the project officer for technology.

This report has been reviewed by the Public Affairs Office (PAS) and is releasable to the National Technical Information Service (NTIS). At NTIS, it will be available to the general public, including foreign nations.

This technical report has been reviewed and is approved for publication. Publication of this report does not constitute Air Force approval of the report's findings or conclusions. It is published only for the exchange and stimulation of ideas.

Robert C. Kline, 2nd Lt, USAF
Project Officer

Florian P. Meinhar`, Lt Col, USAF
Director of Advanced Space Development

FOR THE COMMANDER

William Goldberg, Colonel, USAF
Deputy for Technology

| REPORT DOCUMENTATION PAGE | | READ INSTRUCTIONS BEFORE COMPLETING FORM |
|---|---|---|
| 1. REPORT NUMBER<br>SD-TR-81-53 | 2. GOVT ACCESSION NO.<br>AD-A101152 | 3. RECIPIENT'S CATALOG NUMBER |
| 4. TITLE (and Subtitle)<br>HELIUM PURGE FLOW PREVENTION OF ATMOSPHERIC CONTAMINATION OF THE CRYOGENICALLY COOLED OPTICS OF ORBITING INFRARED TELESCOPES: CALCULATION OF He-O DIFFERENTIAL CROSS SECTION | | 5. TYPE OF REPORT & PERIOD COVERED |
| | | 6. PERFORMING ORG. REPORT NUMBER<br>TR-0081(6432-03)-1 |
| 7. AUTHOR(s)<br>Nancy M. Harvey and Ronald R. Herm | | 8. CONTRACT OR GRANT NUMBER(s)<br>F04701-80-C-0081 |
| 9. PERFORMING ORGANIZATION NAME AND ADDRESS<br>The Aerospace Corporation<br>El Segundo, Calif. 90245 | | 10. PROGRAM ELEMENT, PROJECT, TASK AREA & WORK UNIT NUMBERS |
| 11. CONTROLLING OFFICE NAME AND ADDRESS<br>Space Division<br>Air Force Systems Command<br>Los Angeles, Calif. 90009 | | 12. REPORT DATE<br>5 June 1981 |
| | | 13. NUMBER OF PAGES<br>80 |
| 14. MONITORING AGENCY NAME & ADDRESS(if different from Controlling Office) | | 15. SECURITY CLASS. (of this report)<br>Unclassified |
| | | 15a. DECLASSIFICATION/DOWNGRADING SCHEDULE |

16. DISTRIBUTION STATEMENT *(of this Report)*

Approved for public release; distribution unlimited

17. DISTRIBUTION STATEMENT *(of the abstract entered in Block 20, if different from Report)*

18. SUPPLEMENTARY NOTES

19. KEY WORDS *(Continue on reverse side if necessary and identify by block number)*

| | |
|---|---|
| Contamination Control | Purge Gas |
| He-O Cross Section | SIRE |
| Infrared Telescopes | SIRTF |

20. ABSTRACT *(Continue on reverse side if necessary and identify by block number)*

The ability of an He purge gas to protect the cryogenically cooled optics of orbiting infrared telescopes from the primary atmospheric contaminant, atomic oxygen, can be estimated by Monte Carlo calculations simulating the He-O scattering events that would occur in the operating telescope. We report the results of accurate quantum mechanical calculations of the He-O differential cross sections $\sigma(\theta, E)$ needed in such Monte Carlo calculations. To facilitate the use of these cross sections in Monte Carlo calculations, we have constructed

DD FORM 1473
(FACSIMILE)

19. KEY WORDS (Continued)

20. ABSTRACT (Continued)

a simple separable function of $E$ and $\theta$ which provides an adequate representation of $\sigma(\theta, E)$ for the entire range of relative collision energies studied, $E = 0.02$ to $1.66$ eV. For high relative collision energies, we have also tested the accuracy of the computationally simpler WKB approximation.

## PREFACE

We are grateful to B. R. Johnson for lending us his elastic scattering

codes and for helpful discussions during the course of this work. We also

want to thank A. Straubinger and W. Von der Ohe for critically reviewing this

manuscript and providing many constructive comments.

Accession For
NTIS GRA&I
DTIC TAB
Unannounced
Justification

By
Distribution/
Availability Codes
Avail and/or
Dist Special

A

1

## CONTENTS

4

FIGURES (Continued)

TABLES

# I. Introduction

The performance of an orbiting infrared sensor, such as the SIRE sensor, will be degraded by the condensation of contaminants on its cryogenically cooled optical surfaces. It is estimated that an accumulation of contaminants only 1 μm thick will have a significantly deleterious effect.[1] Two sources will contribute contaminants--the ambient atmosphere and the shuttle orbiter itself. Since the spacecraft will orbit at a velocity of approximately 8 km/sec, molecular species in the space environment will provide a high flux of contaminants, in part simply because they impinge on the shuttle orbiter at high relative velocities. The most abundant constituent of the atmosphere at the altitudes in which the infrared telescopes will operate is atomic oxygen.[1,2] The flux of gases released by the shuttle orbiter and backscattered by the surrounding atmosphere will consist primarily of $H_2O$. Large quantities of $H_2O$ vapor released by the flash evaporators may return to the shuttle orbiter.[1,2]

In contamination control studies for the SIRE sensor, it was suggested that a helium purge gas directed outward through the telescope barrel might prevent contamination of the primary mirror by deflecting contaminants to other surfaces.[1-4] The effectiveness of this He purge system has been investigated both experimentally and theoretically during the last few years. These studies are summarized in the next two paragraphs.

In order to test the feasibility of an He purge, experimentalists investigated the efficiency with which an He purge gas depleted the flux of fast O, $H_2O$, $O_2$, and $N_2$ positive ions entering a scaled-down model of the SIRE telescope.[5] They monitored the ion current reaching a detector placed at the far end of the model telescope barrel as a function of the He gas temperature and pressure and as a function of the velocity of the incident ion beam. However,

9

since the scattering of ions from neutral species is dominated by different forces than the scattering of neutral atoms from neutral atoms, the experiments were criticized for poorly representing the collision processes that would occur in the operating SIRE telescope.[2] The experiments were also criticized for failing to account for nonnegligible sources of experimental error. Because of inadequate pumping in the scattering chamber, the incident ion beam was attenuated by collisions occuring outside the model telescope.[6] Further, since only the ion current was measured by the detector, any quenching of target ions by, e.g., collisions with the walls of the model telescope caused the flux of contaminant molecules at the detector to be underestimated. Thus, the experiments may have overestimated the effectiveness of the He purge gas.

Theoreticians have employed both macroscopic kinetics and detailed molecular dynamics to study how effectively a purge gas can reduce contamination. Murakami based his derivation of analytic expressions describing general features of purge gas systems on the bulk properties of gases.[4] Two groups investigated the effectiveness of an He purge gas against atomic oxygen. Guttman, Furber, and Muntz used a simple model that included only one collision of each incident oxygen atom with the purge gas and treated the He and O atoms as hard spheres for which the differential cross section is isotropic in the center-of-mass reference frame.[2] Simpson and Witteborn used Monte Carlo calculations to provide a more realistic model that allowed multiple He-O collisions in the trajectory of a single O atom traveling through the purge gas.[6] These preliminary calculations yielded useful predictions of the efficiency with which an He purge gas could protect the SIRE sensor. However, in the absence of accurate descriptions of the He flow field, gas-surface interactions, He-contaminant gas cross sections and other important parameters,

they incorporated several assumptions that introduced considerable uncertainty into their final results.

As part of the total appraisal of contamination control, Monte Carlo calculations using measured values for the helium flow field and accurate cross sections for He-O scattering have been proposed. The purpose of this report is to provide the scattering data that would be required as input to calculations modeling purge-gas collisions *with* atomic oxygen. This report gives both the differential cross section $\sigma(\theta, E)$ as a function of the scattering angle $\theta$ and the total elastic scattering cross section $\sigma_{tot}(E)$ for He-O scattering for the wide range of relative collision energies E that would be sampled by collisions occuring in an orbiting telescope. These scattering results, in conjunction with an accurate description of the He flow field, will permit accurate Monte Carlo calculations to be made.

The first collision of an incident oxygen atom with a purge-gas atom will occur at a high relative velocity determined primarily by the orbital speed of the shuttle orbiter. However, since the atmosphere surrounding the shuttle is characterized by exospheric temperatures which rise as high as 2000°K during peak periods of solar activity, the relative collision velocities will sample some distribution of speeds ranging from approximately 6 to 10 km/sec. Subsequent collisions of He and O atoms may take place at significantly smaller relative collision energies. Although the absolute total cross section for He-O scattering has been measured for center-of-mass velocities of 1 to 1.8 km/sec, the angle-dependent He-O differential cross section needed for the Monte Carlo calculations has not been reported in the literature for any collision energy. This report satisfies this need by giving the results of calculations yielding the He-O total and differential cross sections for ten representative relative collision energies, E = 0.02, 0.07, 0.15, 0.27, 0.41,

11

0.60, 0.81, 1.06, 1.34, and 1.66 eV, corresponding to asymptotic relative velocities $v$ = 1, 2, 3, 4, 5, 6, 7, 8, 9, and 10 km/sec, respectively.

The calculation of collision cross sections requires both an accurate description of how the collision partners interact and an accurate and efficient method for treating the collision dynamics. In this work, an approximate, but realistic, model interaction potential is used. This potential function is described in Sec. II. The collision dynamics is treated by a quantum mechanical method that solves the Schrödinger equation exactly for the given interaction potential. The results of some of the high-energy exact calculations are compared to those obtained with the WKB approximation. This approximate quantum mechanical method is computationally simpler and is expected to give reliable results for those energies. The scattering calculations are described in Sec. III.A, and their results are described in Sec. III.B. The detailed angle dependence of the differential cross section for small scattering angles is discussed in Sec. III.C. The uncertainty in the total and differential cross sections due to the uncertainty in the experimentally derived He-O interaction potential is considered in Sec. III.D. In Sec. IV, the He-O differential cross sections obtained by simpler approximate models are compared. A satisfactory analytic fit to the exact differential cross sections for the entire range of relative collision energies is presented in Sec. V. This fit will facilitate the use of the accurate differential cross section in Monte Carlo calculations. The conclusions reached in this work are summarized in Sec. VI.


II.  He-O Interatomic Potential

The He-O interaction is described by a simple analytic function of the interatomic distance $R$. This interatomic potential function neglects the

12

energy differences between the six-fold degenerate (neglecting spin-orbit splitting and $\Lambda$-type doubling) $^3\Pi$ and three-fold degenerate $^3\Sigma^-$ curves that describe the interaction of a ground-state oxygen atom $O(^3P)$ with a rare gas atom $Rg(^1S)$ for small interatomic distances. Although this detailed information on the interatomic potential is not available for the He-O system, it has been reported by Dunning and Hay for the rare gas oxides of Ne, Ar, Kr, and Xe.[7] Their electronic structure calculations on those systems found that for small internuclear separations the $^3\Pi$ and $^3\Sigma^-$ potential curves were approximately parallel and that the $^3\Pi$ curve was displaced from the $^3\Sigma^-$ curve by only about 0.2 Å to smaller R. Thus, one can estimate the effects of neglecting the differences between the $^3\Pi$ and $^3\Sigma^-$ potentials by testing the sensitivity of the scattering results to moderate displacements of the small-R interaction potential. These tests are discussed in Sec. III.D.

The potential function used in this work was constructed from potential functions obtained experimentally. Cross sections for He-O scattering at both high and low relative collision energies have been measured in molecular beam scattering experiments.[8,9] For each energy range a potential function, neglecting the energy differences between the $^3\Pi$ and $^3\Sigma^-$ functions, has been found by inverting the scattering results. Since molecular collisions at different energies are sensitive to different regions of the interatomic potential, the experimentally derived functions can be used to construct an interatomic potential which is realistic for all interatomic distances. The realistic interatomic potential used in this work is predicted on the potential functions provided by Foreman and coworkers[8] and by Aquilanti and coworkers.[9] Foreman and coworkers inverted relative cross section data obtained in high-energy (100-2500 eV in the laboratory frame of reference) molecular

13

beam scattering experiments to obtain an expression for the purely repulsive small-R potential.[8] The interatomic potential derived from their work is

$$v^F(R) = A \exp(-\alpha R) \qquad (1)$$

where $A = 378$ eV and $\alpha = 3.744$ $\text{Å}^{-1}$. They estimate that it accurately represents the interatomic potential for $R = 0.81$ to $1.81$ Å.[8] The accuracy of this expression for the small-R potential is evidenced by its good agreement with statistical theory calculations[10] and is suggested by the agreement between Foreman's experimentally obtained Rg-O interatomic potentials for Rg = Ne, Ar, Kr, and Xe[8] and the ab initio configuration interaction $^3\Pi$ and $^3\Sigma^-$ curves calculated for these systems.[7] Aquilanti and coworkers reported absolute total cross sections obtained by thermal-energy molecular beam experiments.[9] For this energy range, corresponding to relative collision velocities of 1.0 to 1.8 km/sec, the collision dynamics is influenced by both short-range repulsive forces and long-range attractive interactions. Aquilanti and coworkers were able to obtain two analytic forms for the interatomic potential—a Lennard-Jones (12, 6) and an $\exp(\alpha, 6)$ function—which included both attractive and repulsive interactions and provided equally satisfactory fits to their scattering results. Their $\exp(\alpha, 6)$ function is

$$v^{AQ}(R) = \varepsilon \left\{ \left(\frac{6}{\alpha - 6}\right) \exp\left[-\alpha \left(\frac{R}{R_m} - 1\right)\right] - \left(\frac{\alpha}{\alpha - 6}\right)\left(\frac{R_m}{R}\right)^6 \right\} \qquad (2)$$

where $\varepsilon = 2.48 \times 10^{-3}$ eV, $\alpha = 13.772$, and $R_m = 3.08$ Å. It should represent the He-O interatomic potential accurately for $R = 3.8 - 5.5$ Å.[9]

The hybrid interaction potential constructed from $v^F$ and $v^{AQ}$ and used in the scattering calculations reported here is

14

$$V^H(R) = \tanh(aR^{-6}) \, V^F(R) + \tanh(bR^6) \, V^{AQ}(R) \tag{3}$$

where $a = 102.0 \, A^6$ and $b = 0.0001 \, A^{-6}$. This potential is plotted in Fig. 1 as a function of the internuclear separation and is compared, for representative R, to $V^F(R)$ and $V^{AQ}(R)$. The hybrid potential varies smoothly from a repulsive potential to an attractive potential and reproduces $V^F(R)$ and $V^{AQ}(R)$ in their regions of validity. For R = 0.81 to 1.81 A, $V^H(R)$ overestimates $V^F(R)$ by at most 0.02 eV, and for R = 3.8 to 5.5 A, $V^H(R)$ is negligibly less attractive, by at most $1.4 \times 10^{-5}$ eV, than $V^{AQ}(R)$. $V^H(R)$ has a shallow minimum $V(R) = -0.0081$ eV for R = 3.3 A that is not resolved on the scale of Fig. 1.

The repulsive potential is expected to dominate the high-energy collision dynamics. The scattering at energies above 1 eV should be fairly insensitive to the weakly attractive long-range tail of the potential. A test of this assertion is reported in Sec. III. D.

III. He-O Elastic Scattering

A. Calculations

In the theoretical approach to elastic atom-atom scattering, nuclear motion is described by a wave function that satisfies a Schrödinger equation. The solution of this equation, subject to scattering boundary conditions, yields the differential cross section as a function of initial relative kinetic energy and final scattering angle.[11,12] In this study, the numerical solution of the single-channel Schrödinger equation for each partial wave was accomplished with an exact quantum mechanical technique, the renormalized Numerov method.[13] This yields the phase shifts for each partial wave. Additionally, the WKB approximation was used to calculate the phase shifts for the
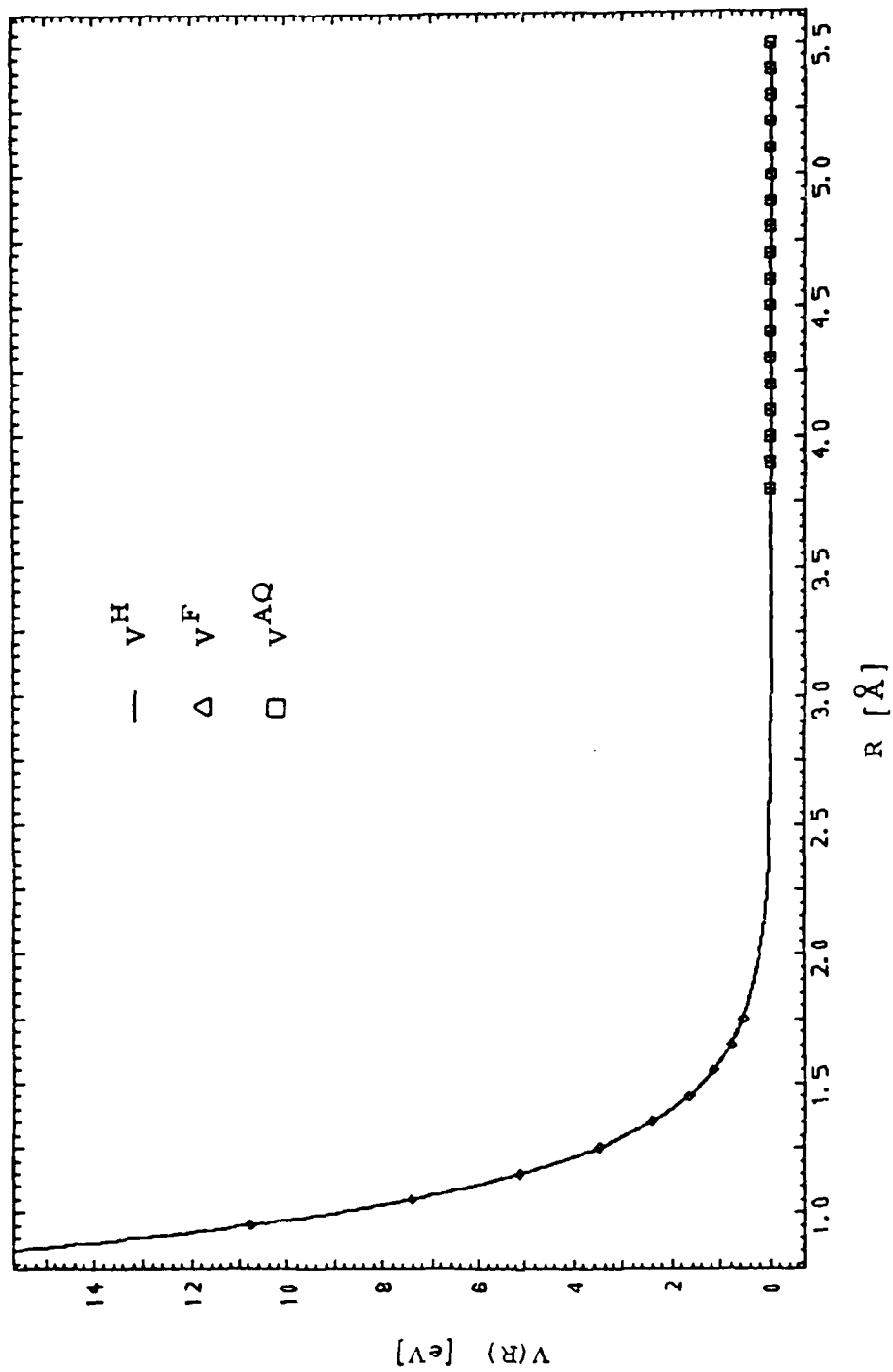
Fig. 1. He-O interatomic potential V(R): hybrid potential $V^H$, Foreman's potential $V^F$, and Aquilanti's potential $V^{AQ}$

high-energy collisions.[12,14] The reason for using the WKB approximation was to assess the applicability of this computationally simpler method.

The total elastic scattering cross section $\sigma_{tot}(E)$ is defined by[15]

$$\sigma_{tot}(E) = \frac{4\pi}{k^2} \sum_{\ell=0}^{\infty} (2\ell + 1) \sin^2 \left[ \eta_\ell(E) \right] \qquad (4)$$

where $k^2 = \frac{2\mu E}{\hbar^2}$, $\mu$ is the reduced mass of the collision partners, $\eta_\ell(E)$ is the phase shift of the $\ell^{th}$ partial wave for collision energy $E$, and $\ell$ is the orbital angular momentum quantum number. In practice, the sum over $\ell$ is truncated at some value $\ell_{max}$, for which $\sigma_{tot}$ is converged to a desired accuracy. For $E = 0.02$ eV, 0.07 to 0.41 eV, and 0.60 to 1.66 eV, the partial wave expansions were truncated at $\ell_{max} = 100$, 200, and 300, respectively. These choices for $\ell_{max}$ and appropriate values for the integration parameters gave total cross sections converged to within 0.01 $Å^2$. The phase shifts $\eta_\ell(E)$ for $0 \leqslant \ell \leqslant \ell_{max}$ calculated for the ten relative collision energies studied in this work are tabulated in Appendices A and B.

The total cross section can also be expressed as the integral of the differential scattering cross section $\sigma(\theta, E)$ over all the values of the scattering angle $\theta$

$$\sigma_{tot}(E) = 2\pi \int_0^\pi \sigma(\theta, E) \sin\theta \, d\theta \qquad (5)$$

where $\sigma(\theta, E)$ is defined in terms of the partial wave phase shifts by[15]

$$\sigma(\theta, E) = \frac{1}{k^2} \left| \sum_{\ell=0}^{\ell_{max}} (2\ell + 1) \exp[i\eta_\ell(E)] \sin \left[ \eta_\ell(E) \right] P_\ell(\cos \theta) \right|^2 \qquad (6)$$

17

The differential cross sections $\sigma(\theta, E)$ calculated for each of the ten colli-
sion energies studied in this work are tabulated for representative scattering
angles $\theta$ in Appendices C and D.


B.    Cross Sections

   1.   Total Cross Section $\sigma_{tot}(E)$

   The total cross sections obtained by exact quantum mechanical calcu-
lations for He-O elastic scattering for ten relative collision energies rang-
ing from 0.02 to 1.66 eV are listed in Table I and plotted as a function of E
in Fig. 2.  As expected, $\sigma_{tot}$ decreases monotonically with increasing colli-
sion energy.  For relative collision energies E > 0.27 eV, $\sigma_{tot}(E)$ is only
slightly energy dependent, varying from 41.76 to 35.65 $\AA^2$ with increasing
energy.  However, as illustrated in Fig. 2, $\sigma_{tot}(E)$ increases dramatically at
lower energies.   An   additional   calculation   for   E = 0.01   eV   gave
$\sigma_{tot}$ = 126.32 $\AA^2$.  The total cross sections for the lowest energy calcula-
tions can be compared to the molecular beam scattering results of Aquilanti et
al.[9]   The absolute total cross sections obtained experimentally were
approximately 90 ± 3 $\AA^2$ and 55 ± 3 $\AA^2$ for relative collision velocities of 1
and 2 km/sec, respectively.  Table I shows that the exact quantum mechanical
calculations yielded $\sigma_{tot}(E)$ = 87.94 $\AA^2$ and 53.99 $\AA^2$, respectively, for these
energies.   In comparison, one should note that in previous studies requiring
$\sigma_{tot}$, the He-O total elastic scattering cross section has been assigned
values including 0.1 to 10.0 $\AA^2$,[2] 45 $\AA^2$ (for helium-air),[4] and 70 $\AA^2$.[6]

   For E > 0.60 eV, the WKB approximation was also used to generate the
phase shifts from which $\sigma_{tot}(E)$ was calculated by eq. (4).  The total cross
sections calculated in this way agree to within 0.1% with those obtained by
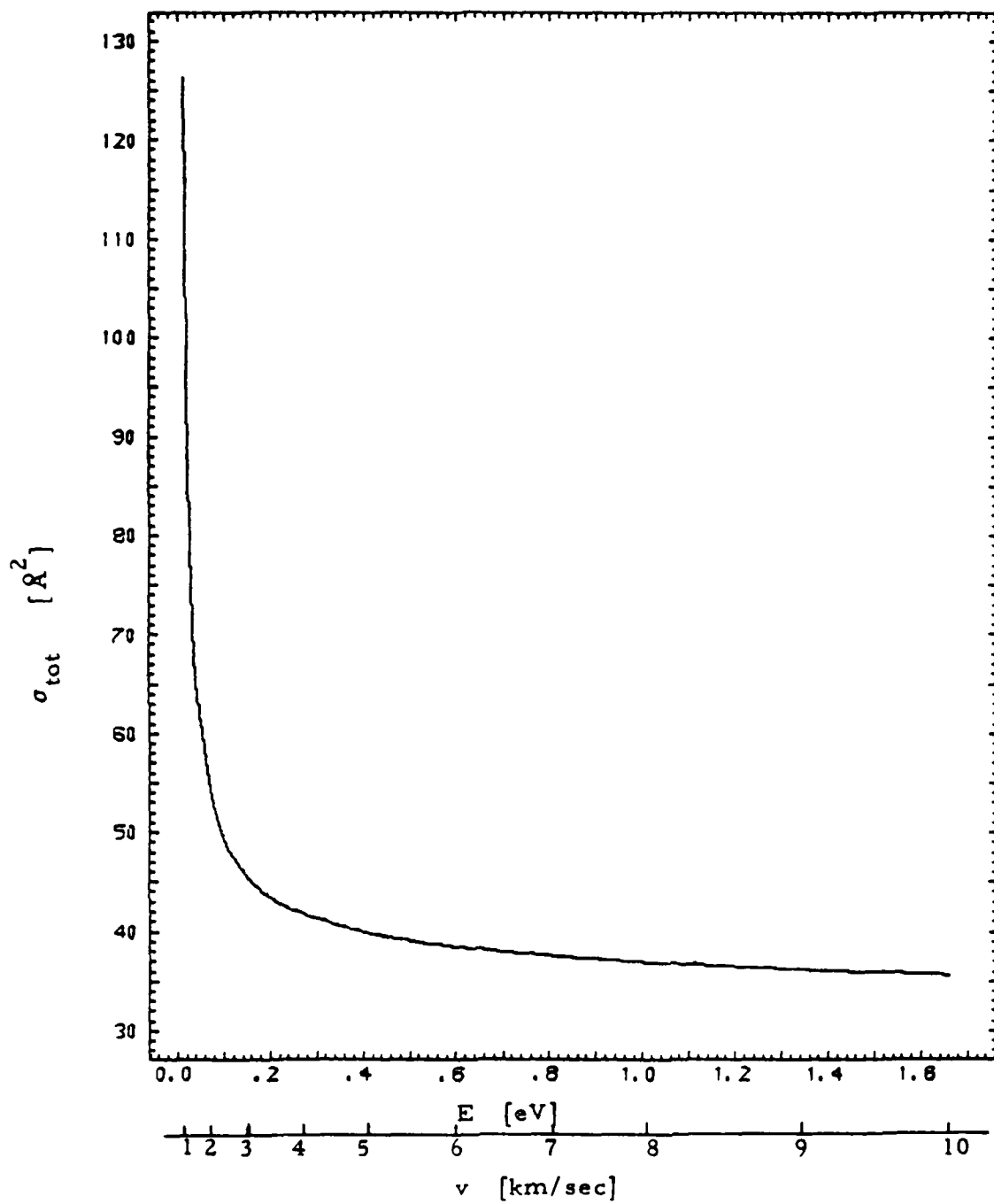
Fig. 2. He–O total cross section $\sigma_{tot}$ (E) as a function of the relative collision energy E and relative velocity v

19

Table I. He-O total cross section $\sigma_{tot}$ for each of ten relative collision
energies Å

| E [eV] | $\sigma_{tot}[\text{Å}^2]$ |
|--------|--------|
| 0.02 | 87.94 |
| 0.07 | 53.99 |
| 0.15 | 45.51 |
| 0.27 | 41.76 |
| 0.41 | 39.88 |
| 0.60 | 38.48 |
| 0.81 | 37.56 |
| 1.06 | 36.81 |
| 1.34 | 36.19 |
| 1.66 | 35.65 |

the exact quantum mechanical calculation. This demonstrates the accuracy with which the WKB approximation treats high-energy collisions.

2. Differential Cross Section $\sigma(\theta, E)$

The differential cross sections $\sigma(\theta, E)$ for the ten collision energies studied are plotted in Figures 3 through 12 as a function of the scattering angle $\theta$ and are tabulated for representative scattering angles in Appendices C and D. Since the initial collision of an O atom with an He purge-gas atom occurs at a high relative collision energy, consider first the differential cross section for E = 1.06 eV. The scattering at this collision energy, corresponding to a relative velocity of 8 km/sec, is representative of the scattering for velocities of about 4 to 10 km/sec. As shown in Fig. 10, $\sigma(\theta, E)$ is strongly peaked in the forward direction and decreases monotonically for $\theta > 15$ deg. Some oscillatory structure is imposed on $\sigma(\theta, E)$ for smaller scattering angles. Fig. 13 shows that this angle dependence is representative of the behavior exhibited by the differential cross sections for the seven highest energies. In order to emphasize the strikingly similar angle dependence of the differential cross sections for $E > 0.27$ eV, the cross sections are plotted on a linear scale. As shown in Figures 3 through 5, at lower collision energies the oscillations modulating the angle dependence of the differential cross section extend to larger scattering angles. Indeed for E = 0.02 eV, the lowest energy studied, Fig. 3 shows that the oscillations in the differential cross section continue to $\theta \simeq 90$ deg. Although the detailed angle dependence of the differential cross section changes as the energy decreases, the differential cross sections are qualitatively similar for the entire range of energies studied here. The gradual modifications of the angle dependence of the differential cross section as a function of the collision

21
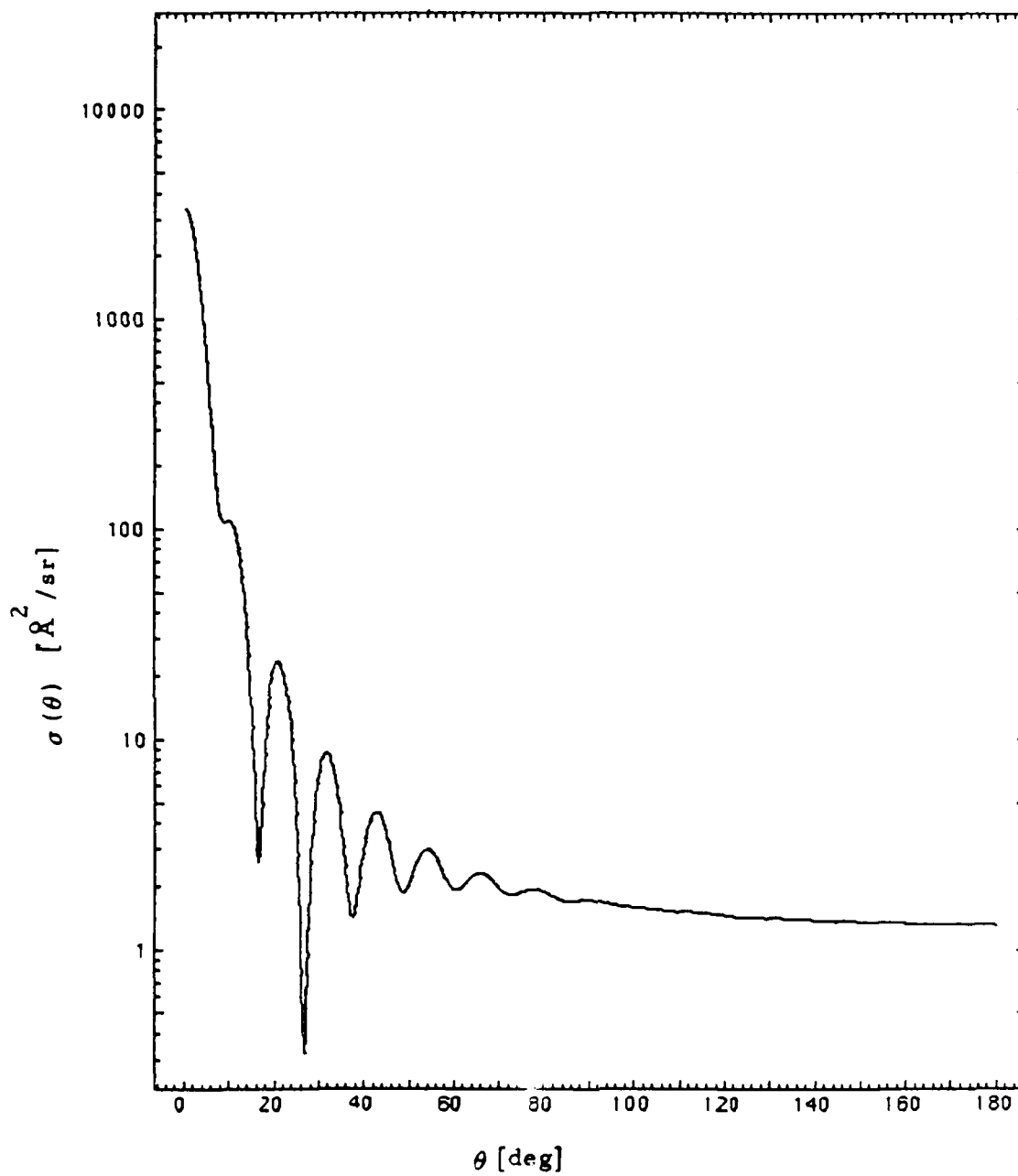
Fig. 3. Semilog plot of the He-O differential cross section σ(θ) as a function of the scattering angle θ for E = 0.02 eV

22
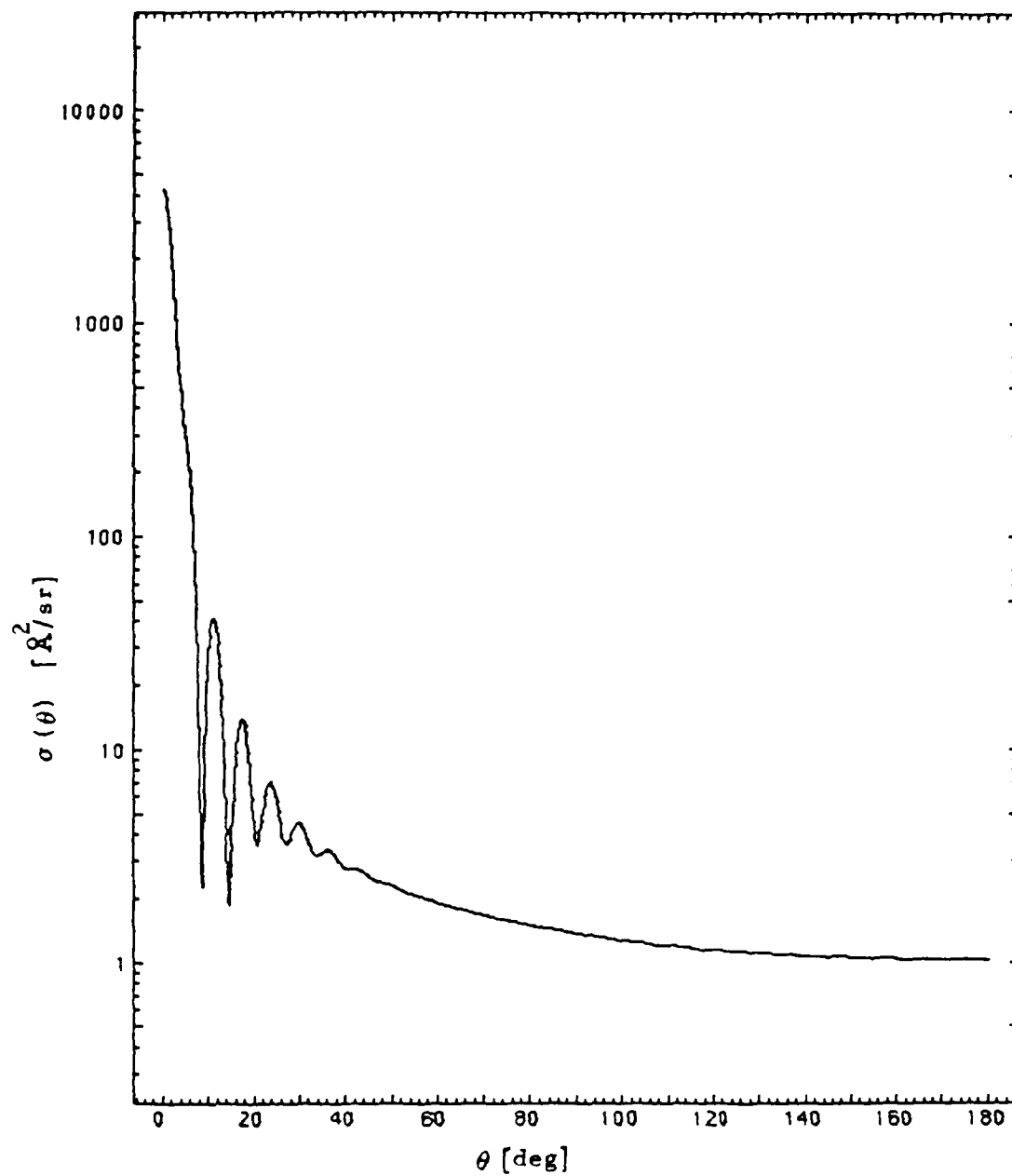
Fig. 4.   Semilog plot of the He-O differential cross section $\sigma(\theta)$
as a function of the scattering angle $\theta$ for E = 0.07 eV

23
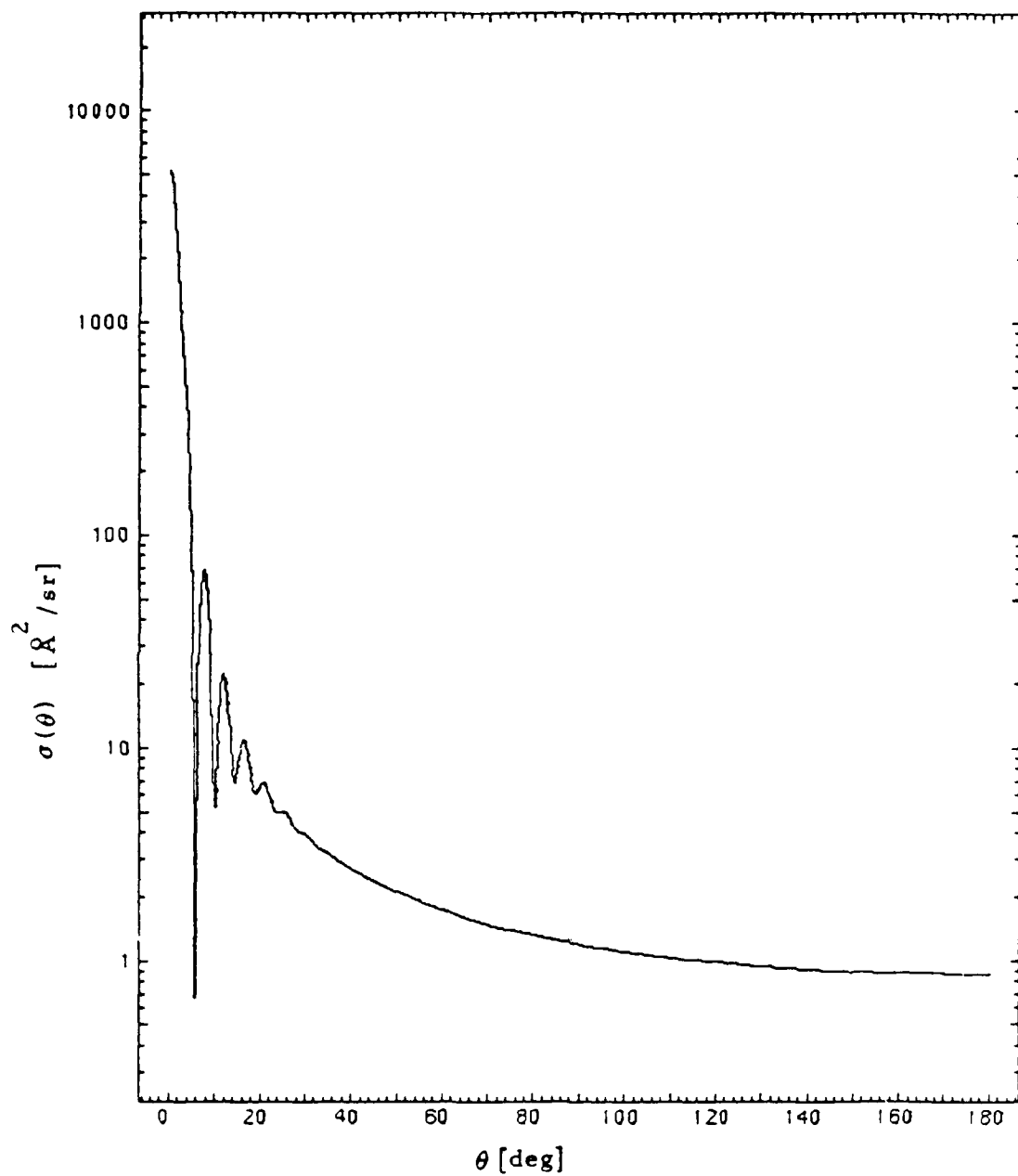
Fig. 5.   Semilog plot of the He-O differential cross section σ(θ)
          as a function of the scattering angle θ for E = 0.15 eV
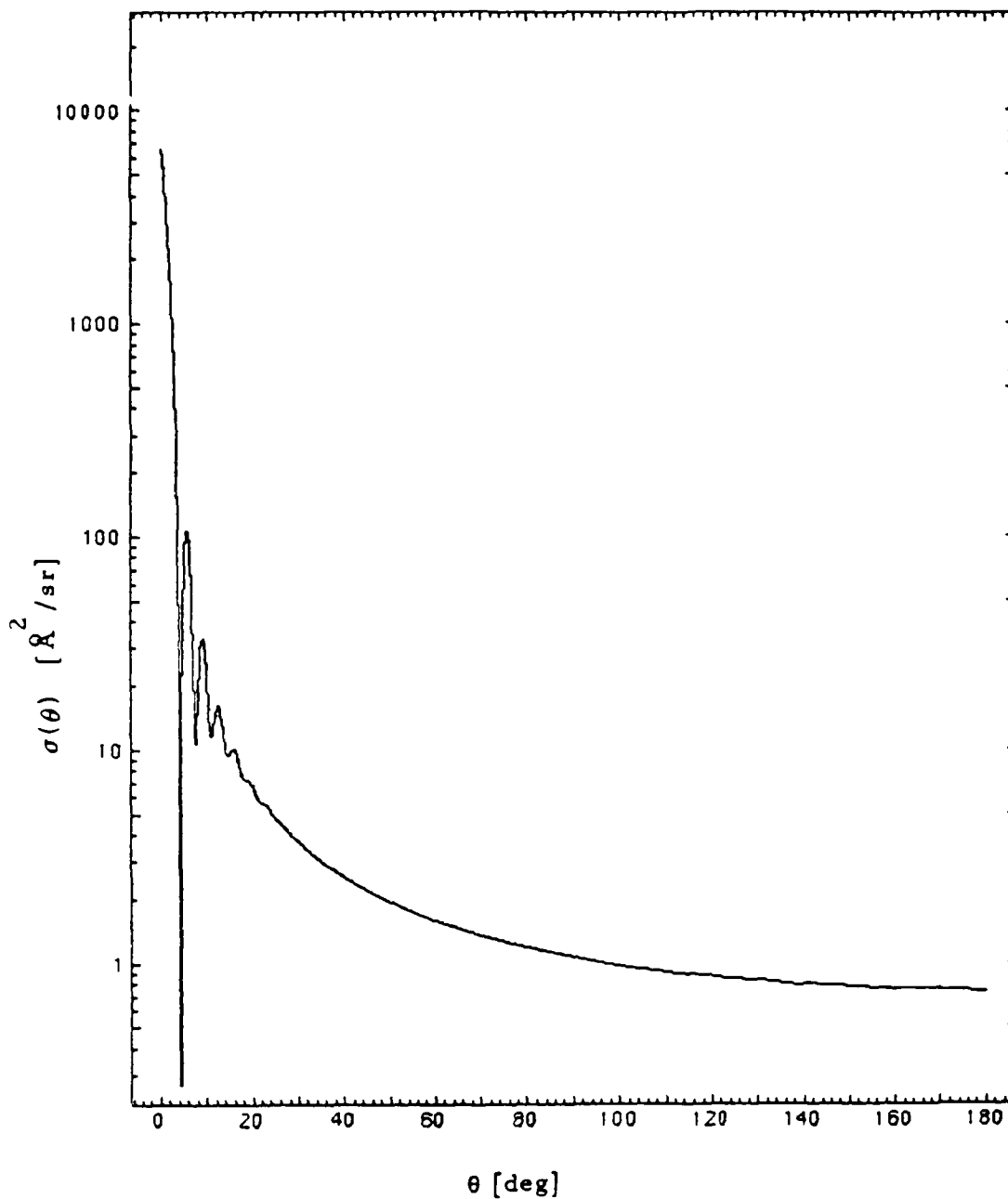
Fig. 6.  Semilog plot of the He-O differential cross section σ(θ)
as a function of the scattering angle θ for E = 0.27 eV
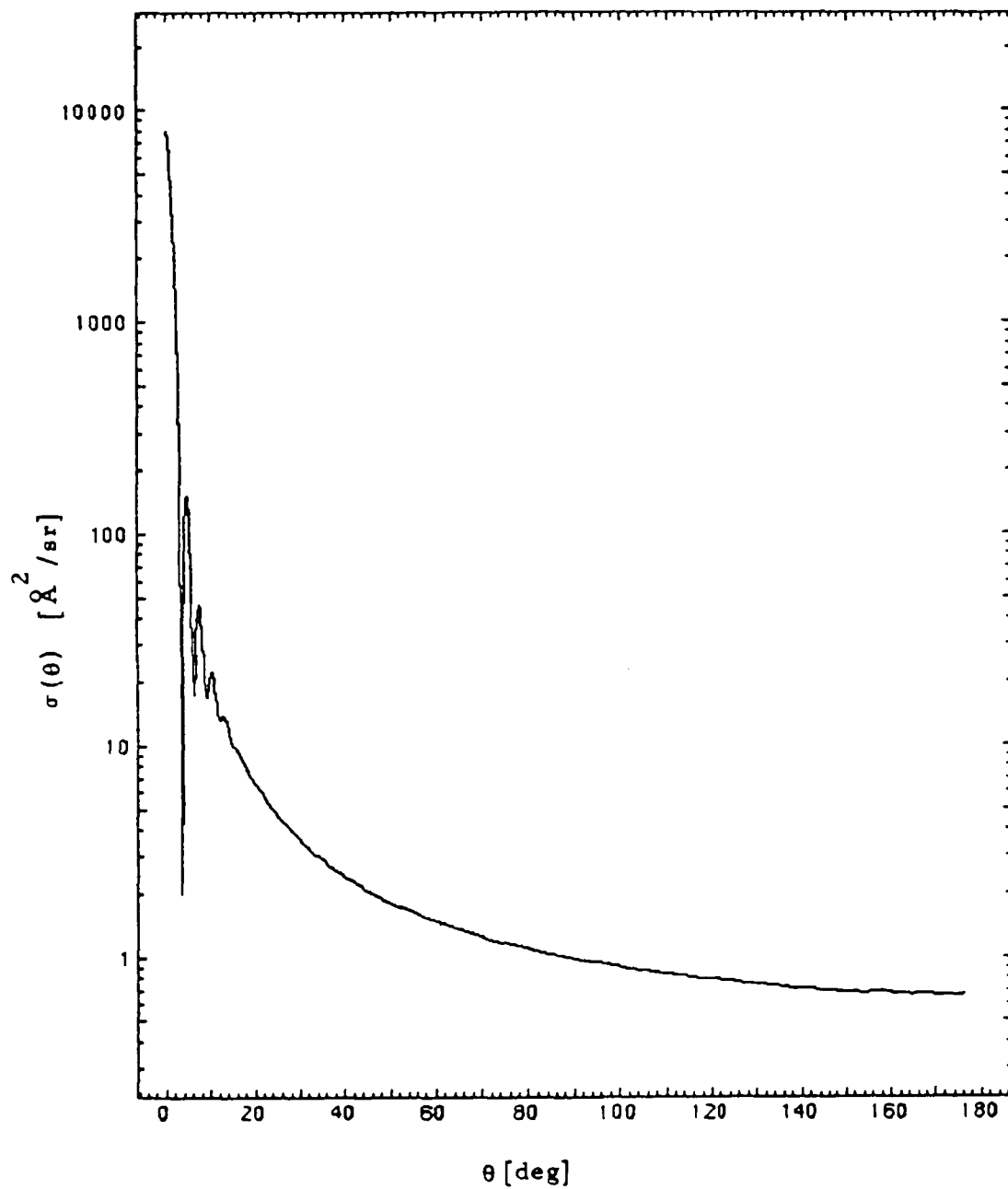
Fig. 7. Semilog plot of the He-O differential cross section σ(θ) as a function of the scattering angle θ for E = 0.41 eV
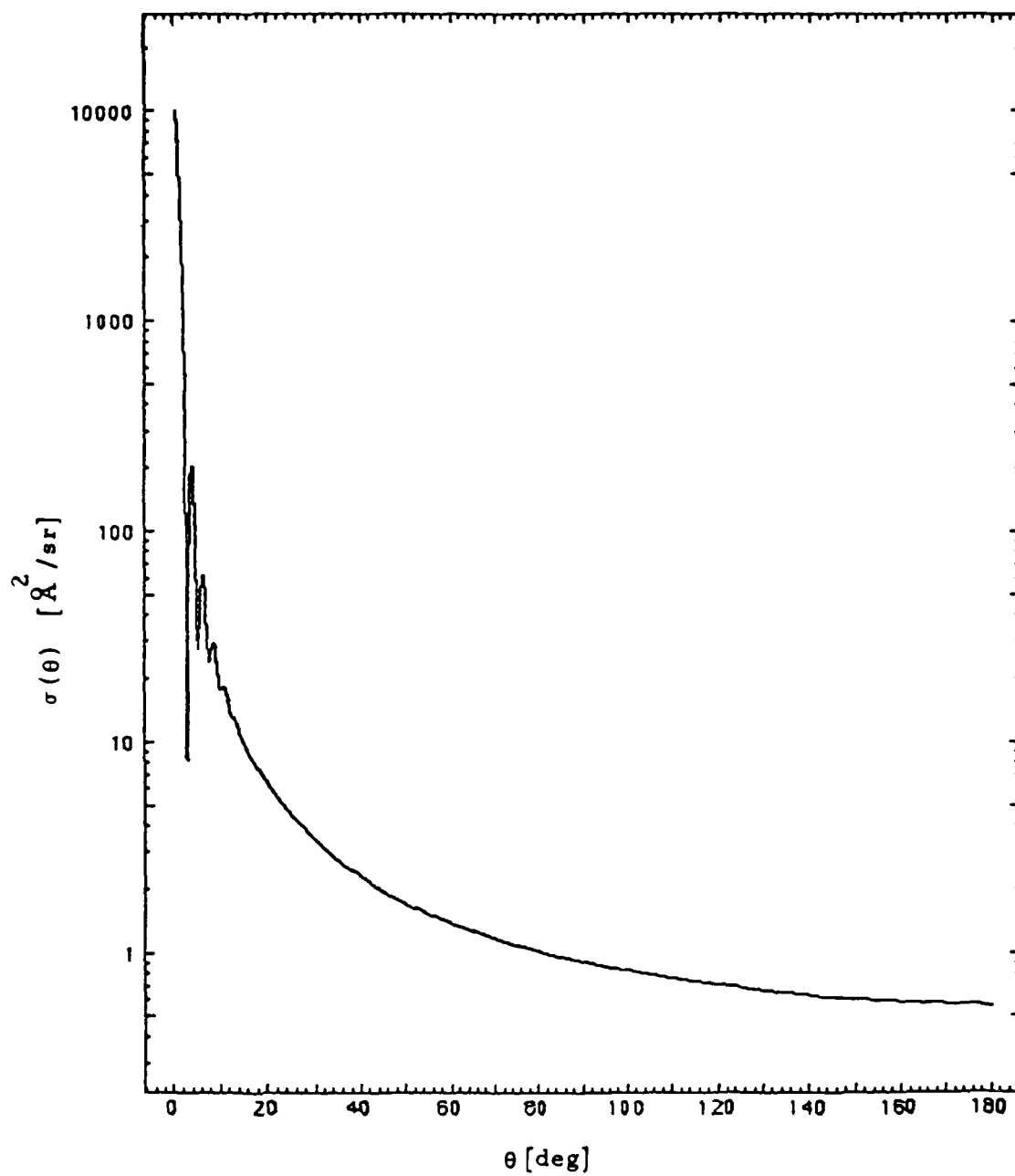
Fig. 8. Semilog plot of the He-O differential cross section $\sigma(\theta)$ as a function of the scattering angle $\theta$ for E = 0.60 eV

27
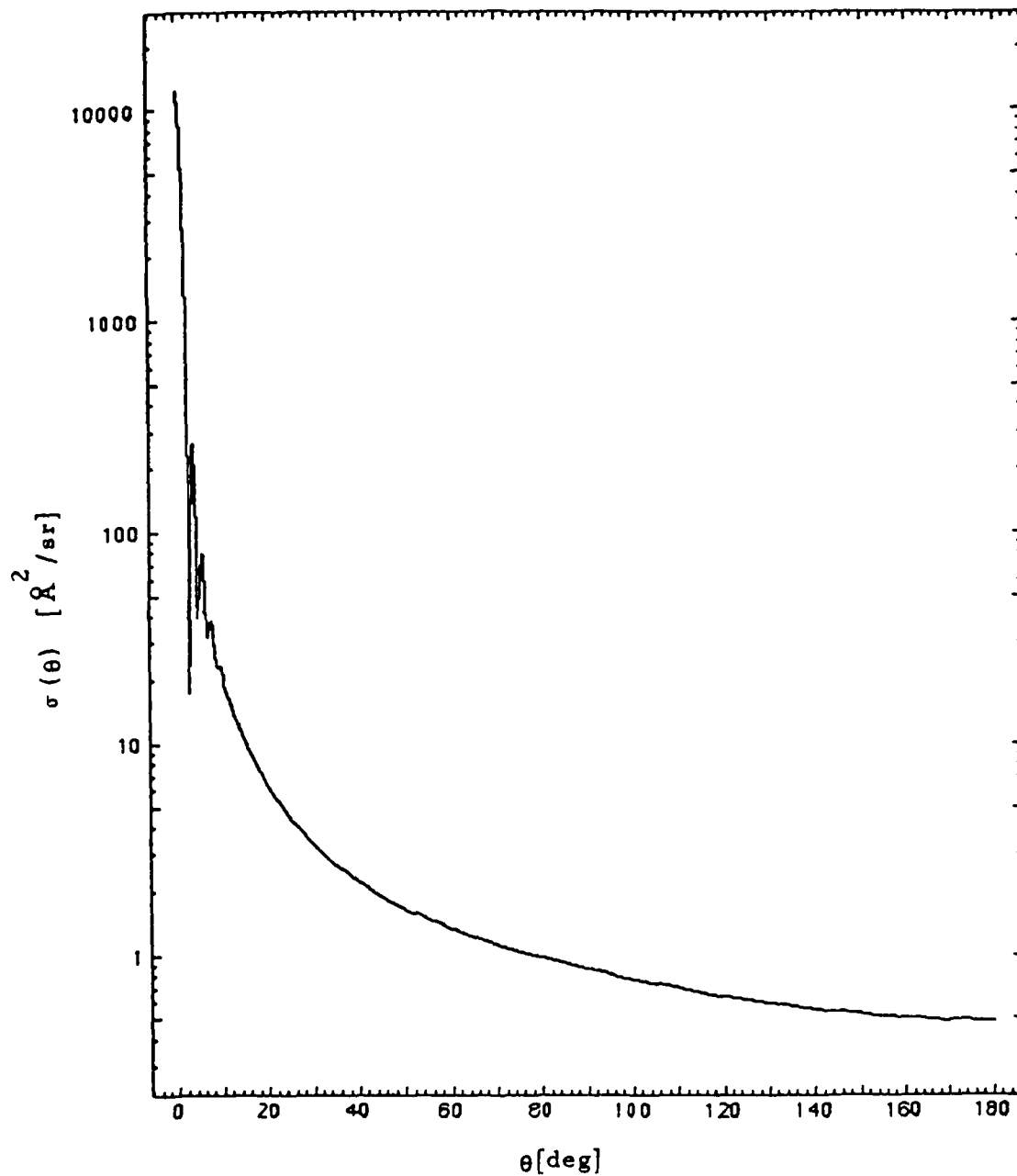
Fig. 9.   Semilog plot of the He-O differential cross section σ(θ)
          as a function of the scattering angle θ for E = 0.81 eV
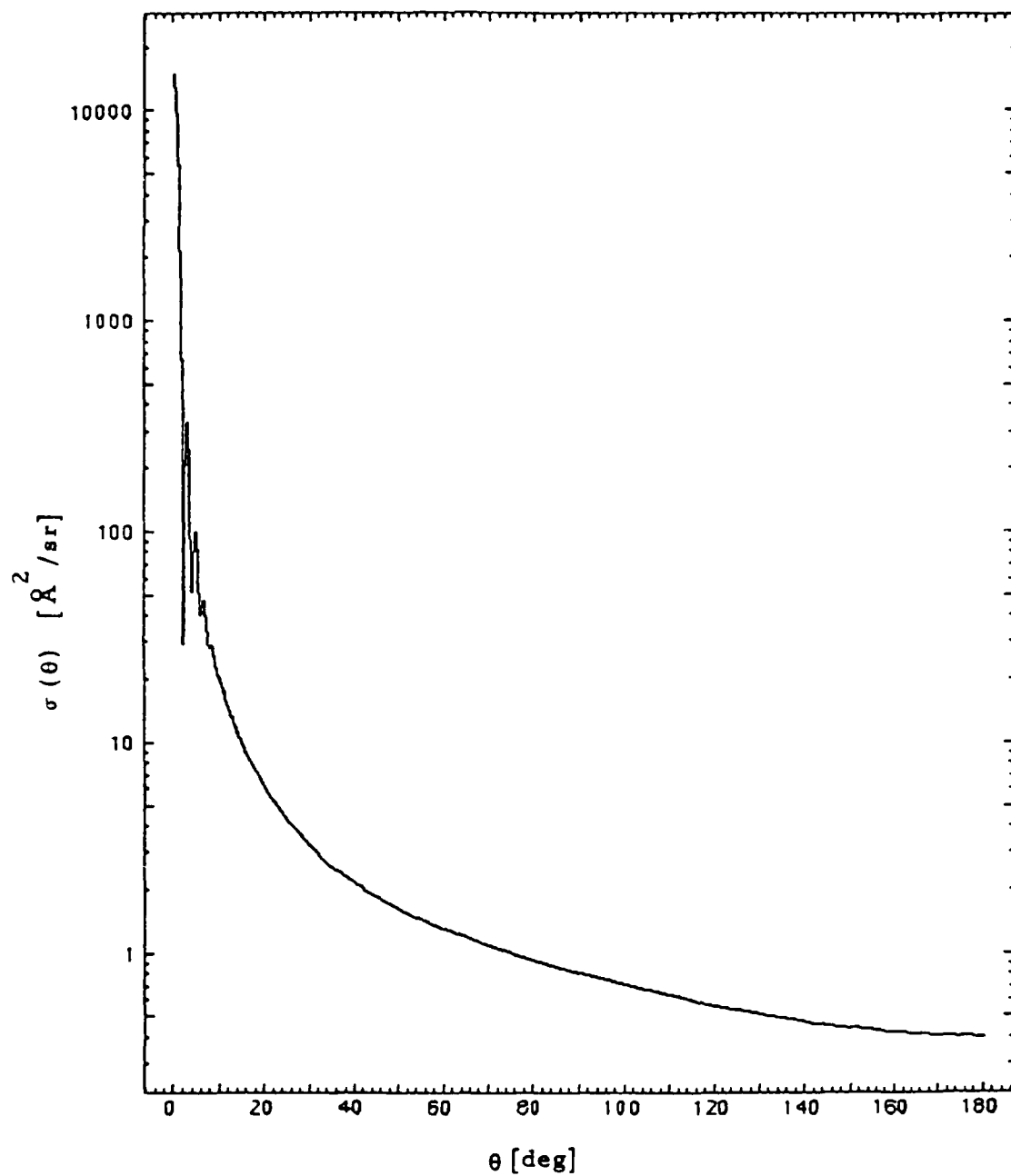
Fig. 10. Semilog plot of the He-O differential cross section $\sigma(\theta)$ as a function of the scattering angle $\theta$ for E = 1.06 eV

29
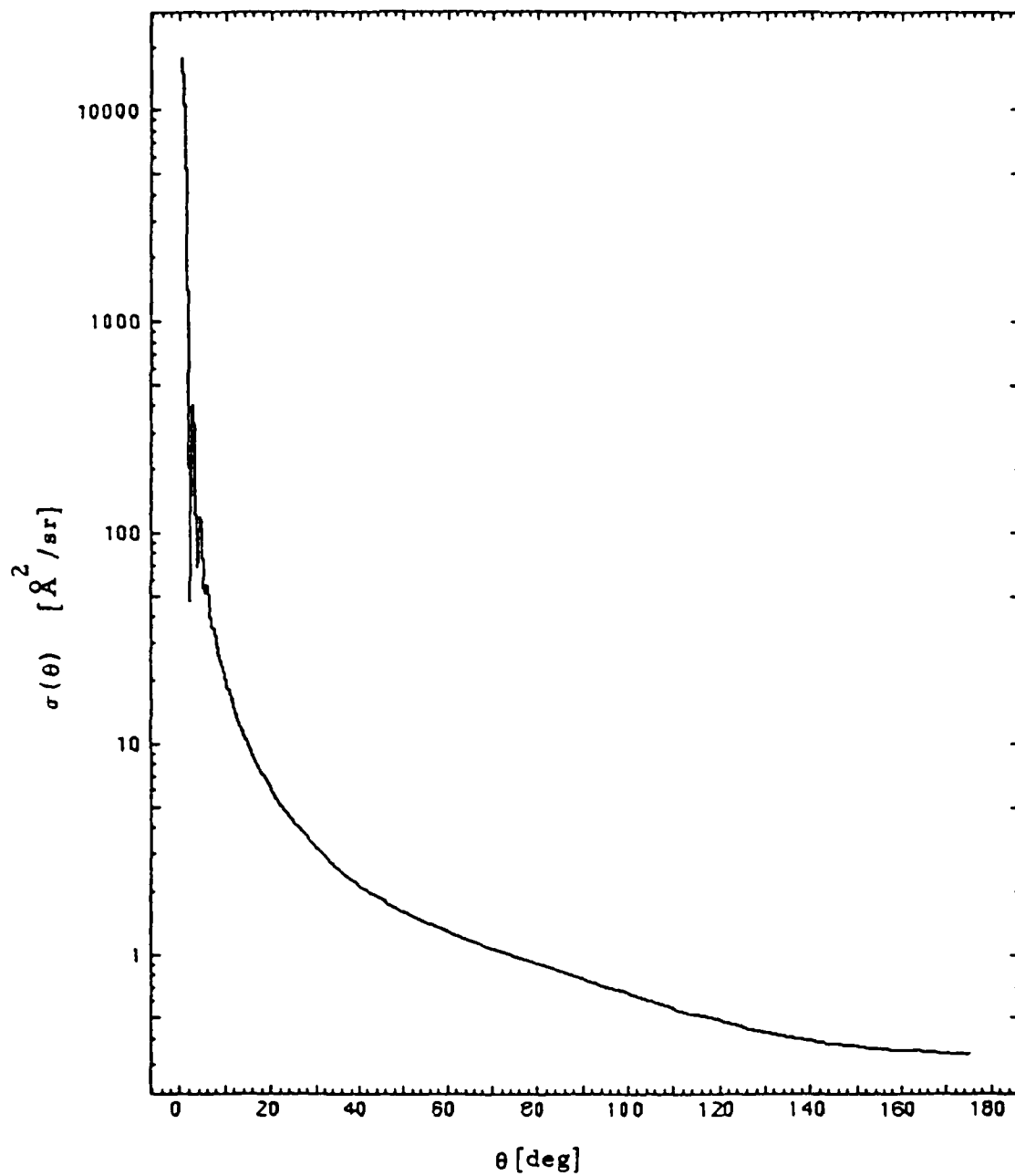
Fig. 11. Semilog plot of the He-O differential cross section σ(θ) as a function of the scattering angle θ for E = 1.34 eV
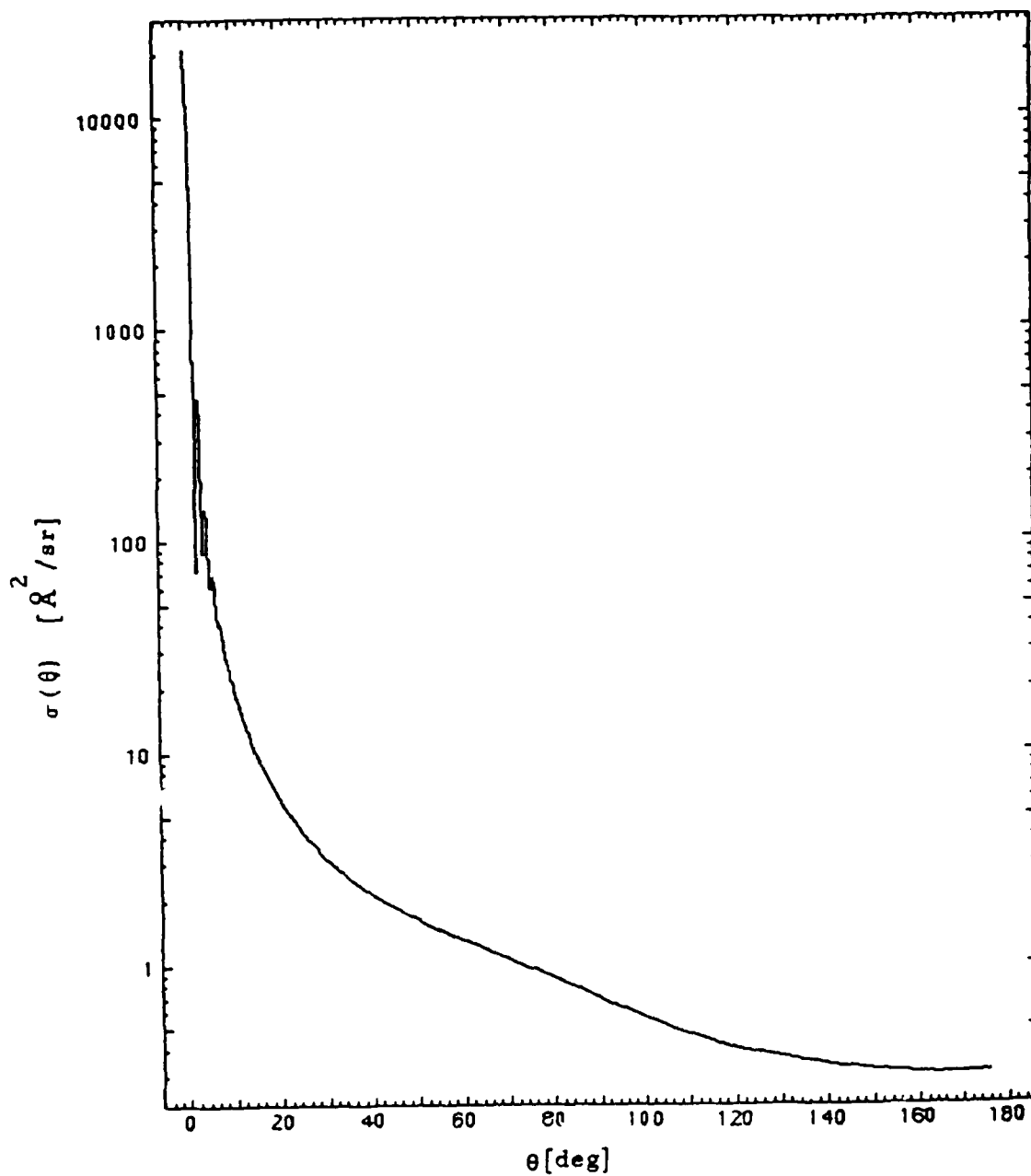
Fig. 12.  Semilog plot of the He-O differential cross section σ(θ)
as a function of the scattering angle θ for E = 1.66 eV
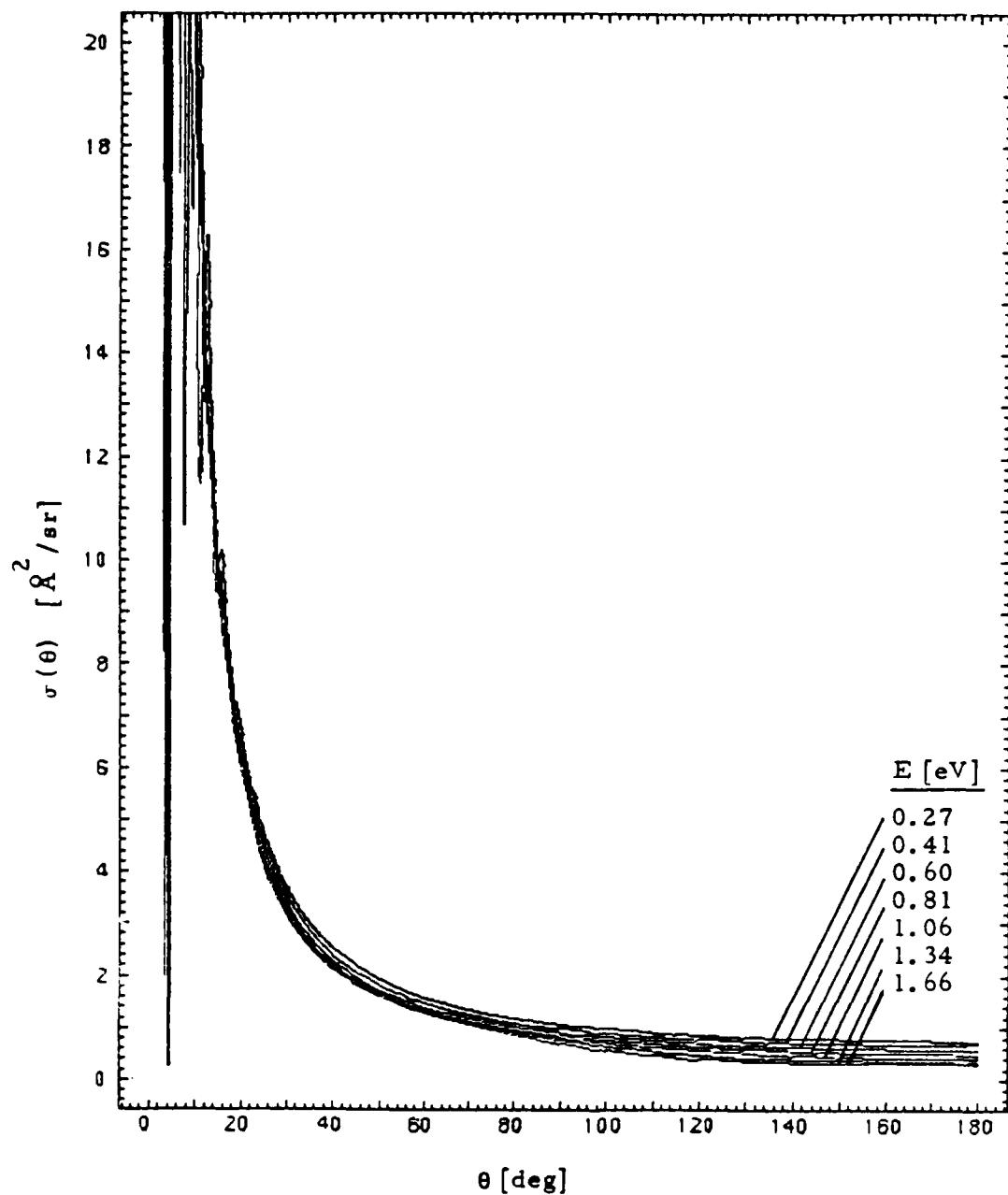
Fig. 13.  Linear plot of the He-O differential cross section $\sigma(\theta,E)$
for seven relative collision energies E > 0.27 eV

energy are displayed in Fig. 14 where the differential cross sections for the ten energies from 0.02 to 1.66 eV are compared.

The accuracy reported in Sec. III.B.1 for the WKB total cross sections for high energies, $E > 0.60$ eV, is not fortuitous. It is predicated on accurate differential cross sections. For those energies for which the WKB approximation was tested, the differential cross sections obtained using the WKB aproximation differ from the exact quantum results by less than 1%, except for energies in the range from 0.60 to 1.06 eV where, in the region of strong quantum mechanical oscillations, the error in $\sigma(\theta, E)$ for a few scattering angles is as large as 4%.

C. Quantum Mechanical Oscillations

The differential cross section for all collision energies is modulated by a strong quantum mechanical interference pattern. For collisions occuring at high energies, the oscillations in the angle dependence of the differential cross section are confined to small scattering angles. For example, for $v > 6$ km/sec, Fig. 15 compares these oscillations, which cannot be distinguished on the scale of Fig. 14. As expected, the wavelength of the quantum mechanical diffraction pattern, measured for example by the peak-to-peak distance $\Delta\theta$, decreases as the collision energy increases and the system behaves more classically.[15] $\Delta\theta$ decreases from 2.3 deg at $E = 0.60$ eV to 1.5 deg at $E = 1.66$ eV.

For lower energies, the quantum mechanical interference pattern is more pronounced and affects the differential cross section for a wider range of scattering angles. This is easily seen even in Fig. 14. For very low collision energies, the quantum mechanical "rainbow" moves away from the origin to sufficiently large scattering angles that its strong amplitude

33
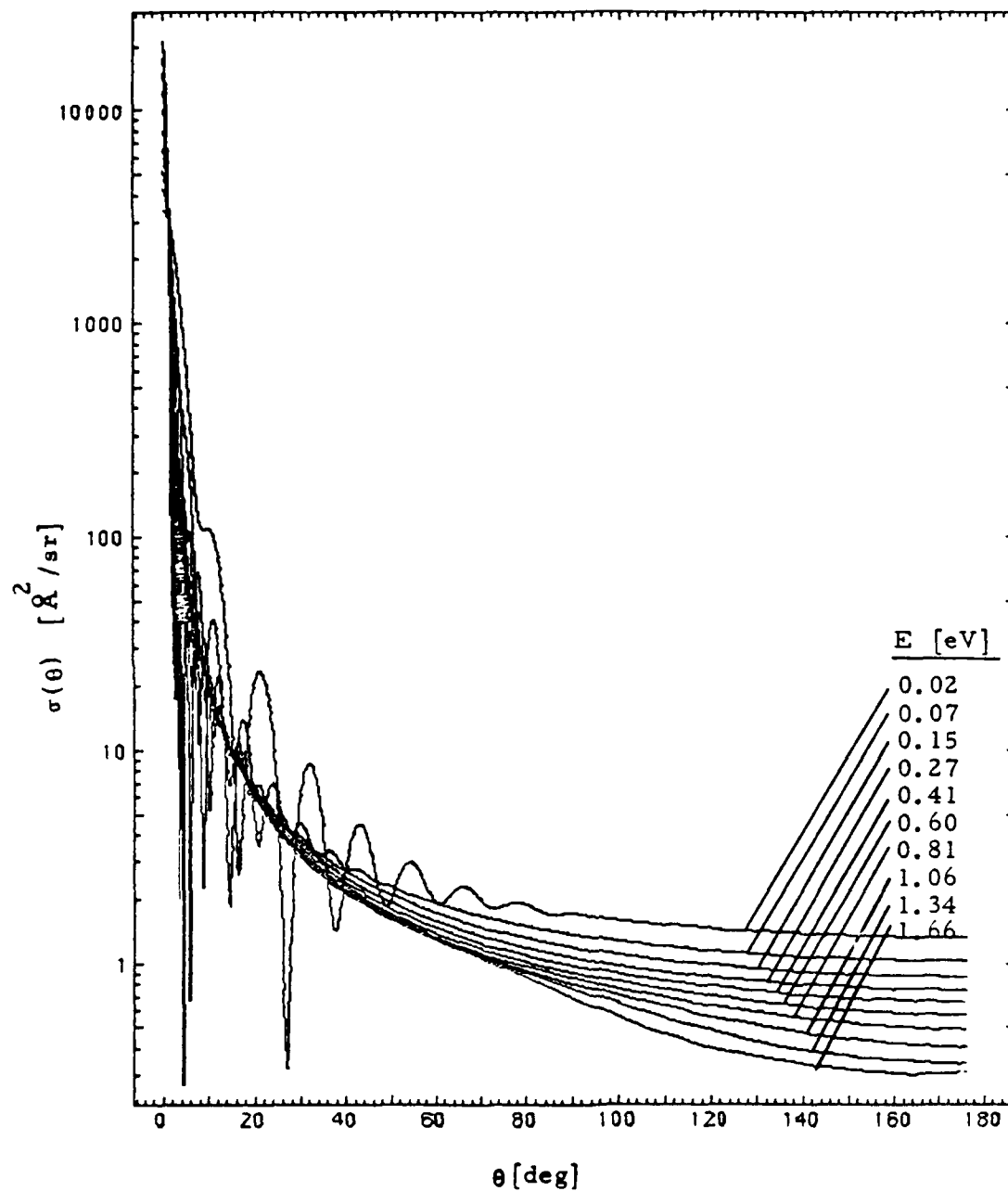
Fig. 14. Semilog plot of the He-O differential cross section $\sigma(\theta,E)$ for ten relative collision energies $0.02 \leqslant E[eV] \leqslant 1.66$

34
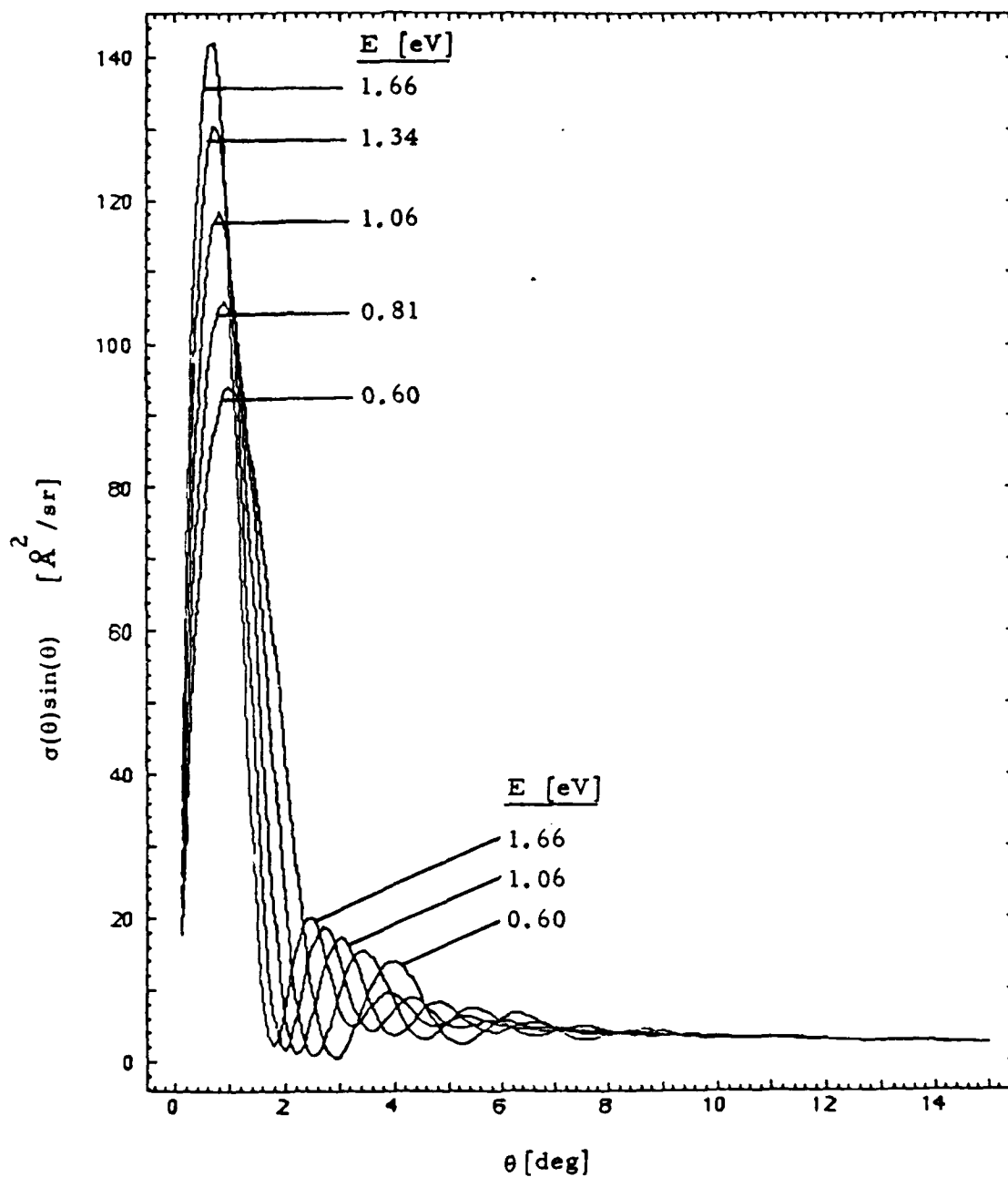
Fig. 15. Linear plot of $\sigma(\theta,E)\sin(\theta)$ showing the oscillations in the He-O differential cross section for small scattering angles $\theta$ for five relation collision energies $0.60 \leqslant E[eV] \leqslant 1.66$

35

oscillation can be easily identified.[15] This is illustrated in Fig. 16. There the differential cross sections for $E = 0.045$, $0.02$, and $0.01$ eV are plotted and the rainbows at $\theta \approx 11$, $27$, and $37$ deg, respectively, are well resolved.

D. Dependence of $\sigma_{tot}(E)$ and $\sigma(\theta, E)$ on the Interatomic Potential

The uncertainty in the scattering cross sections due to errors in the representation of the He-O interatomic potential by the model $V^H(R)$ defined by eq. (3) can be estimated by comparing the results of scattering calculations carried out using moderately different potentials to the results obtained using the realistic, but approximate, hybrid potential $V^H(R)$. It is not necessary to make this comparison for the low-energy calculations since the excellent agreement between the total cross sections obtained experimentally by Aquilanti and coworkers[9] and by the quantum mechanical calculations here confirms that $V^H(R)$ provides a satisfactory representation of the potential. However, since no such comparison of calculated and experimental results is available for the high-energy collisions, a test of the sensitivity of the high-energy scattering calculations to the interaction potential is important.

Three model interaction potentials are illustrated in Fig. 17. $V^F(R)$ is Foreman's repulsive potential. This differs from $V^H(R)$ in that it lacks a long-range attractive tail and is slightly more repulsive than $V^H(R)$ for R approximately 2.0 to 2.5 Å. The other potentials shown in Fig. 17, $V^{F\pm2}(R)$, were obtained by shifting $V^F(R)$ to smaller R, $V^{F+2}(R) = V^F(R + .2 \text{ Å})$, and to larger R, $V^{F-2}(R) = V^F(R - 0.2 \text{ Å})$.

Exact quantum mechanical calculations of He-O scattering using $V^H(R)$, $V^{F\pm2}(R)$, or $V^{F\pm1}(R) = V^F(R \pm 0.1 \text{ Å})$ were compared for the intermediate energy $E = 1.06$ eV. These potentials were chosen for the following reason. As noted in Sec. II., the potential used in this work, $V^H$, neglects the energy differ-

36
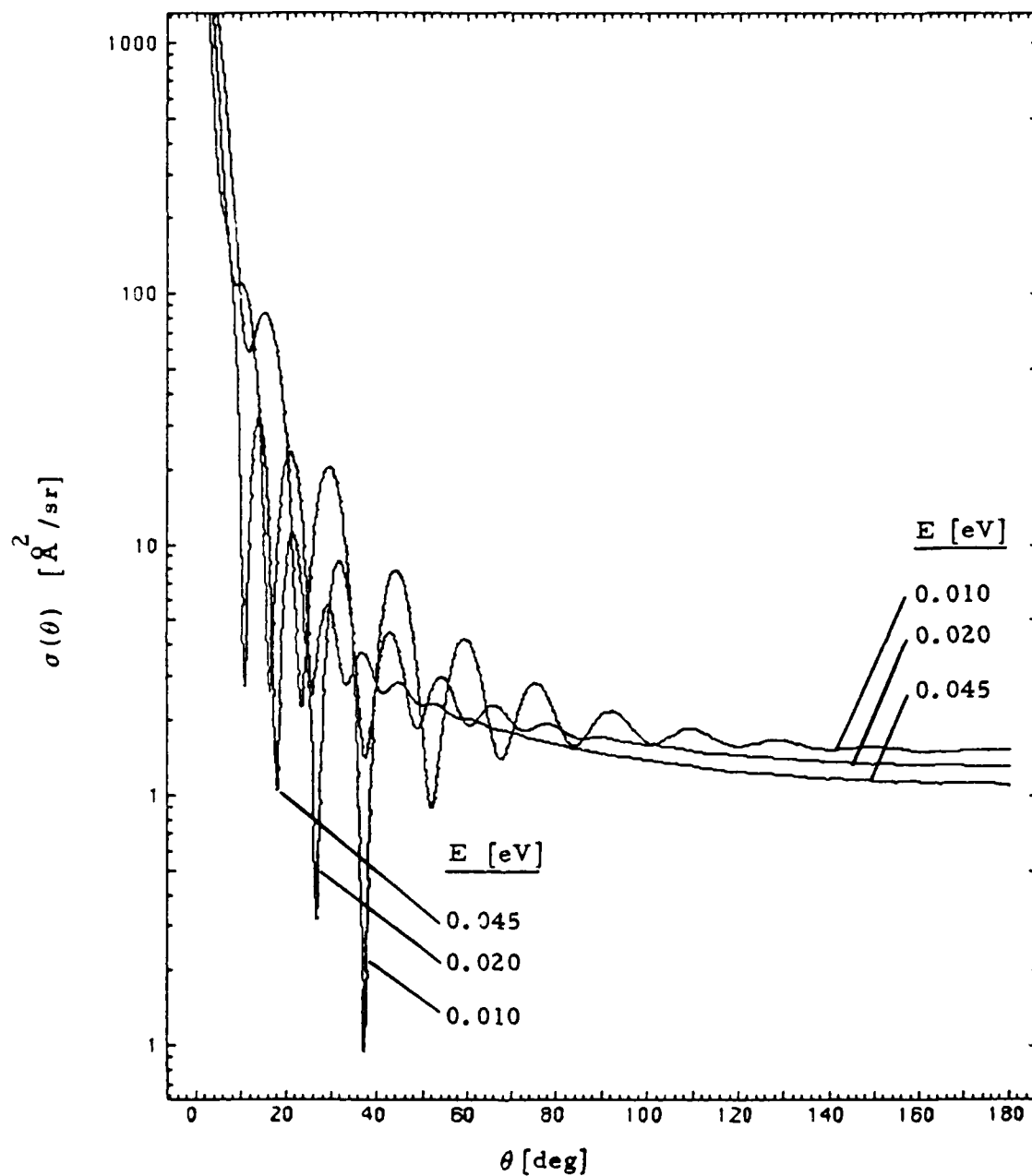
Fig. 16. Semilog plot of the He-O differential cross section s($\theta$,E) showing the quantum mechanical rainbow for three low collision energies E $\leqslant$ 0.10 Ev

37
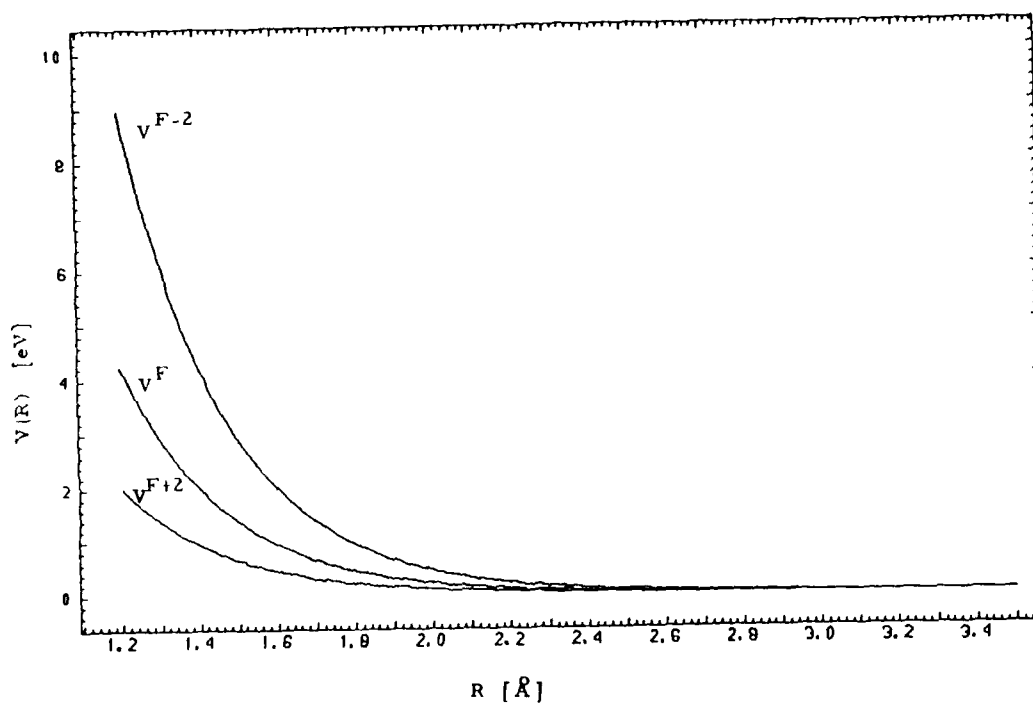
Fig. 17.   Comparison of representative model interatomic potentials:
Foreman's potential $V^F$, eq. (1), and $V^{F\pm2}$, Sec. III.D

38

ences between the $^3\Pi$ and $^3\Sigma^-$ potential functions which described the interactions of ground-state oxygen and helium atoms. Instead, for small R, $V^H$ is equivalent to $V^F$, the potential obtained by Foreman and coworkers[8] by inverting high-energy molecular beam scattering results. The ab initio calculations of Dunning and Hay[7] on the rare-gas oxides of Ne, Ar, Kr, and Xe provide the only information on the differences between the $^3\Pi$ and $^3\Sigma^-$ potential functions. As mentioned in Sec. II., these calculations found that the $^3\Pi$ and $^3\Sigma^-$ potential functions are similar in shape and differ significantly only for small R. For small interatomic separations, the $^3\Sigma^-$ potential is shifted to larger R than the $^3\Pi$ function, and the experimentally derived potential function more closely approximates the $^3\Pi$ function. For NeO the $^3\Sigma^-$ curve is shifted by about 0.16 Å from the $^3\Pi$ curve; for HeO the splitting between the two potential curves should be less than that. This suggests that the small-R $^3\Pi$ and $^3\Sigma^-$ potential functions for HeO should lie between $V^{F+2}$ and $V^{F-2}$. Therefore, the differences between the scattering results obtained using $V^F$ and $V^{F\pm2}$ should indicate the largest errors associated with using a single potential function $V^F$ to describe the small-R He-O interatomic potential when the elastic scattering is really mediated by two slightly different potential functions.

The total cross sections for He-O scattering at E = 1.06 eV, obtained by exact quantum mechanical calculations employing $V^H$, $V^F$, $V^{F\pm1}$, and $V^{F\pm2}$, are given in Table II. The total cross sections obtained by calculations using the five purely repulsive potentials differ by at most a factor of 1.5 from $\sigma_{tot}$ calculated using the realistic hybrid potential, $V^H$. Although $V^H$ has a long-range attractive potential, and, in contrast, the purely repulsive potentials die off more quickly as a function of the internuclear separation, $\sigma_{tot}$ obtained in scattering calculations using any of the purely repulsive

39

Table II.  Comparison of the total cross sections $\sigma_{tot}$ obtained using the realistic hybrid potential $V^H$, Foreman's potential $V^F$, or four other model interatomic potentials (see Sec. III.D) for scattering at $E = 1.06$ eV

| Potential | $\sigma_{tot} [A^2]$ |
|-----------|----------------------|
| $V^H$     | 36.8                 |
| $V^{F+2}$ | 39.6                 |
| $V^{F+1}$ | 43.1                 |
| $V^F$     | 46.6                 |
| $V^{F-1}$ | 50.3                 |
| $V^{F-2}$ | 54.1                 |

potentials is larger than that given by calculations using the hybrid potential because the purely repulsive potentials are of greater magnitude than $V^H$ in an important intermediate-R region. The differential scattering cross sections for He-O scattering at E = 1.06 eV, mediated by $V^H$ or any of the five model interatomic potentials, are very similar. The differential cross sections obtained with the potentials $V^H$, $V^F$, and $V^{F\pm2}$ are plotted in Fig. 18. These cross sections are all strongly peaked toward small scattering angles. Except for small $\theta$ where $\sigma(\theta, E)$ obtained using $V^H$ has larger amplitude oscillations than the differential cross sections for any of the purely repulsive potentials, the results obtained for the five test potentials closely bracket $\sigma(\theta, E)$ obtained using $V^H$.

These results suggest that errors in the model interaction potential $V^H(R)$ used in the quantum scattering calculators give rise to no more than a factor of two error in the calculated total elastic scattering cross section. Additionally, Fig. 18 implies that the angle dependence of the differential cross sections is known to about the same degree of accuracy.


IV. Hard-Sphere Models

It is interesting to consider how accurately simple alternative models of the He-O collision process can mimic the exact collision dynamics. In this section, two hard-sphere models are compared to the exact quantum mechanical treatment for the representative high-energy E = 1.06 eV.

The simplest model of the elastic scattering of two atoms treats the atoms as hard spheres and uses classical mechanics to determine their motion. This classical mechanical hard-sphere (CMHS) model yields the following energy-independent expression for the total cross section[16]
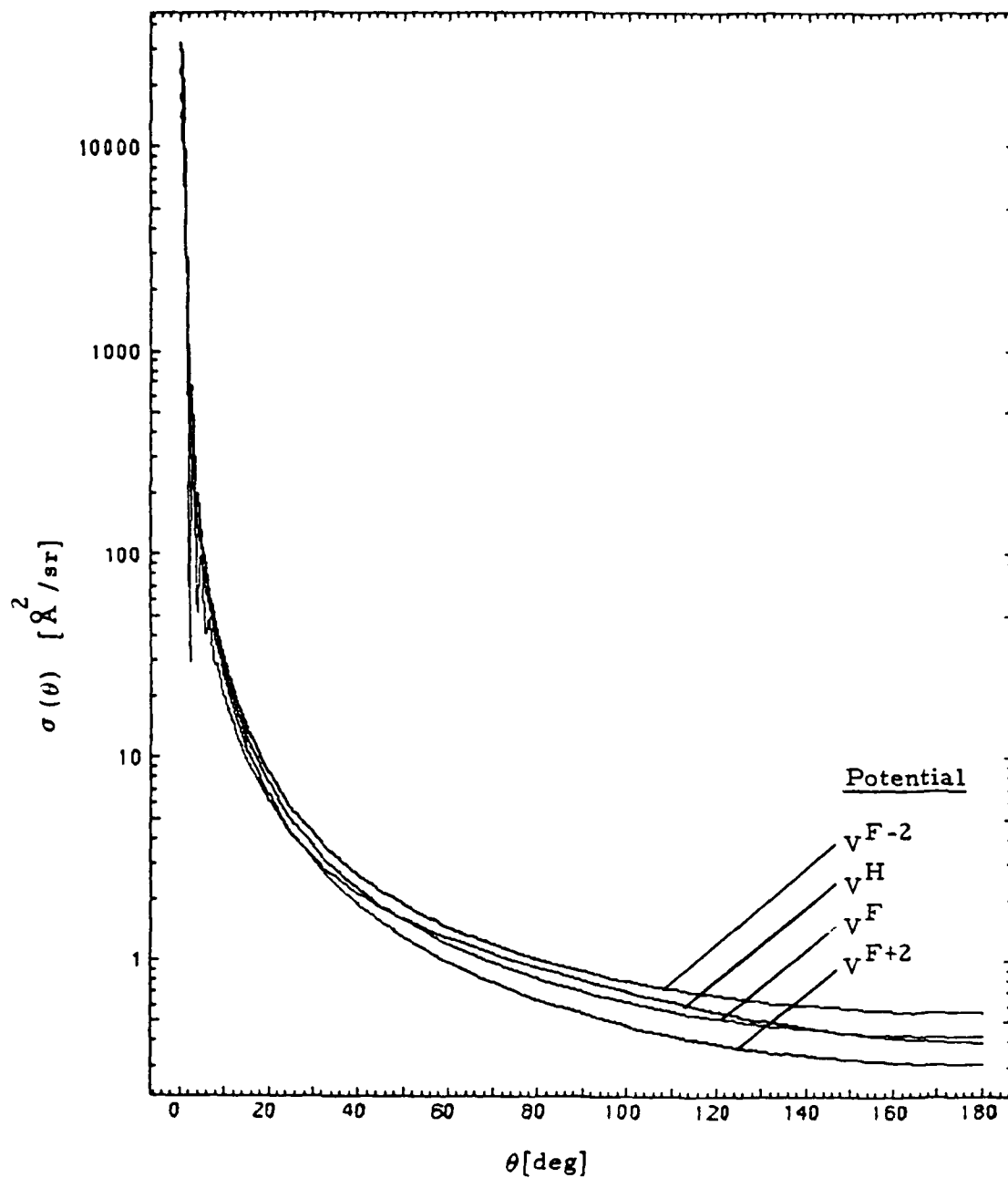
Fig. 18. Semilog plot comparing the differential cross section for the three model interatomic potentials, $V^F$ and $V^{F\pm2}$, to that for the realistic hybrid potential, $V^H$, for scattering at $E = 1.06$ eV

42

$$\sigma_{tot}^{CMHS} = \pi \, r_o^2 \tag{7}$$

where $r_o$ is an effective collision radius. If $r_o = 3.42$ A, $\sigma_{tot}^{CMHS} = 36.8$ A$^2$, the value of the exact quantum mechanical cross section for E = 1.06 eV. The classical mechanical hard-sphere differential cross section is given by[16]

$$\sigma^{CMHS}(\theta) = \frac{1}{4} \, r_o^2 \tag{8}$$

and for $r_o = 3.42$ A yields $\sigma^{CHMS} = 2.92$ A$^2$/sr. In Fig. 19, the classical mechanical hard-sphere differential cross section is compared to the exact quantum mechanical result for E = 1.06 eV. The isotropic classical mechanical hard-sphere differential cross section severely underestimates the small-angle scattering and overestimates the scattering into large angles.

Using quantum mechanics to treat the hard-sphere collision dynamics gives a better approximation to the exact differential cross section. The quantum mechanical model of high-energy hard-sphere elastic scattering gives[17]

$$\sigma_{tot}^{QMHS} \simeq 2\pi r_o^2 \tag{9}$$

Quantum mechanical calculations using $r_o = 2.42$ A yield $\sigma_{tot}^{QMHS} = 38.5$ A$^2$ and the differential cross section plotted in Fig. 19. The quantum mechanical hard-sphere differential cross section is forward peaked, but like the classical mechanical result, it strongly overestimates the large-angle scattering.

Previous models of He purge-gas collisions with O atoms have described the He-O scattering by a classical mechanical hard-sphere collision model characterized by some value for $\sigma_{tot}$. In addition to neglecting the energy dependence of the differential cross section, such a model gives a very poor
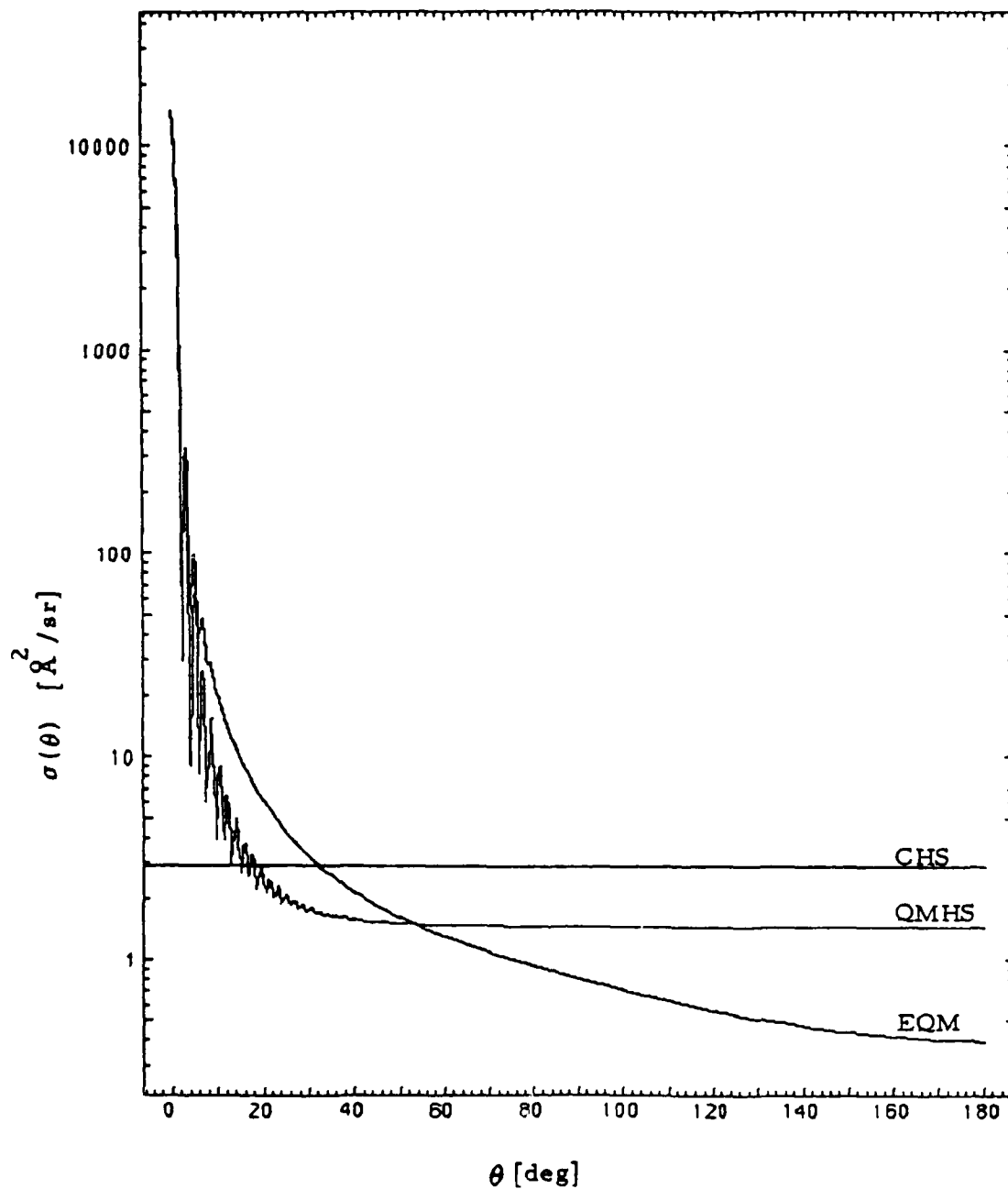
Fig. 19.   Semilog plot comparing the exact quantum mechanical (EQM),
classical hard sphere (CHS), and quantum mechanical hard
sphere (QMHS) differential cross sections for E - 1.06 eV

representation of the strong angle dependence of the exact differential cross section and consequently can lead to incorrect estimates of the purge gas efficiency.

V.   Analytic Fit to Differential Cross Section

The accurate He-O differential cross section is a function of both the relative collision energy and the scattering angle.   This dependence on E and $\theta$ presents a major impediment to the use of the accurate differential cross section in Monte Carlo calculations.   In order to facilitate the use of the accurate cross sections presented in this report, the differential cross sections have been fitted by a simple separable analytic function of E and $\theta$. In this section, this analytic function $s(\theta, E)$, which separates the dependence on E and $\theta$ and provides an adequate representation of $\sigma(\theta, E)$ for all $\theta$ for the energies tested here, is described.   For each of the ten energies studied, it is compared with the accurate differential cross sections.

The general features of the He-O differential cross sections that might need to be incorporated into the fitting function can be summarized as follows.   For all energies, the differential cross section is strongly forward peaked.   For each energy, it is a monotonically decreasing function of $\theta$ except for some range of small scattering angles where it is modulated by a quantum mechanical diffraction pattern.   Since the Monte Carlo calculations will sample collisions occuring at many different energies, the quantum mechanical oscillations in $\sigma(\theta, E)$ can be neglected since they average out over a range of energies.

The function $s(\theta, E)$, which provides the approximate fit to the differential cross section $\sigma(\theta, E)$ for all $\theta$ and E, is the product of two functions. One function, $\bar{s}(\theta)$, furnishes the dominant angle dependence of $\sigma(\theta, E)$ and the

other accounts for some of the variation in this angle dependence as a function of the collision energy. This factorization was guided by the weak energy dependence and strong angle dependence displayed in Figures 13 and 14.

The predominant angle dependence can be expressed by

$$\bar{s}(\theta) = \exp(a_i \theta^2 + b_i \theta + c_i) \quad \text{for } \theta_{i-1} \leq \theta \leq \theta_i \tag{10}$$

where $\theta_0 = 0$ and the parameters $a_i$, $b_i$, $c_i$, and $\theta_i$ for the five regions of $\theta$ indexed by i are listed in Table III. In Fig. 20, $\bar{s}(\theta)$ is compared with $\sigma(\theta, v = 10 \text{ km/sec})$. The plot shows that $\bar{s}(\theta)$ provides an excellent fit to the accurate differential cross section for all $\theta$ for the highest relative collision energy studied. For very small scattering angles, $\bar{s}(\theta)$ remains within the limits of the quantum oscillations, and for larger scattering angles, $\bar{s}(\theta)$ is almost indistinguishable from the differential cross section. Because $\sigma(\theta, E)$ is only weakly dependent on the collision energy, $\bar{s}(\theta)$ provides a fair approximation to the differential cross section for $v <$ 10 km/sec as well. In fact, Figures 13, 14, and 20 suggest that $\bar{s}(\theta)$ may provide an adequate representation of $\sigma(\theta, E)$ for some applications. For the worst case considered here, the use of $\bar{s}(\theta)$ to represent $\sigma(\theta, v = 1 \text{ km/sec})$, $\bar{s}(\theta)$ underestimates the accurate cross section by, e.g., only factors of 1.2 and 2.2 for $\theta = 50$ and 80 deg, respectively. However, the differences between $\bar{s}(\theta)$ and $\sigma(\theta, v = 1 \text{ km/sec})$ increase with the scattering angle until at $\theta = 175$ deg, $\bar{s}(\theta)$ is 4.4 times less than $\sigma(\theta, v = 1 \text{ km/sec})$.

One possible function that can represent both the energy and angle dependence of the accurate differential cross section is

Table III. Parameters for $\bar{s}(\theta)$[a]

| $i$ | $\theta_i$ [deg] | $a_i$ [deg$^{-2}$] | $b_i$ [deg$^{-1}$] | $c_i$ |
|---|---|---|---|---|
| 1 | 12.0 | 7.23029 (−3)[b] | −3.67150 (−1) | 6.00370 |
| 2 | 40.0 | 1.76033 (−3) | −1.59291 (−1) | 4.29707 |
| 3 | 110.0 | 3.29386 (−5) | −2.64174 (−2) | 1.74593 |
| 4 | 180.0 | 1.00125 (−4) | −3.53582 (−2) | 1.91647 |

[a]See eq. (10)

[b]The number in parentheses denotes the power of ten by which the entry should be multiplied.

Fig. 29.    Semilog plot comparing the exact differential cross section
σ(θ) to the analytic fit $\overline{s}(\theta) = s(\theta)$ for v = 10 km/sec

48

$$s(\theta, v) = \bar{s}(\theta) \left[ 1 + f(\theta)(\frac{\bar{v}}{\tilde{v}} - 1) \right] \qquad (11)$$

where $\bar{s}(\theta)$ is given by eq. (10), $\bar{v} = 10$ km/sec, $\tilde{v}$ is defined by

$$\tilde{v} = v \qquad\qquad \text{for } v > 5 \text{ km/sec}$$

$$\tilde{v} = (5 + v)/2 \qquad \text{for } v < 5 \text{ km/sec}$$

and $f(\theta)$ is given by

$$f(\theta) = 0.59 \left\{ \tanh\left[0.8\pi \left(\frac{\theta - 100}{70}\right)\right] + 1 \right\} \qquad (12)$$

Thus $s(\theta, v = 10 \text{ km/sec}) = \bar{s}(\theta)$. The function $f(\theta)$ is designed to account for those differences between the accurate differential cross sections and $\bar{s}(\theta)$ which increase as $\theta$ increases. For $\theta < 70$ deg $f(\theta)$ is $< 0.12$, but for larger scattering angles, $f(\theta)$ increases rapidly, reaching half its asymptotic value of 1.18 by $\theta = 100$ deg. As a consequence of this, at $\theta = 70$ deg $s(\theta, v)$ differs from $\bar{s}(\theta)$ by $< 5\%$ for relative collision velocities $v > 7$ km/sec, by $< 18\%$ for $v = 3-6$ km/sec, and by $< 29\%$ for $v = 1-2$ km/sec. For larger scattering angles, $\bar{s}(\theta)$ and $s(\theta, v)$ differ more significantly. For example, $s(\theta, v = 5 \text{ km/sec})$ and $s(\theta, v = 1 \text{ km/sec})$ are 2.18 and 3.74 times greater than $\bar{s}(\theta)$ for $\theta = 175$ deg.

The analytic fits $s(\theta, v)$ to the accurate differential cross sections $\sigma(\theta, v)$ are compared for collision velocities of less than 10 km/sec in Figures 21 through 29. The agreement between $s(\theta, v)$ and $\sigma(\theta, v)$ is very good for the higher collision energies and acceptable for the lower energies. The poorest agreement between $s(\theta, v)$ and $\sigma(\theta, v)$ is exhibited for intermediate scattering angles, i.e., for scattering angles ranging from approximately 20

49

Fig. 21. Semilog plot comparing the exact differential cross section $\sigma(\theta)$ to the analytic fit $s(\theta)$ for $v = 9$ km/sec

Fig. 22.   Semilog plot comparing the exact differential cross section
           σ(θ) to the analytic fit s(θ) for v = 8 km/sec
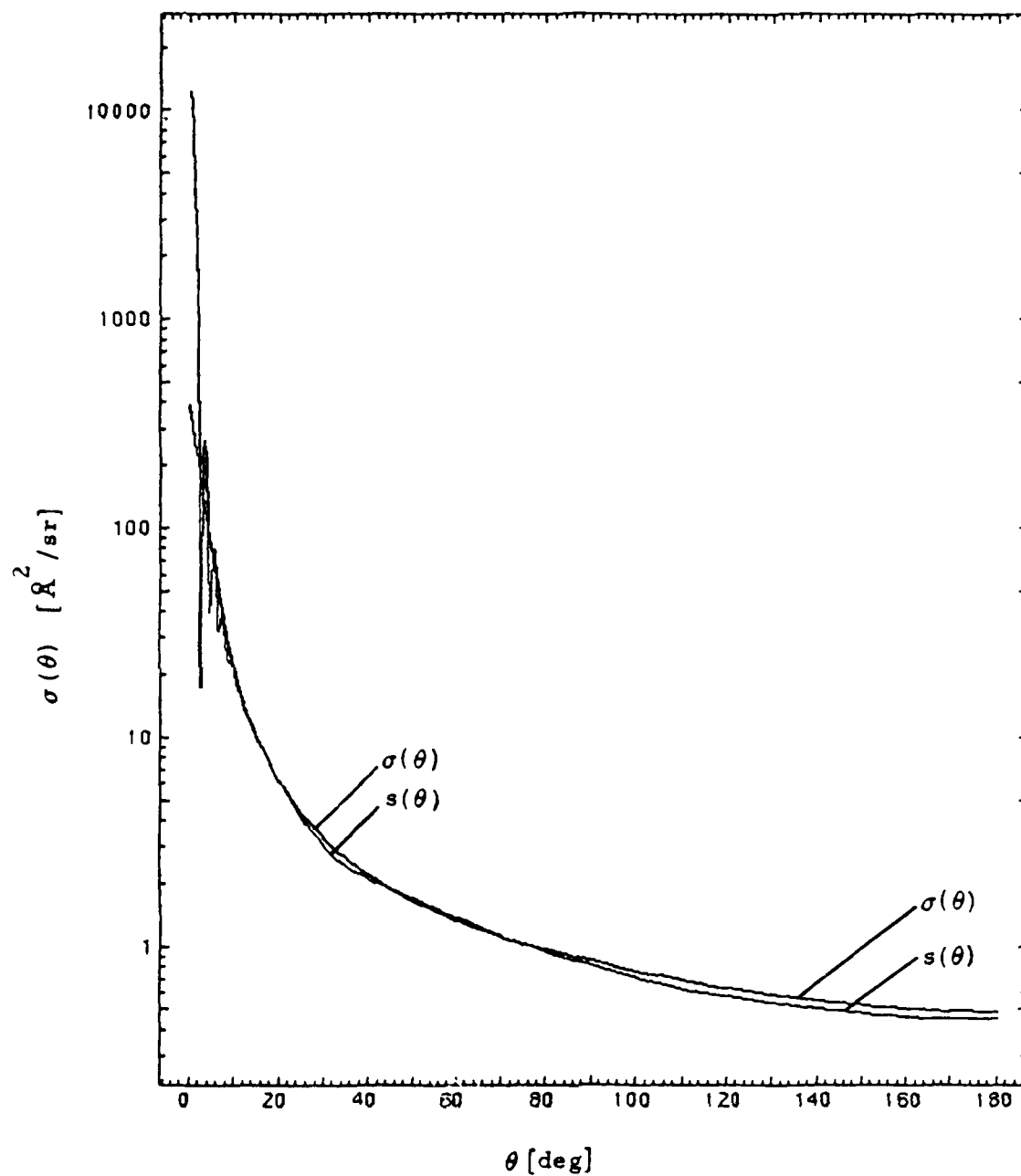
Fig. 23. Semilog plot comparing the exact differential cross section
$\sigma(\theta)$ to the analytic fit $s(\theta)$ for $v = 7$ km/sec

52
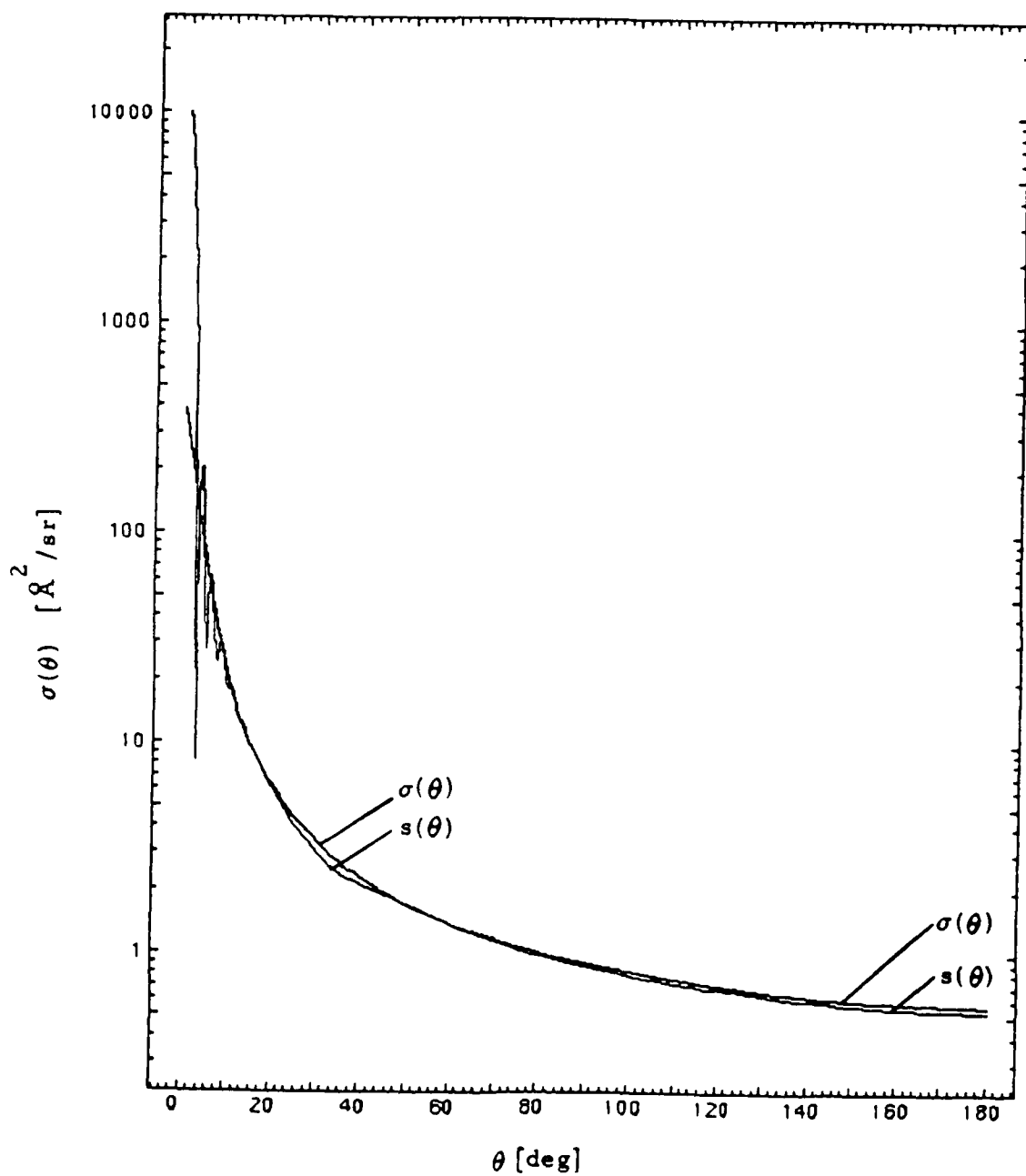
Fig. 24.   Semilog plot comparing the exact differential cross section
$\sigma(\theta)$ to the analytic fit $s(\theta)$ for $v = 6$ km/sec

53
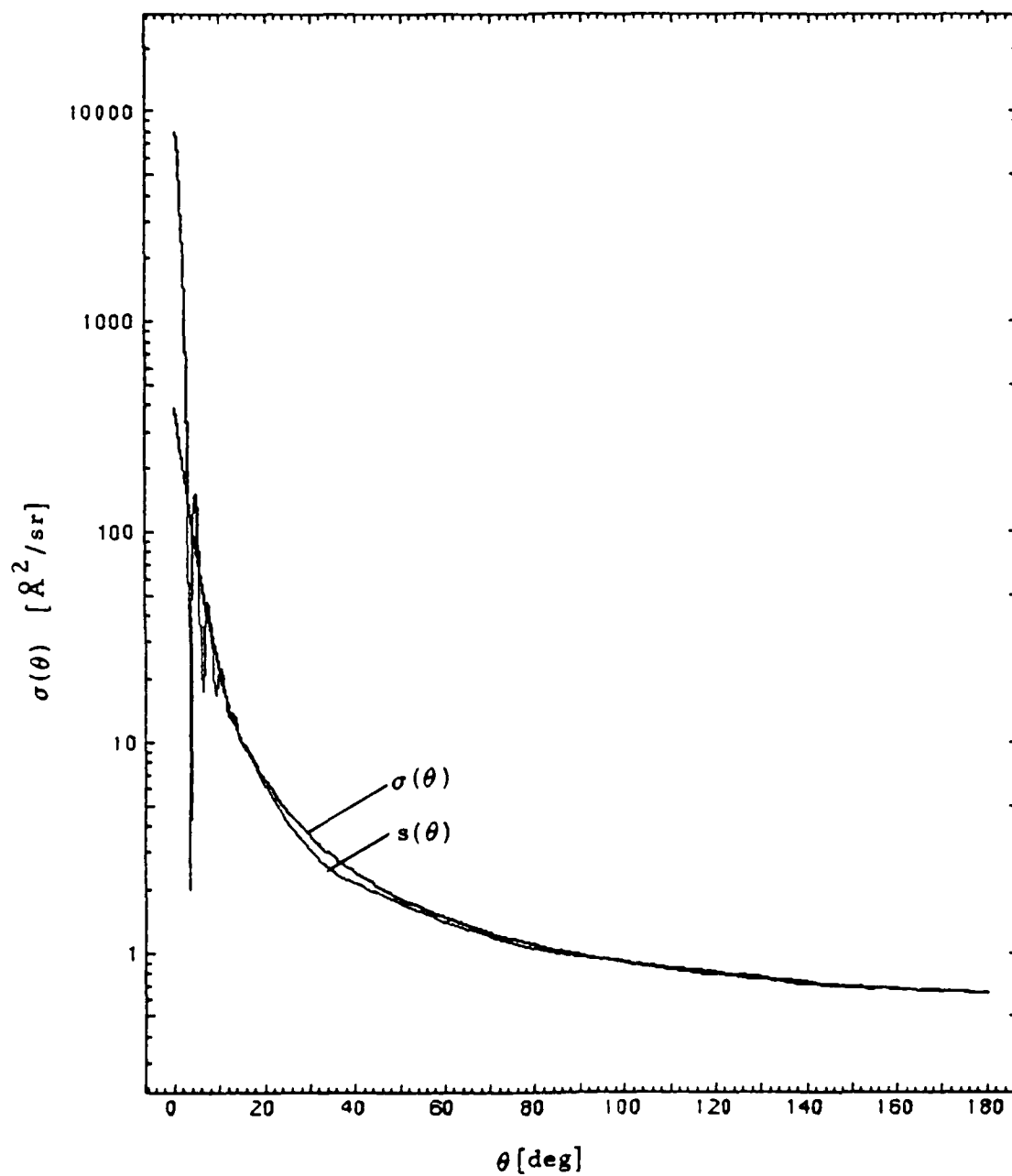
Fig. 25.    Semilog plot comparing the exact differential cross section
$\sigma(\theta)$ to the analytic fit $s(\theta)$ for $v = 5$ km/sec
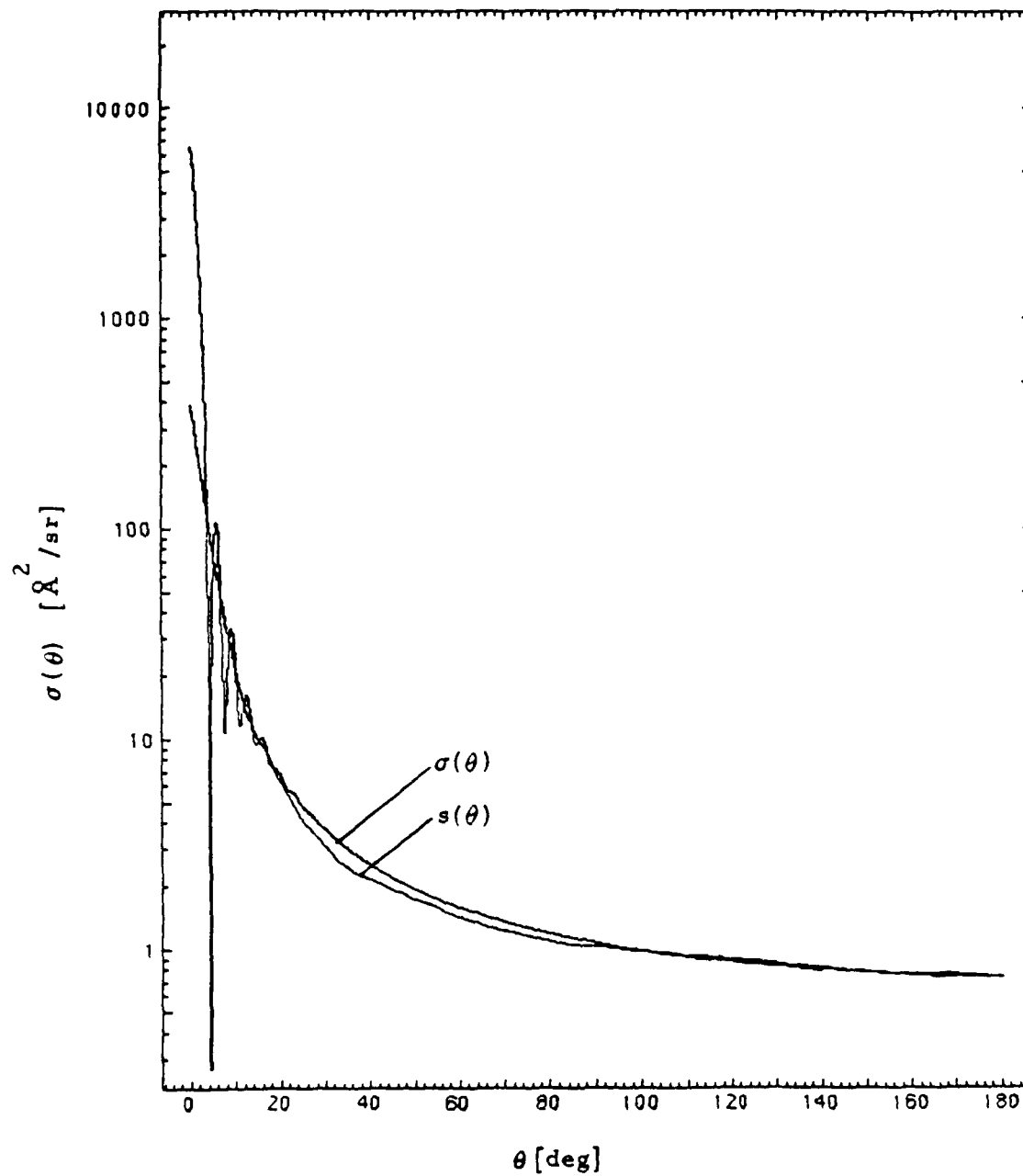
Fig. 26. Semilog plot comparing the exact differential cross section
$\sigma(\theta)$ to the analytic fit $s(\theta)$ for $v = 4$ km/sec
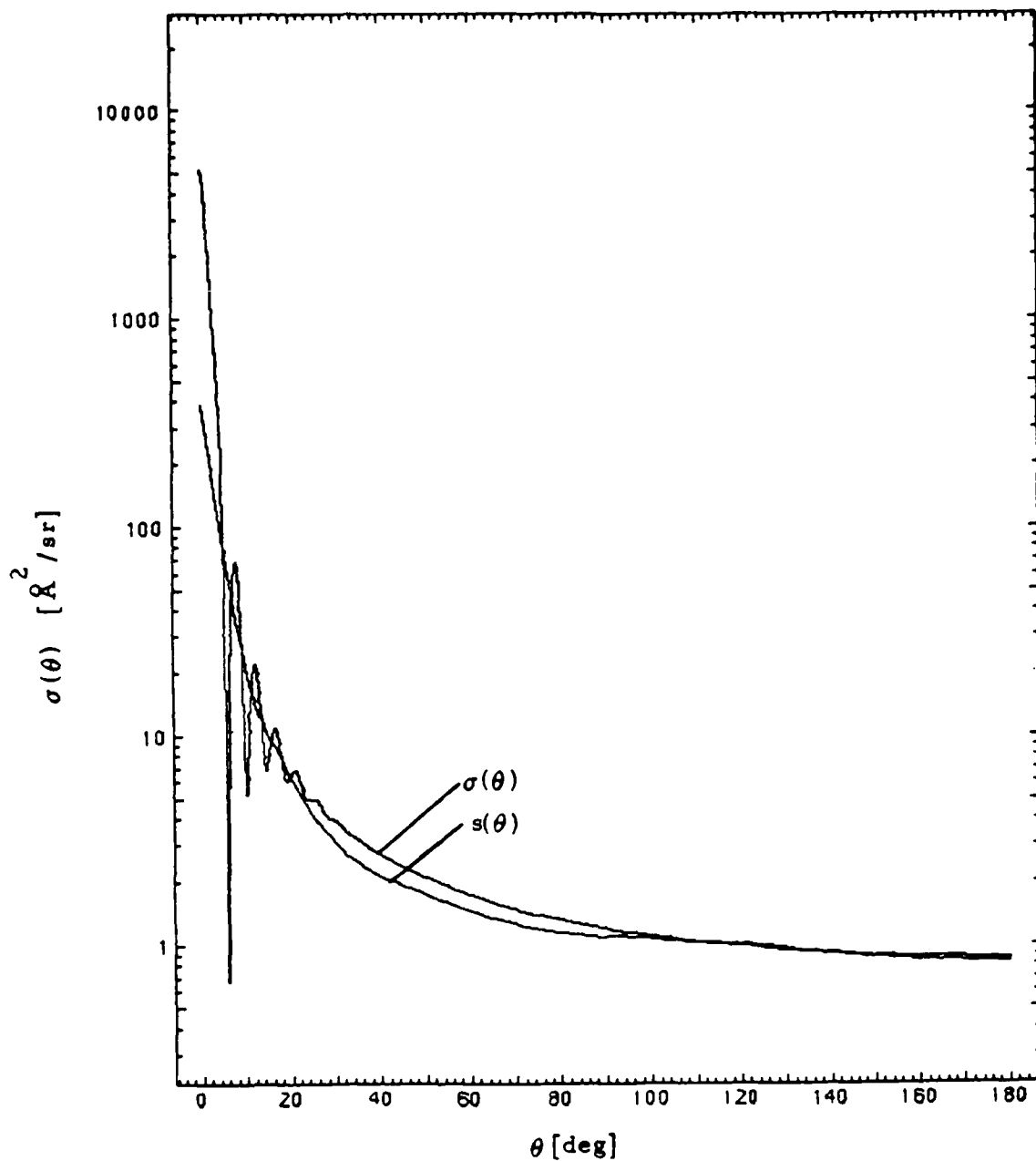
Fig. 27.    Semilog plot comparing the exact differential cross section
$\sigma(\theta)$ to the analytic fit $s(\theta)$ for $v = 3$ km/sec

56
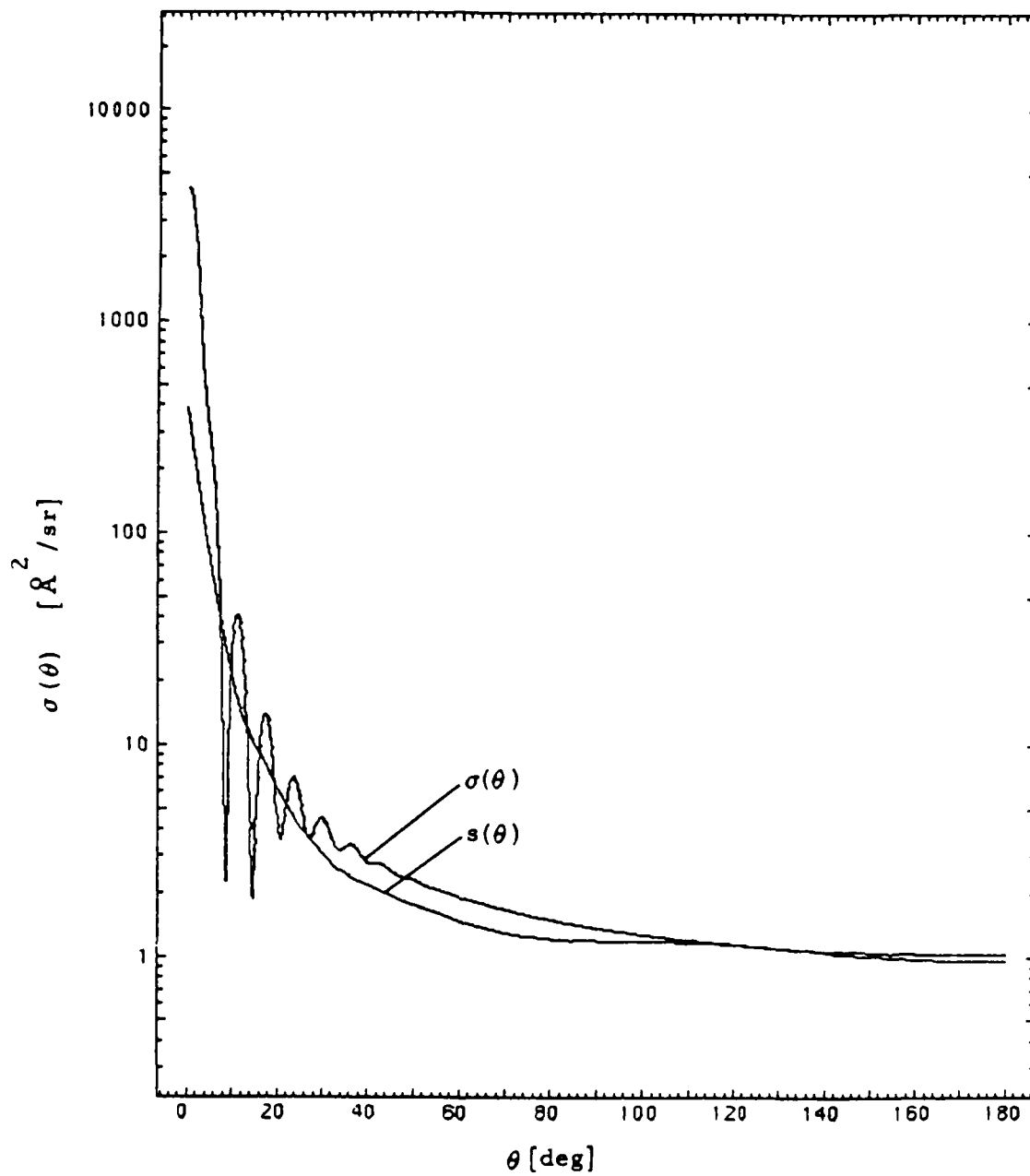
Fig. 28.    Semilog plot comparing the exact differential cross section
σ(θ) to the analytic fit s(θ) for v = 2 km/sec
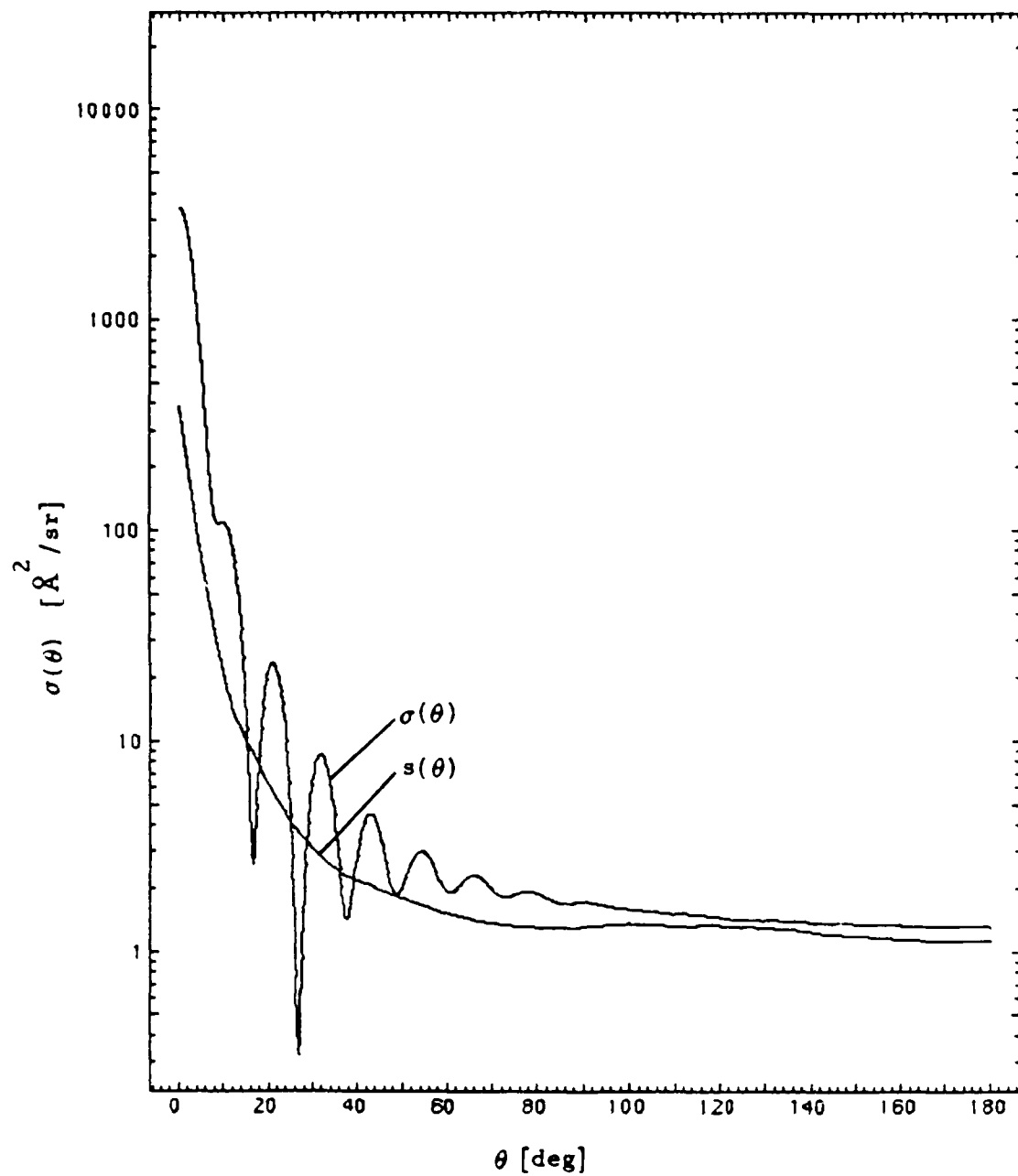
Fig. 29.    Semilog plot comparing the exact differential cross section
σ(θ) to the analytic fit s(θ) for v = 1 km/sec

to 90 deg, for v < 4 km/sec. Figures 30 through 34 again compare $\sigma(\theta, v)$ to $s(\theta, v)$ for v = 9, 7, 5, 3, and 1 km/sec, respectively. The latter five plots use a linear scale to emphasize the agreement between $s(\theta, v)$ and $\sigma(\theta, v)$. Indeed, two representative points showing poor agreement between $s(\theta, v)$ and $\sigma(\theta, v)$, $s(\theta = 40$ deg, v = 3 km/sec) and $s(\theta = 70$ deg, v = 1 km/sec) differ from the accurate cross sections for those scattering angles and collision energies by only 21% and 30%, respectively.

## VI. Conclusions

The total elastic scattering cross section $\sigma_{tot}(E)$ and the differential cross section $\sigma(\theta, E)$ have been reported for He-O scattering at ten representative collision energies in the range E = 0.02 to 1.66 eV. These results should be of interest to those involved in contamination control for cryogenically cooled sensors of orbiting infrared telescopes.

For the ten collision energies studied here, a simple separable analytic function of E and $\theta$ which fits $\sigma(\theta, E)$ reasonably well was found. This function permits the interpolation of the differential cross section for energies and scattering angles other than those tabulated here and facilitates the use of accurate differential cross sections in Monte Carlo calculations.

Additionally, the WKB approximation was used to calculate the cross sections for relative collision velocities of 6 to 10 km/sec. This computationally simpler approximate method yielded cross sections in excellent agreement with those obtained by the exact quantum mechanical calculations. This suggests that the WKB approximation will provide an accurate and efficient means by which to calculate cross sections for high-energy collisions of He with other contaminants, e.g., $H_2O$.
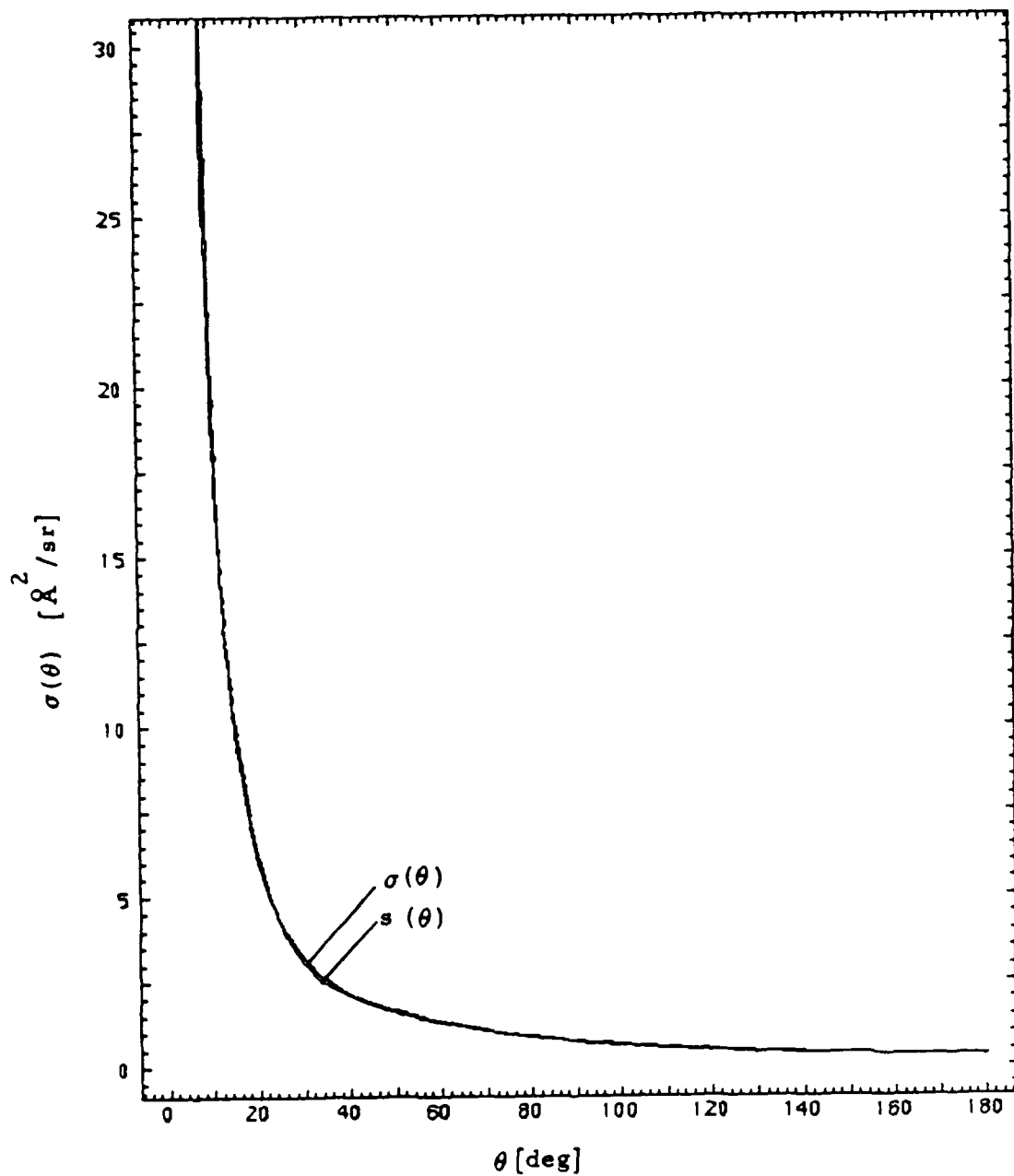
Fig. 30. Linear plot comparing the exact differential cross section $\sigma(\theta)$ to the analytic fit $s(\theta)$ for $v = 9$ km/sec
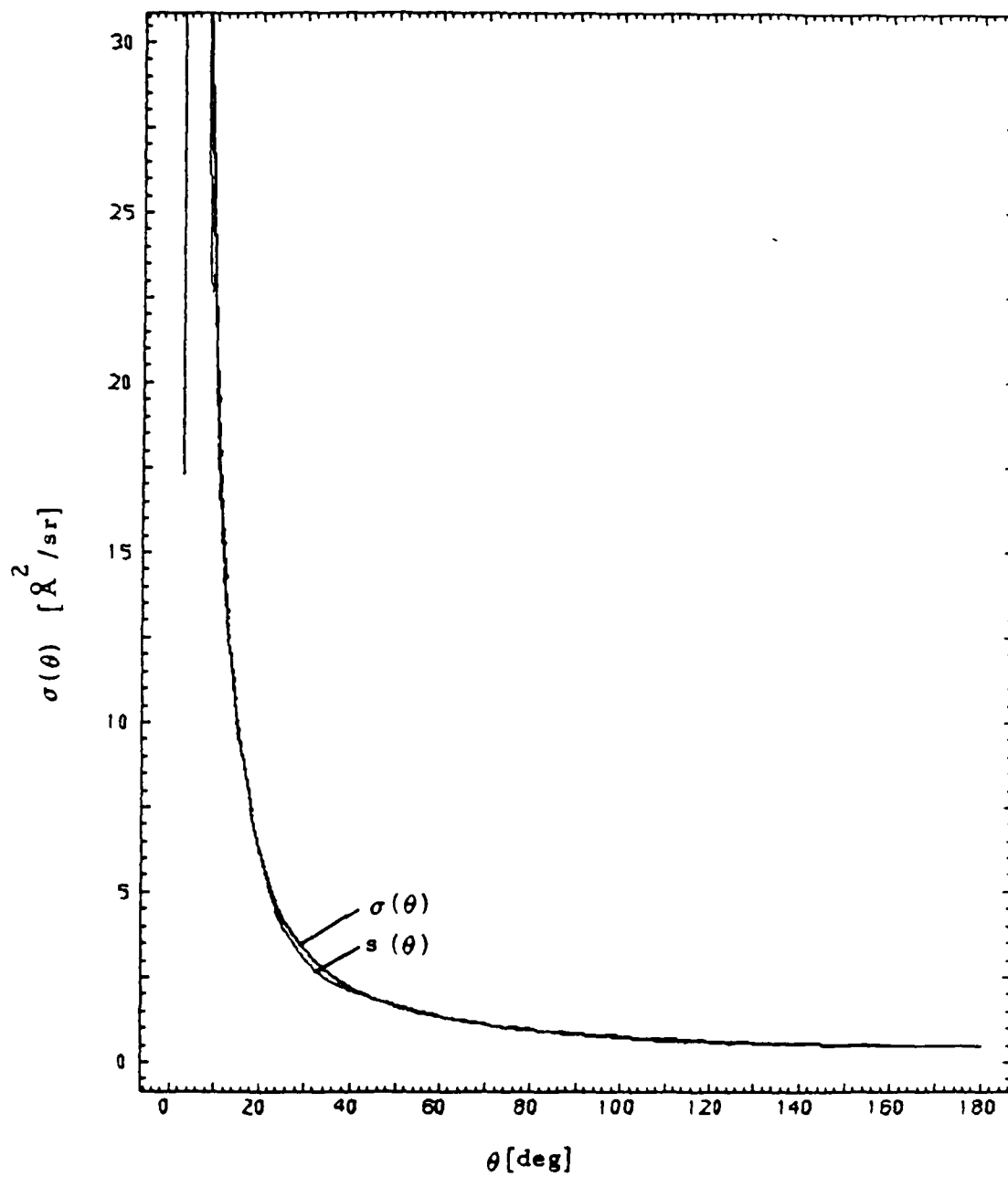
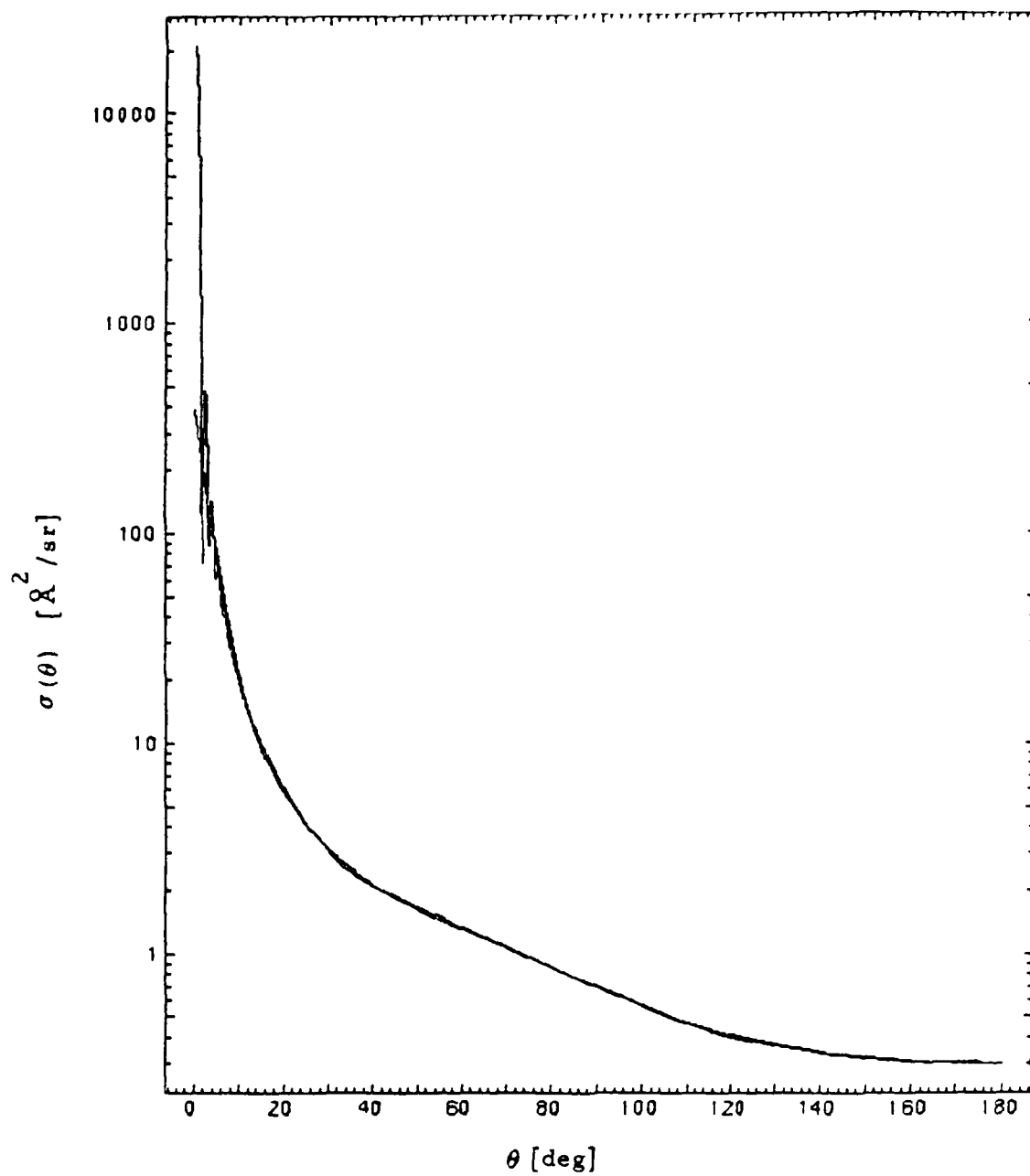Fig. 31. Linear plot comparing the exact differential cross section $\sigma(\theta)$ to the analytic fit $s(\theta)$ for $v = 7$ km/sec

61
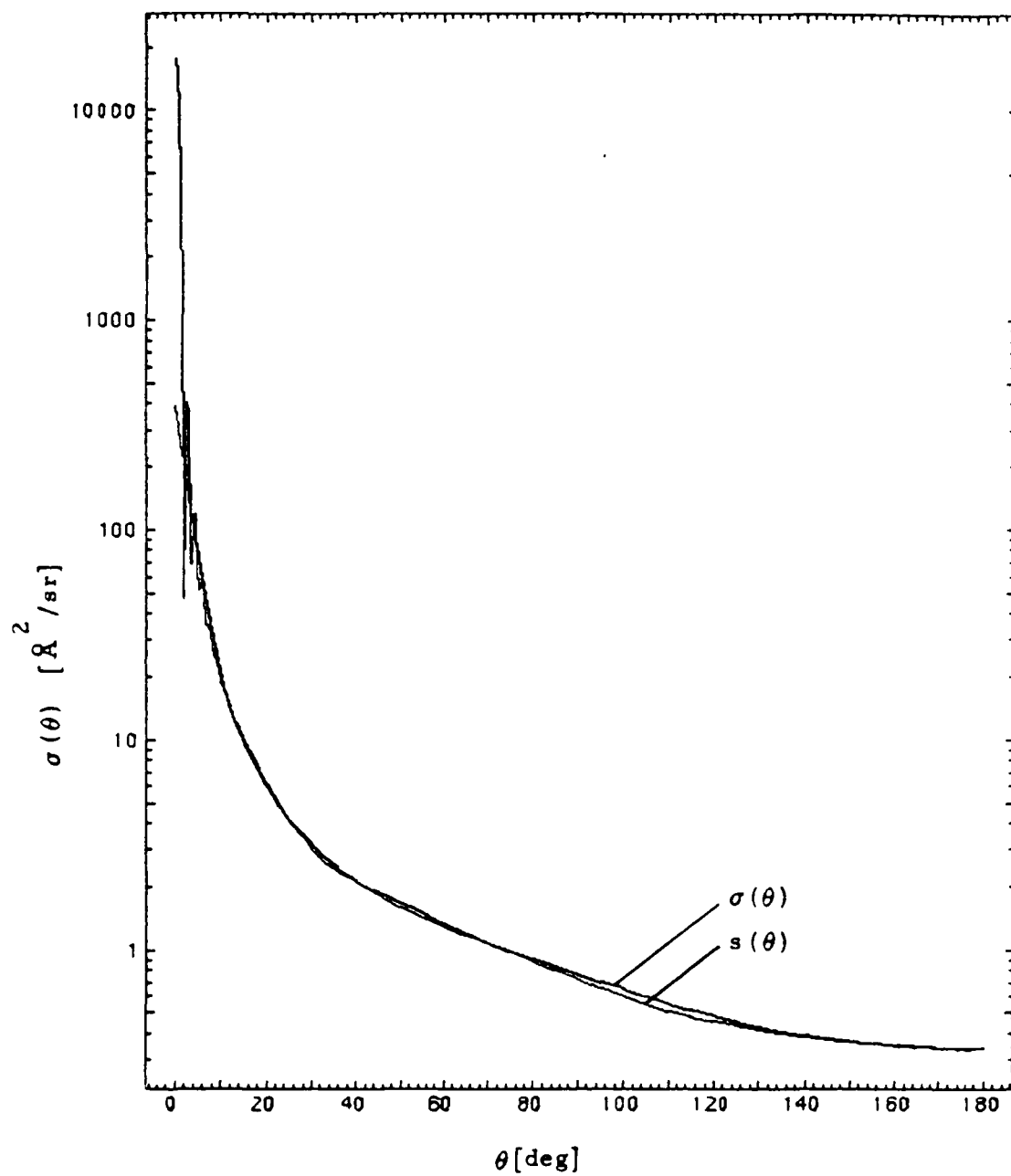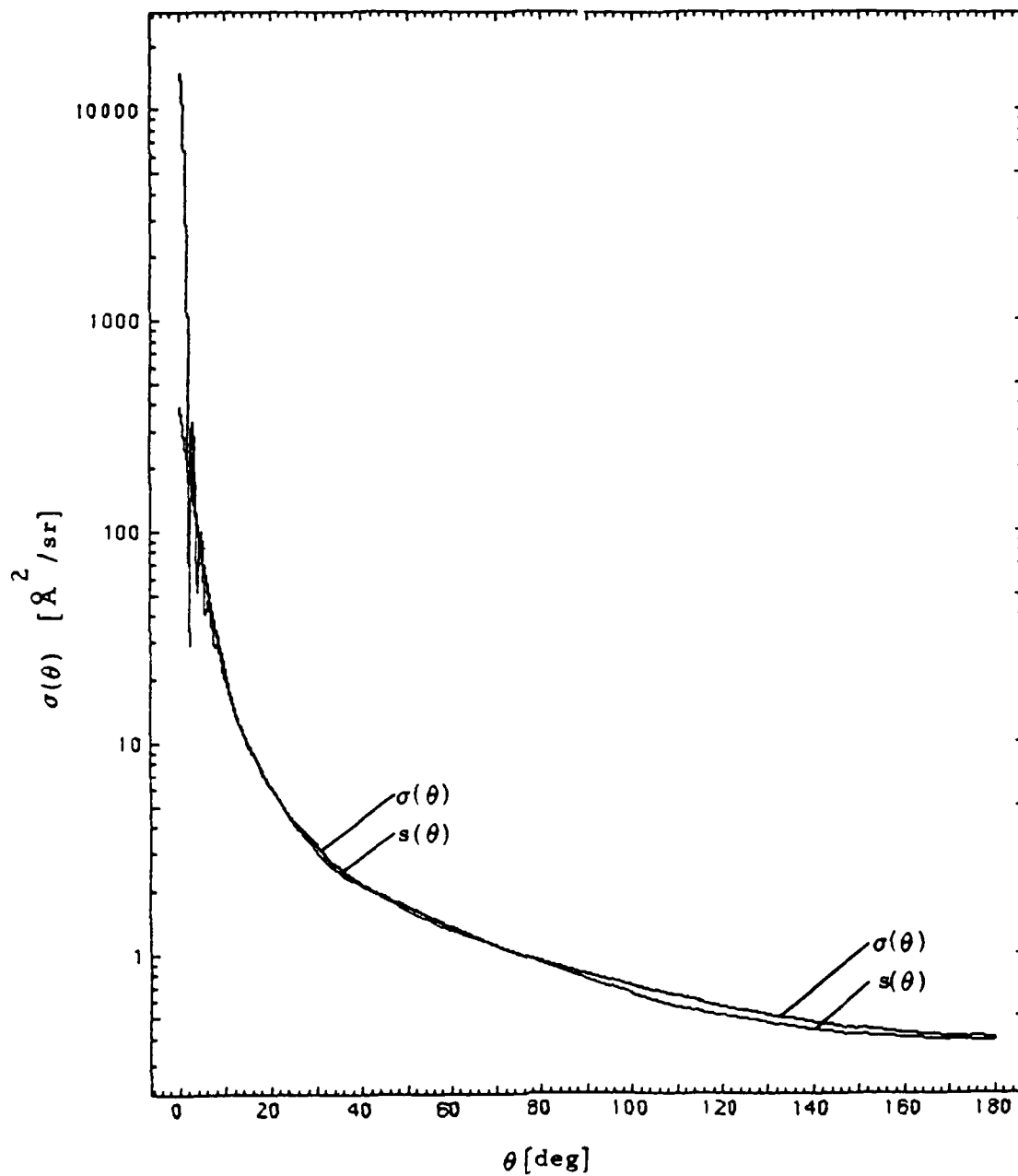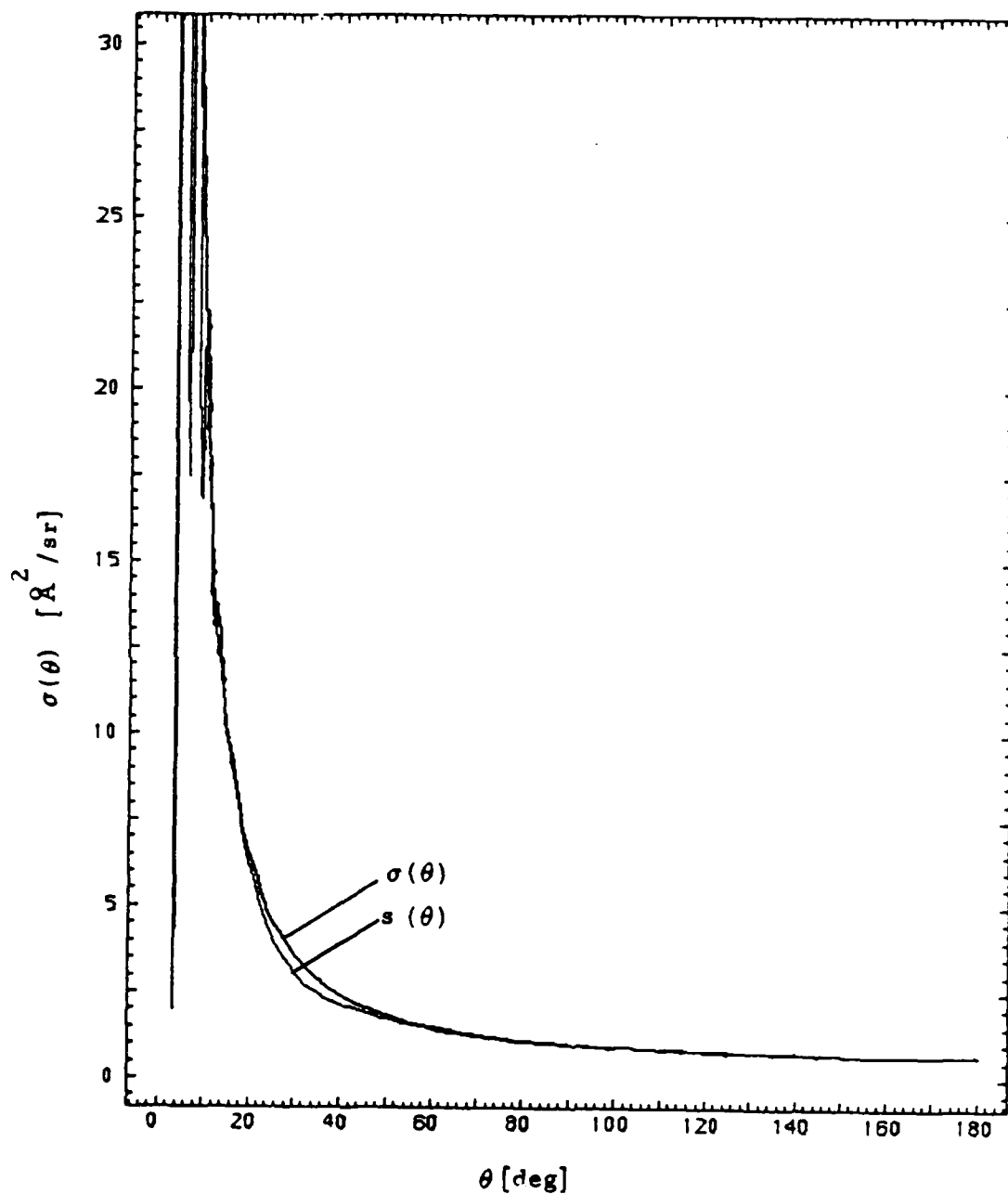
Fig. 32.   Linear plot comparing the exact differential cross section
$\sigma(\theta)$ to the analytic fit $s(\theta)$ for $v = 5$ km/sec
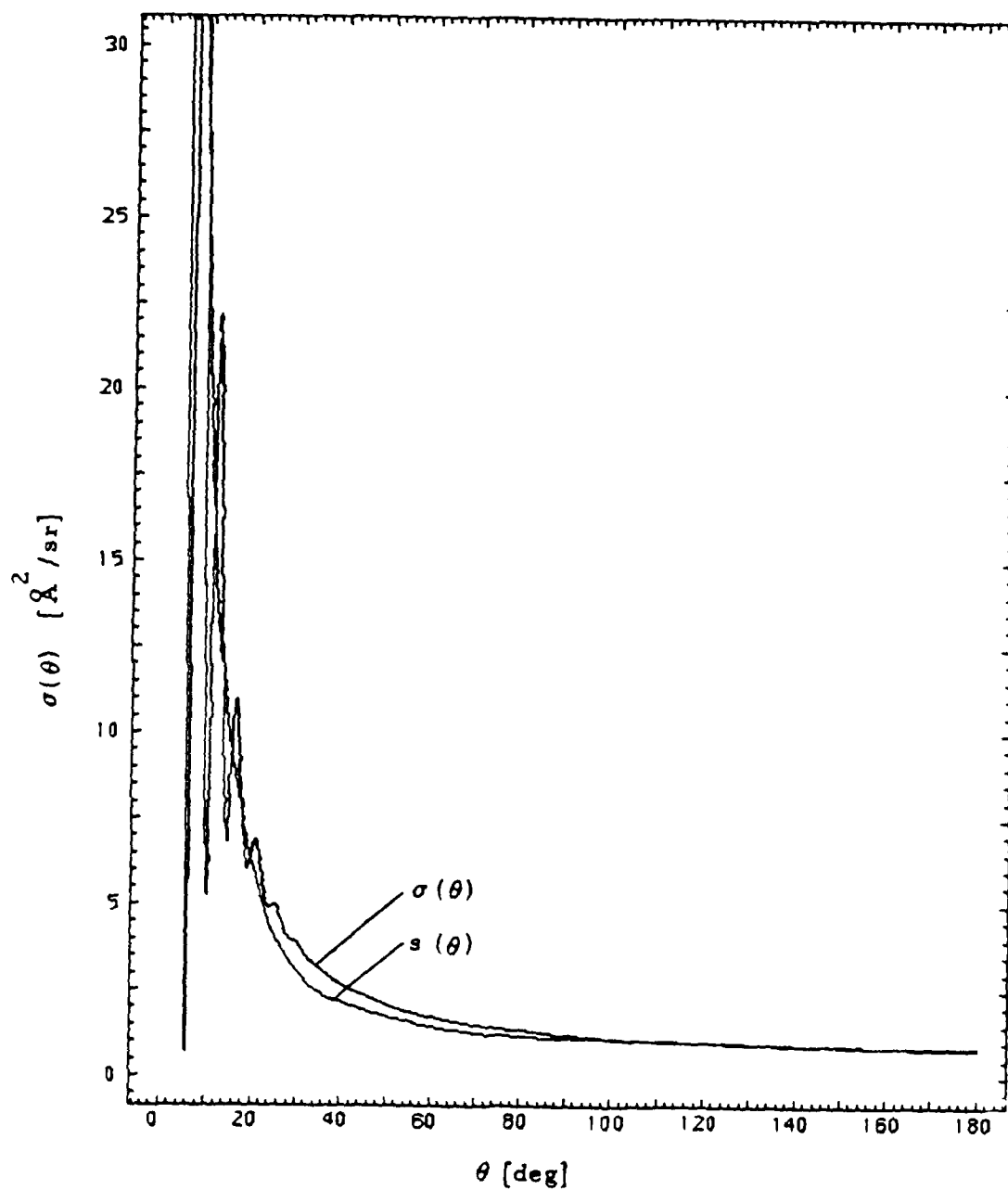
Fig. 33.   Linear plot comparing the exact differential cross section
σ(θ) to the analytic fit s(θ) for v = 3 km/sec
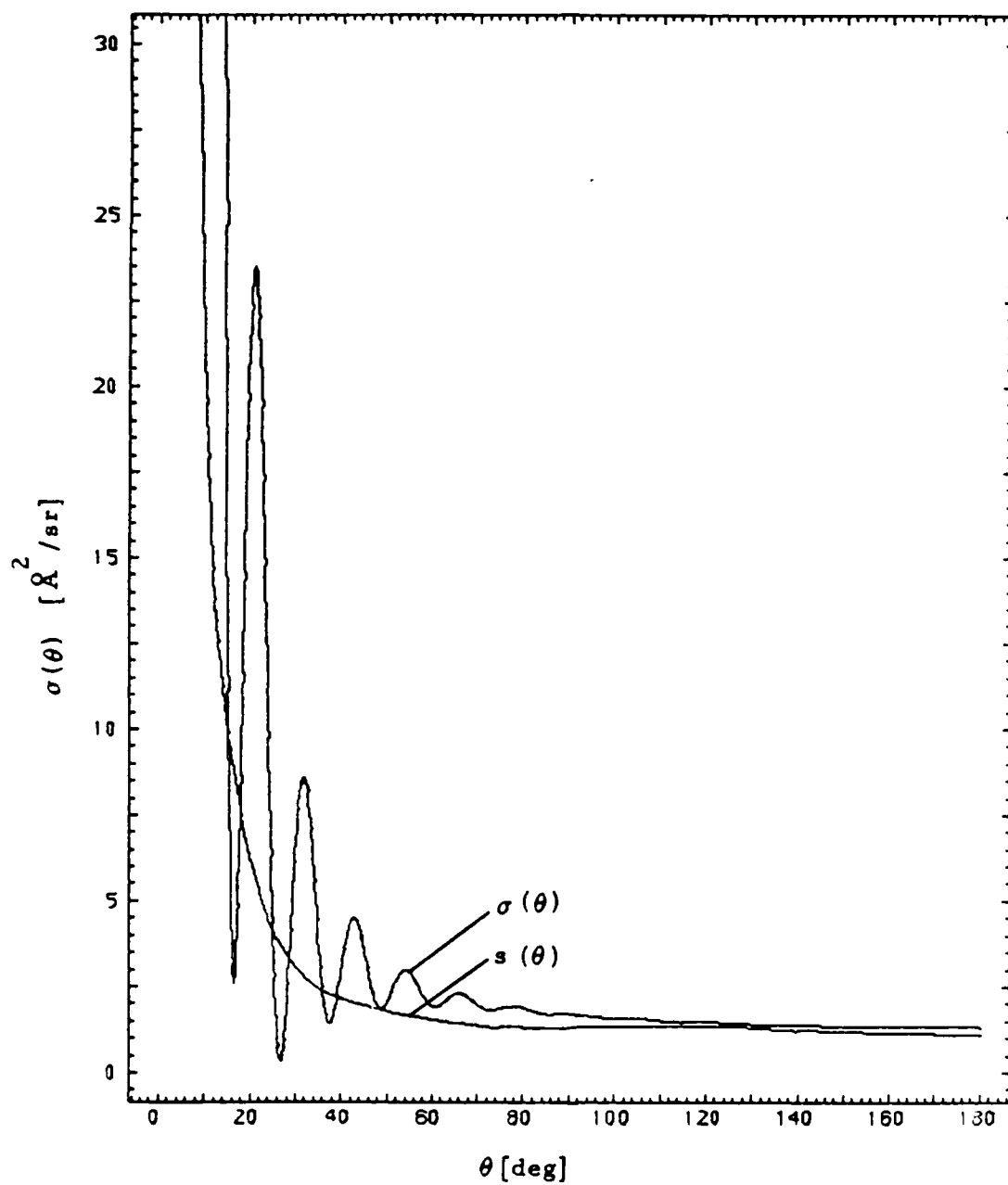
Fig. 34.  Linear plot comparing the exact differential cross section
σ(θ) to the analytic fit s(θ) for v = 1 km/sec

# References

1. Simpson, J. P., and Witteborn, F. C., "Effect of the Shuttle Contaminant Environment on a Sensitive Infrared Telescope," _Applied Optics_, Vol. 16, August 1977, pp. 2051-2073.

2. Guttman, A., Furber, R. D., and Muntz, E. P., "Protection of Satellite Infrared Experiment (SIRE) Cryogenic Infrared (IR) Optics in Shuttle Orbiter," _Optics in Adverse Environments_, Proceedings of the Society of Photo-Optical Instrumentation Engineers, Vol. 216, 1980, pp. 174-185.

3. Witteborn, F. C., and Young, L. S., "Spacelab Infrared Telescope Facility (SIRTF)," _Journal of Spacecraft_, Vol. 13, Nov. 1976, pp. 667-674.

4. Murakami, M., "Theoretical Contamination of Cryogenic Satellite Telescopes," NASA Technical Paper 1177, 1978.

5. Hetrick, M. A., Rantanen, R. O., Ress, E. B., and Froechtenight, J. F., "Experimental Investigation of Contamination Prevention Techniques to Cryogenic Surfaces on Board Orbiting Spacecraft," Martin Marietta Aerospace, MCR-78-578, Aug. 1978.

6. J. P. Simpson and F. C. Witteborn, "Monte Carlo Calculations of Helium Purge Gas Scattering," private communication to G. Borson, The Aerospace Corporation.

7. Dunning, Jr., T. H., and Hay, P. J., "Low-lying Electronic States of the Rare Gas Oxides," _Journal of Chemical Physics_, Vol. 66, Apr. 1977, pp. 3767-3777.

8. Foreman, P. B., Lees, A. B., and Rol, P. K., "Repulsive Potentials for the Interaction of Oxygen Atoms with the Noble Gases and Atmospheric Molecules," _Chemical Physics_, Vol. 12, Feb. 1976, pp. 213-224.

9. Aquilanti, V., Liuti, G., Pirani, F., Vecchiocattivi, F., and Volpi, G. G., "Absolute Total Elastic Cross Sections for Collisions of Oxygen Atoms with the Rare Gases at Thermal Energies," _Journal of Chemical Physics_, Vol. 65, Dec. 1976, pp. 4751-4755.

10. Gaydaenko, V. I., and Nikulin, V. K., "Born-Mayer Interatomic Potential for Atoms with Z=2 to Z=36," _Chemical Physics Letters_, Vol. 7, Nov. 1970, pp. 360-362.

11. Schiff, L. I., _Quantum Mechanics_, 3rd Ed., McGraw-Hill, New York, 1968, Sections 18-19.

12. Pauly, H., and Toennies, J. P., "The Study of Intermolecular Potentials with Molecular Beams at Thermal Energies," _Advances in Atomic and Molecular Physics_, Vol. 1, 1965, pp. 195-344.

13. Johnson, B. R., "The Log Derivative and Renomalized Numerov Algorithms," _Proceedings of the Workshop Algorithms and Computer Codes for Atomic and_

Molecular Scattering Theory, Vol. I, National Resource for Computation in Chemistry, 1979, pp. 86-104.

14. Schiff, L. I., Quantum Mechanics, 3rd Ed., McGraw-Hill, New York, 1968, Section 34.

15. Bernstein, R. B., "Quantum Effects in Elastic Molecular Scattering," Advances in Chemical Physics, Vol. 10, 1966, pp. 75-134.

16. Levine, R. D., and Bernstein, R. B., Molecular Reaction Dynamics, 1st Ed., Oxford University Press, 1974, pp. 22,53.

17. Schiff, L. I., Quantum Mechanics, 3rd Ed., McGraw-Hill, New York, 1968, pp. 124-126.

Phase Shifts $\eta_\ell$ Modulo $\pi$ for Orbital Angular

Momentum $\ell = 0 - \ell_{max}$ and Relative

Collision Energy $E \leqslant 0.41$ eV

| $\ell$ | E [eV] | | | | |
|---|---|---|---|---|---|
| | .02 | .07 | .15 | .27 | .41 |
| 0 | -6.57(-2)[a] | -9.48(-1) | -6.74(-1) | -3.04(-1) | 1.44( 0) |
| 1 | 1.43( 0) | 5.75(-1) | 8.62(-1) | 1.24( 0) | -1.51(-1) |
| 2 | -3.03(-1) | -1.09( 0) | -7.80(-1) | -3.89(-1) | 1.37( 0) |
| 3 | 1.03( 0) | 3.35(-1) | 6.84(-1) | 1.10( 0) | -2.73(-1) |
| 4 | -9.59(-1) | -1.43( 0) | -1.03( 0) | -5.89(-1) | 1.20( 0) |
| 5 | 3.13(-1) | -9.64(-2) | 3.63(-1) | 8.39(-1) | -4.95(-1) |
| 6 | 1.40( 0) | 1.19( 0) | -1.42( 0) | -9.03(-1) | 9.29(-1) |
| 7 | -7.34(-1) | -7.22(-1) | -1.00(-1) | 4.68(-1) | -8.14(-1) |
| 8 | 1.84(-1) | 4.68(-1) | 1.19( 0) | -1.33( 0) | 5.60(-1) |
| 9 | 1.01( 0) | -1.54( 0) | -7.08(-1) | -1.70(-2) | -1.23( 0) |
| 10 | -1.39( 0) | -4.60(-1) | 5.05(-1) | 1.27( 0) | 9.21(-2) |
| 11 | -7.46(-1) | 5.75(-1) | -1.46( 0) | -6.17(-1) | 1.39( 0) |
| 12 | -2.01(-1) | 1.56( 0) | -3.20(-1) | 6.10(-1) | -4.74(-1) |
| 13 | 2.39(-1) | -6.50(-1) | 7.83(-1) | -1.33( 0) | 7.77(-1) |
| 14 | 5.70(-1) | 2.30(-1) | -1.29( 0) | -1.64(-1) | -1.14( 0) |
| 15 | 7.86(-1) | 1.06( 0) | -2.63(-1) | 9.77(-1) | 6.23(-2) |
| 16 | 8.87(-1) | -1.31( 0) | 7.29(-1) | -1.05( 0) | 1.24( 0) |
| 17 | 8.81(-1) | -5.90(-1) | -1.46( 0) | 2.80(-2) | -7.51(-1) |
| 18 | 7.93(-1) | 7.44(-2) | -5.43(-1) | 1.09( 0) | 3.76(-1) |
| 19 | 6.66(-1) | 6.83(-1) | 3.36(-1) | -1.04( 0) | 1.48( 0) |
| 20 | 5.37(-1) | 1.24( 0) | 1.18( 0) | -4.44(-2) | -5.87(-1) |
| 21 | 4.26(-1) | -1.41( 0) | -1.17( 0) | 9.19(-1) | 4.65(-1) |
| 22 | 3.33(-1) | -9.76(-1) | -4.04(-1) | -1.29( 0) | 1.49( 0) |
| 23 | 2.69(-1) | -5.99(-1) | 3.19(-1) | -3.84(-1) | -6.47(-1) |
| 24 | 2.17(-1) | -2.80(-1) | 1.00( 0) | 4.90(-1) | 3.30(-1) |
| 25 | 1.76(-1) | -1.99(-2) | -1.50( 0) | 1.33( 0) | 1.28( 0) |
| 26 | 1.44(-1) | 1.84(-1) | -8.95(-1) | -9.95(-1) | -9.33(-1) |
| 27 | 1.19(-1) | 3.33(-1) | -3.33(-1) | -2.12(-1) | -3.17(-2) |
| 28 | 9.91(-2) | 4.33(-1) | 1.89(-1) | 5.40(-1) | 8.44(-1) |
| 29 | 8.31(-2) | 4.90(-1) | 6.69(-1) | 1.26( 0) | -1.45( 0) |
| 30 | 7.01(-2) | 5.11(-1) | 1.11( 0) | -1.19( 0) | -6.22(-1) |
| 31 | 5.95(-2) | 5.06(-1) | 1.51( 0) | -5.30(-1) | 1.78(-1) |
| 32 | 5.03(-2) | 4.82(-1) | -1.28( 0) | 9.82(-2) | 9.52(-1) |
| 33 | 4.36(-2) | 4.48(-1) | -9.60(-1) | 6.95(-1) | -1.44( 0) |
| 34 | 3.75(-2) | 4.09(-1) | -6.82(-1) | 1.26( 0) | -7.20(-1) |
| 35 | 3.25(-2) | 3.68(-1) | -4.42(-1) | -1.35( 0) | -2.32(-2) |
| 36 | 2.83(-2) | 3.29(-1) | -2.40(-1) | -8.44(-1) | 6.47(-1) |
| 37 | 2.47(-2) | 2.93(-1) | -7.25(-2) | -3.73(-1) | 1.29( 0) |
| 38 | 2.16(-2) | 2.60(-1) | 6.18(-2) | 6.73(-2) | -1.23( 0) |
| 39 | 1.90(-2) | 2.31(-1) | 1.66(-1) | 4.76(-1) | -6.39(-1) |
| 40 | 1.67(-2) | 2.05(-1) | 2.43(-1) | 8.54(-1) | -7.27(-2) |
| 41 | 1.48(-2) | 1.82(-1) | 2.98(-1) | 1.20( 0) | 4.67(-1) |
| 42 | 1.31(-2) | 1.62(-1) | 3.32(-1) | 1.52( 0) | 9.82(-1) |
| 43 | 1.17(-2) | 1.44(-1) | 3.51(-1) | -1.34( 0) | 1.47( 0) |
| 44 | 1.04(-2) | 1.29(-1) | 3.57(-1) | -1.09( 0) | -1.21( 0) |
| 45 | 9.32(-3) | 1.15(-1) | 3.54(-1) | -8.47(-1) | -7.74(-1) |
| 46 | 8.35(-3) | 1.03(-1) | 3.44(-1) | -6.44(-1) | -3.64(-1) |
| 47 | 7.50(-3) | 9.30(-2) | 3.30(-1) | -4.65(-1) | 2.13(-2) |
| 48 | 6.76(-3) | 8.37(-2) | 3.13(-1) | -3.13(-1) | 3.81(-1) |
| 49 | 6.09(-3) | 7.56(-2) | 2.94(-1) | -1.83(-1) | 7.16(-1) |
| 50 | 5.51(-3) | 6.83(-2) | 2.75(-1) | -7.3?(-2) | 1.03( 0) |
| 51 | 4.99(-3) | 6.19(-2) | 2.56(-1) | 1.53(-2) | 1.31( 0) |
| 52 | 4.53(-3) | 5.62(-2) | 2.33(-1) | 8.32(-2) | -1.57( 0) |
| 53 | 4.12(-3) | 5.11(-2) | 2.20(-1) | 1.45(-1) | -1.33( 0) |
| 54 | 3.75(-3) | 4.66(-2) | 2.03(-1) | 1.83(-1) | -1.11( 0) |
| 55 | 3.42(-3) | 4.25(-2) | 1.87(-1) | 2.21(-1) | -2.15(-1) |

APPENDIX A. (continued)

| $\ell$ | E [eV] | | | | |
|---|---|---|---|---|---|
| | .02 | .07 | .15 | .27 | .41 |
| 56 | 3.12(-3) | 3.89(-2) | 1.73(-1) | 2.44(-1) | -7.40(-1) |
| 57 | 2.86(-3) | 3.56(-2) | 1.59(-1) | 2.58(-1) | -5.84(-1) |
| 58 | 2.62(-3) | 3.26(-2) | 1.47(-1) | 2.66(-1) | -4.47(-1) |
| 59 | 2.40(-3) | 3.00(-2) | 1.36(-1) | 2.69(-1) | -3.27(-1) |
| 60 | 2.21(-3) | 2.76(-2) | 1.25(-1) | 2.68(-1) | -2.23(-1) |
| 61 | 2.03(-3) | 2.54(-2) | 1.16(-1) | 2.63(-1) | -1.33(-1) |
| 62 | 1.67(-3) | 2.34(-2) | 1.07(-1) | 2.56(-1) | -5.75(-2) |
| 63 | 1.72(-3) | 2.16(-2) | 9.90(-2) | 2.48(-1) | 6.00(-3) |
| 64 | 1.59(-3) | 2.00(-2) | 9.16(-2) | 2.38(-1) | 5.85(-2) |
| 65 | 1.47(-3) | 1.85(-2) | 8.49(-2) | 2.28(-1) | 1.01(-1) |
| 66 | 1.36(-3) | 1.71(-2) | 7.88(-2) | 2.17(-1) | 1.36(-1) |
| 67 | 1.26(-3) | 1.59(-2) | 7.32(-2) | 2.07(-1) | 1.63(-1) |
| 68 | 1.16(-3) | 1.48(-2) | 6.80(-2) | 1.96(-1) | 1.83(-1) |
| 69 | 1.08(-3) | 1.37(-2) | 6.33(-2) | 1.85(-1) | 1.98(-1) |
| 70 | 1.00(-3) | 1.28(-2) | 5.89(-2) | 1.75(-1) | 2.09(-1) |
| 71 | 9.29(-4) | 1.19(-2) | 5.49(-2) | 1.65(-1) | 2.15(-1) |
| 72 | 8.63(-4) | 1.11(-2) | 5.12(-2) | 1.56(-1) | 2.18(-1) |
| 73 | 8.05(-4) | 1.04(-2) | 4.73(-2) | 1.47(-1) | 2.19(-1) |
| 74 | 7.48(-4) | 9.70(-3) | 4.47(-2) | 1.39(-1) | 2.18(-1) |
| 75 | 6.95(-4) | 9.07(-3) | 4.18(-2) | 1.30(-1) | 2.15(-1) |
| 76 | 6.48(-4) | 8.49(-3) | 3.91(-2) | 1.23(-1) | 2.11(-1) |
| 77 | 6.06(-4) | 7.95(-3) | 3.67(-2) | 1.16(-1) | 2.05(-1) |
| 78 | 5.64(-4) | 7.46(-3) | 3.44(-2) | 1.09(-1) | 2.00(-1) |
| 79 | 5.24(-4) | 7.00(-3) | 3.23(-2) | 1.03(-1) | 1.93(-1) |
| 80 | 4.90(-4) | 6.57(-3) | 3.03(-2) | 9.67(-2) | 1.86(-1) |
| 81 | 4.60(-4) | 6.18(-3) | 2.85(-2) | 9.12(-2) | 1.79(-1) |
| 82 | 4.28(-4) | 5.81(-3) | 2.68(-2) | 8.60(-2) | 1.72(-1) |
| 83 | 3.98(-4) | 5.47(-3) | 2.52(-2) | 8.11(-2) | 1.65(-1) |
| 84 | 3.72(-4) | 5.15(-3) | 2.38(-2) | 7.65(-2) | 1.58(-1) |
| 85 | 3.50(-4) | 4.86(-3) | 2.24(-2) | 7.22(-2) | 1.51(-1) |
| 86 | 3.27(-4) | 4.58(-3) | 2.12(-2) | 6.82(-2) | 1.44(-1) |
| 87 | 3.03(-4) | 4.32(-3) | 2.00(-2) | 6.45(-2) | 1.38(-1) |
| 88 | 2.81(-4) | 4.08(-3) | 1.89(-2) | 6.10(-2) | 1.32(-1) |
| 89 | 2.64(-4) | 3.86(-3) | 1.78(-2) | 5.77(-2) | 1.25(-1) |
| 90 | 2.49(-4) | 3.65(-3) | 1.69(-2) | 5.46(-2) | 1.20(-1) |
| 91 | 2.32(-4) | 3.45(-3) | 1.60(-2) | 5.17(-2) | 1.14(-1) |
| 92 | 2.14(-4) | 3.27(-3) | 1.51(-2) | 4.90(-2) | 1.09(-1) |
| 93 | 1.97(-4) | 3.10(-3) | 1.43(-2) | 4.64(-2) | 1.03(-1) |
| 94 | 1.84(-4) | 2.94(-3) | 1.36(-2) | 4.40(-2) | 9.85(-2) |
| 95 | 1.74(-4) | 2.78(-3) | 1.29(-2) | 4.18(-2) | 9.38(-2) |
| 96 | 1.63(-4) | 2.64(-3) | 1.22(-2) | 3.97(-2) | 8.94(-2) |
| 97 | 1.50(-4) | 2.51(-3) | 1.16(-2) | 3.77(-2) | 8.52(-2) |
| 98 | 1.36(-4) | 2.38(-3) | 1.10(-2) | 3.58(-2) | 8.11(-2) |
| 99 | 1.22(-4) | 2.26(-3) | 1.05(-2) | 3.41(-2) | 7.73(-2) |
| 100 | 1.12(-4) | 2.15(-3) | 9.98(-3) | 3.24(-2) | 7.37(-2) |
| 101 | | 2.05(-3) | 9.49(-3) | 3.08(-2) | 7.03(-2) |
| 102 | b | 1.95(-3) | 9.04(-3) | 2.94(-2) | 6.71(-2) |
| 103 | | 1.85(-3) | 8.61(-3) | 2.80(-2) | 6.40(-2) |
| 104 | | 1.77(-3) | 8.21(-3) | 2.67(-2) | 6.11(-2) |
| 105 | | 1.68(-3) | 7.82(-3) | 2.54(-2) | 5.83(-2) |
| 106 | | 1.60(-3) | 7.46(-3) | 2.42(-2) | 5.57(-2) |
| 107 | | 1.53(-3) | 7.12(-3) | 2.31(-2) | 5.32(-2) |
| 108 | | 1.46(-3) | 6.80(-3) | 2.21(-2) | 5.08(-2) |
| 109 | | 1.39(-3) | 6.49(-3) | 2.11(-2) | 4.86(-2) |
| 110 | | 1.33(-3) | 6.20(-3) | 2.02(-2) | 4.64(-2) |
| 111 | | 1.27(-3) | 5.93(-3) | 1.93(-2) | 4.44(-2) |
| 112 | | 1.21(-3) | 5.67(-3) | 1.84(-2) | 4.25(-2) |
| 113 | | 1.16(-3) | 5.42(-3) | 1.76(-2) | 4.07(-2) |
| 114 | | 1.11(-3) | 5.19(-3) | 1.69(-2) | 3.89(-2) |
| 115 | | 1.06(-3) | 4.97(-3) | 1.62(-2) | 3.73(-2) |

| $\ell$ | E [eV] | | | | |
|---|---|---|---|---|---|
| | .02 | .07 | .15 | .27 | .41 |
| 116 | | 1.02(-3) | 4.76(-3) | 1.55(-2) | 3.57(-2) |
| 117 | | 9.72(-4) | 4.56(-3) | 1.49(-2) | 3.43(-2) |
| 118 | | 9.31(-4) | 4.37(-3) | 1.42(-2) | 3.29(-2) |
| 119 | | 8.92(-4) | 4.19(-3) | 1.36(-2) | 3.15(-2) |
| 120 | | 8.54(-4) | 4.02(-3) | 1.31(-2) | 3.02(-2) |
| 121 | | 8.18(-4) | 3.85(-3) | 1.26(-2) | 2.90(-2) |
| 122 | | 7.85(-4) | 3.70(-3) | 1.20(-2) | 2.79(-2) |
| 123 | | 7.52(-4) | 3.55(-3) | 1.16(-2) | 2.67(-2) |
| 124 | | 7.21(-4) | 3.41(-3) | 1.11(-2) | 2.57(-2) |
| 125 | | 6.92(-4) | 3.28(-3) | 1.07(-2) | 2.47(-2) |
| 126 | | 6.65(-4) | 3.15(-3) | 1.03(-2) | 2.37(-2) |
| 127 | | 6.39(-4) | 3.03(-3) | 9.87(-3) | 2.28(-2) |
| 128 | | 6.12(-4) | 2.91(-3) | 9.49(-3) | 2.20(-2) |
| 129 | | 5.89(-4) | 2.80(-3) | 9.13(-3) | 2.11(-2) |
| 130 | | 5.65(-4) | 2.69(-3) | 8.78(-3) | 2.03(-2) |
| 131 | | 5.43(-4) | 2.57(-3) | 8.45(-3) | 1.96(-2) |
| 132 | | 5.22(-4) | 2.49(-3) | 8.14(-3) | 1.89(-2) |
| 133 | | 5.02(-4) | 2.40(-3) | 7.84(-3) | 1.82(-2) |
| 134 | | 4.82(-4) | 2.31(-3) | 7.55(-3) | 1.75(-2) |
| 135 | | 4.63(-4) | 2.23(-3) | 7.28(-3) | 1.69(-2) |
| 136 | | 4.46(-4) | 2.15(-3) | 7.02(-3) | 1.63(-2) |
| 137 | | 4.29(-4) | 2.07(-3) | 6.77(-3) | 1.57(-2) |
| 138 | | 4.12(-4) | 2.00(-3) | 6.53(-3) | 1.51(-2) |
| 139 | | 3.97(-4) | 1.93(-3) | 6.29(-3) | 1.46(-2) |
| 140 | | 3.83(-4) | 1.86(-3) | 6.08(-3) | 1.41(-2) |
| 141 | | 3.68(-4) | 1.79(-3) | 5.85(-3) | 1.36(-2) |
| 142 | | 3.54(-4) | 1.73(-3) | 5.66(-3) | 1.31(-2) |
| 143 | | 3.41(-4) | 1.67(-3) | 5.47(-3) | 1.27(-2) |
| 144 | | 3.29(-4) | 1.61(-3) | 5.28(-3) | 1.22(-2) |
| 145 | | 3.17(-4) | 1.56(-3) | 5.10(-3) | 1.18(-2) |
| 146 | | 3.05(-4) | 1.50(-3) | 4.93(-3) | 1.14(-2) |
| 147 | | 2.94(-4) | 1.45(-3) | 4.76(-3) | 1.11(-2) |
| 148 | | 2.84(-4) | 1.40(-3) | 4.61(-3) | 1.07(-2) |
| 149 | | 2.73(-4) | 1.36(-3) | 4.45(-3) | 1.03(-2) |
| 150 | | 2.63(-4) | 1.31(-3) | 4.31(-3) | 1.00(-2) |
| 151 | | 2.53(-4) | 1.27(-3) | 4.17(-3) | 9.69(-3) |
| 152 | | 2.45(-4) | 1.23(-3) | 4.03(-3) | 9.37(-3) |
| 153 | | 2.36(-4) | 1.19(-3) | 3.91(-3) | 9.07(-3) |
| 154 | | 2.27(-4) | 1.15(-3) | 3.78(-3) | 8.78(-3) |
| 155 | | 2.19(-4) | 1.11(-3) | 3.66(-3) | 8.50(-3) |
| 156 | | 2.12(-4) | 1.08(-3) | 3.55(-3) | 8.24(-3) |
| 157 | | 2.04(-4) | 1.04(-3) | 3.43(-3) | 7.99(-3) |
| 158 | | 1.96(-4) | 1.01(-3) | 3.33(-3) | 7.74(-3) |
| 159 | | 1.89(-4) | 9.78(-4) | 3.22(-3) | 7.50(-3) |
| 160 | | 1.83(-4) | 9.48(-4) | 3.12(-3) | 7.27(-3) |
| 161 | | 1.76(-4) | 9.18(-4) | 3.03(-3) | 7.05(-3) |
| 162 | | 1.70(-4) | 8.90(-4) | 2.94(-3) | 6.84(-3) |
| 163 | | 1.63(-4) | 8.62(-4) | 2.85(-3) | 6.63(-3) |
| 164 | | 1.57(-4) | 8.36(-4) | 2.76(-3) | 6.44(-3) |
| 165 | | 1.52(-4) | 8.11(-4) | 2.68(-3) | 6.24(-3) |
| 166 | | 1.47(-4) | 7.86(-4) | 2.60(-3) | 6.06(-3) |
| 167 | | 1.41(-4) | 7.62(-4) | 2.53(-3) | 5.89(-3) |
| 168 | | 1.35(-4) | 7.40(-4) | 2.45(-3) | 5.71(-3) |
| 169 | | 1.31(-4) | 7.18(-4) | 2.39(-3) | 5.55(-3) |
| 170 | | 1.27(-4) | 6.96(-4) | 2.31(-3) | 5.39(-3) |
| 171 | | 1.22(-4) | 6.76(-4) | 2.24(-3) | 5.23(-3) |
| 172 | | 1.17(-4) | 6.55(-4) | 2.18(-3) | 5.09(-3) |
| 173 | | 1.12(-4) | 6.37(-4) | 2.12(-3) | 4.94(-3) |
| 174 | | 1.08(-4) | 6.18(-4) | 2.06(-3) | 4.81(-3) |
| 175 | | 1.04(-4) | 6.00(-4) | 2.00(-3) | 4.67(-3) |

| $\ell$ | E [eV] | | | | |
|---|---|---|---|---|---|
| | .02 | .07 | .15 | .27 | .41 |
| 175 | | 1.01(-4) | 5.83(-4) | 1.94(-3) | 4.54(-3) |
| 177 | | 9.71(-5) | 5.66(-4) | 1.87(-3) | 4.42(-3) |
| 178 | | 9.24(-5) | 5.50(-4) | 1.84(-3) | 4.29(-3) |
| 179 | | 8.82(-5) | 5.35(-4) | 1.79(-3) | 4.18(-3) |
| 180 | | 8.49(-5) | 5.19(-4) | 1.74(-3) | 4.06(-3) |
| 181 | | 8.24(-5) | 5.05(-4) | 1.69(-3) | 3.95(-3) |
| 182 | | 7.99(-5) | 4.91(-4) | 1.64(-3) | 3.85(-3) |
| 183 | | 7.63(-5) | 4.77(-4) | 1.60(-3) | 3.74(-3) |
| 184 | | 7.22(-5) | 4.64(-4) | 1.55(-3) | 3.65(-3) |
| 185 | | 6.82(-5) | 4.51(-4) | 1.51(-3) | 3.55(-3) |
| 186 | | 6.50(-5) | 4.39(-4) | 1.48(-3) | 3.45(-3) |
| 187 | | 6.28(-5) | 4.27(-4) | 1.44(-3) | 3.37(-3) |
| 188 | | 6.10(-5) | 4.15(-4) | 1.40(-3) | 3.28(-3) |
| 189 | | 5.89(-5) | 4.04(-4) | 1.36(-3) | 3.19(-3) |
| 190 | | 5.59(-5) | 3.93(-4) | 1.33(-3) | 3.11(-3) |
| 191 | | 5.21(-5) | 3.82(-4) | 1.29(-3) | 3.03(-3) |
| 192 | | 4.82(-5) | 3.72(-4) | 1.26(-3) | 2.96(-3) |
| 193 | | 4.49(-5) | 3.62(-4) | 1.23(-3) | 2.85(-3) |
| 194 | | 4.24(-5) | 3.52(-4) | 1.19(-3) | 2.81(-3) |
| 195 | | 4.03(-5) | 3.43(-4) | 1.16(-3) | 2.74(-3) |
| 196 | | 3.97(-5) | 3.34(-4) | 1.13(-3) | 2.67(-3) |
| 197 | | 3.84(-5) | 3.25(-4) | 1.11(-3) | 2.60(-3) |
| 198 | | 3.64(-5) | 3.16(-4) | 1.08(-3) | 2.54(-3) |
| 199 | | 3.34(-5) | 3.03(-4) | 1.05(-3) | 2.48(-3) |
| 200 | | 2.95(-5) | 3.00(-4) | 1.02(-3) | 2.42(-3) |

[a]The number in parentheses denotes the power of ten by which the entry should be multiplied.

[b]For E = .02 eV $\ell_{max}$ = 100.

## APPENDIX B

### Phase Shifts $\eta_\ell$ Modulo $\pi$ for Orbital Angular

### Momentum $\ell = 0 - \ell_{max}$ and Relative

### Collision Energy $E \geq 0.60$ eV

| $\ell$ | E [eV] | | | | |
|---|---|---|---|---|---|
| | 0.60 | 0.81 | 1.06 | 1.34 | 1.66 |
| | a | | | | |
| 0 | -1.81(-1) | -6.48(-1) | -5.91(-1) | 2.89(-1) | -1.54( 0) |
| 1 | 1.37( 0) | 9.02(-1) | 9.60(-1) | -1.30( 0) | 8.41(-3) |
| 2 | -2.46(-1) | -7.07(-1) | -6.50(-1) | 2.32(-1) | 1.54( 0) |
| 3 | 1.26( 0) | 8.03(-1) | 8.62(-1) | -1.40( 0) | -8.22(-2) |
| 4 | -3.93(-1) | -8.52(-1) | -7.86(-1) | 9.94(-2) | 1.42( 0) |
| 5 | 1.05( 0) | 6.19(-1) | 6.87(-1) | -1.57( 0) | -2.45(-1) |
| 6 | -6.40(-1) | -1.03( 0) | -1.00( 0) | -1.09(-1) | 1.22( 0) |
| 7 | 7.78(-1) | 3.54(-1) | 4.34(-1) | 1.33( 0) | -4.81(-1) |
| 8 | -9.67(-1) | -1.39( 0) | -1.29( 0) | -3.93(-1) | 9.45(-1) |
| 9 | 4.07(-1) | 8.93( 3) | 1.03(-1) | 1.01( 0) | -7.89(-1) |
| 10 | -1.39( 0) | 1.33( 0) | 1.49( 0) | -7.52(-1) | 6.02(-1) |
| 11 | -5.06(-2) | -4.16(-1) | -3.05(-1) | 6.11(-1) | -1.17( 0) |
| 12 | 1.25( 0) | 9.12(-1) | 1.03( 0) | -1.19( 0) | 1.86(-1) |
| 13 | -5.96(-1) | -9.22(-1) | -7.82(-1) | 1.40(-1) | 1.52( 0) |
| 14 | 6.70(-1) | 3.06(-1) | 5.11(-1) | 1.45( 0) | -3.02(-1) |
| 15 | -1.23( 0) | -1.51( 0) | -1.35( 0) | -4.06(-1) | 9.93(-1) |
| 16 | -4.33(-3) | -2.53(-1) | -3.61(-2) | 8.65(-1) | -8.61(-1) |
| 17 | 1.20( 0) | 9.70(-1) | 1.16( 0) | -1.02( 0) | 4.03(-1) |
| 18 | -7.67(-1) | -9.63(-1) | -7.59(-1) | 2.10(-1) | -1.49( 0) |
| 19 | 3.91(-1) | 2.26(-1) | 4.49(-1) | 1.43( 0) | -2.63(-1) |
| 20 | 1.53( 0) | 1.40( 0) | -1.51( 0) | -5.18(-1) | 9.49(-1) |
| 21 | -5.01(-2) | -5.96(-1) | -3.35(-1) | 6.63(-1) | -1.00( 0) |
| 22 | 5.92(-1) | 5.34(-1) | 8.17(-1) | -1.32( 0) | 1.77(-1) |
| 23 | -1.49( 0) | -1.50( 0) | -1.19( 0) | -1.71(-1) | 1.34( 0) |
| 24 | -4.29(-1) | -4.05(-1) | -7.57(-2) | 9.57(-1) | -6.65(-1) |
| 25 | 6.00(-1) | 6.68(-1) | 1.02( 0) | -1.07( 0) | 4.59(-1) |
| 26 | -1.54( 0) | -1.42( 0) | -1.04( 0) | 1.83(-2) | 1.57( 0) |
| 27 | -5.51(-1) | -3.87(-1) | 2.26(-2) | 1.09( 0) | -4.85(-1) |
| 28 | 4.13(-1) | 6.27(-1) | 1.07( 0) | -9.88(-1) | 5.68(-1) |
| 29 | 1.35( 0) | -1.52( 0) | -1.05( 0) | 5.45(-2) | -1.50( 0) |
| 30 | -8.67(-1) | -5.43(-1) | -3.75(-2) | 1.08( 0) | -4.58(-1) |
| 31 | 3.18(-2) | 4.14(-1) | 9.55(-1) | -1.05( 0) | 5.65(-1) |
| 32 | 9.09(-1) | 1.35( 0) | -1.21( 0) | -5.85(-2) | -1.57( 0) |
| 33 | -1.39( 0) | -8.70(-1) | -2.53(-1) | 9.19(-1) | -5.79(-1) |
| 34 | -5.44(-1) | 3.00(-2) | 6.83(-1) | -1.25( 0) | 3.95(-1) |
| 35 | 2.69(-1) | 9.11(-1) | -1.53( 0) | -3.17(-1) | 1.35( 0) |
| 36 | 1.05( 0) | -1.37( 0) | -6.23(-1) | 6.13(-1) | -8.44(-1) |
| 37 | -1.31( 0) | -5.25(-1) | 2.67(-1) | 1.53( 0) | 8.39(-2) |
| 38 | -5.67(-1) | 2.99(-1) | 1.14( 0) | -7.16(-1) | 9.97(-1) |
| 39 | 1.58(-1) | 1.10( 0) | -1.14( 0) | 1.63(-1) | -1.25( 0) |
| 40 | 8.61(-1) | -1.25( 0) | -3.04(-1) | 1.04( 0) | -3.65(-1) |
| 41 | 1.54( 0) | -4.82(-1) | 5.20(-1) | -1.25( 0) | 5.04(-1) |
| 42 | -9.40(-1) | 2.66(-1) | 1.33( 0) | -4.14(-1) | 1.36( 0) |
| 43 | -3.02(-1) | 9.96(-1) | -1.02( 0) | 4.10(-1) | -9.45(-1) |
| 44 | 3.13(-1) | -1.43( 0) | -2.50(-1) | 1.22( 0) | -1.19(-1) |
| 45 | 9.07(-1) | -7.42(-1) | 5.09(-1) | -1.13( 0) | 6.93(-1) |
| 46 | 1.49( 0) | -6.91(-2) | 1.25( 0) | -3.49(-1) | 1.49( 0) |
| 47 | -1.11( 0) | 5.85(-1) | -1.17( 0) | 4.16(-1) | -9.66(-1) |
| 48 | -5.85(-1) | 1.22( 0) | -4.59(-1) | 1.17( 0) | -9.45(-2) |
| 49 | -7.92(-2) | -1.30( 0) | 2.33(-1) | -1.24( 0) | 6.64(-1) |
| 50 | 4.05(-1) | -7.07(-1) | 9.03(-1) | -5.17(-1) | 1.41( 0) |
| 51 | 8.67(-1) | -1.29(-1) | 1.57( 0) | 1.91(-1) | -1.00( 0) |
| 52 | 1.31( 0) | 4.31(-1) | -9.31(-1) | 8.85(-1) | -2.80(-1) |
| 53 | -1.41( 0) | 9.72(-1) | -3.04(-1) | 1.55( 0) | 4.27(-1) |
| 54 | -1.02( 0) | 1.43( 0) | 3.06(-1) | -9.12(-1) | 1.12( 0) |
| 55 | -6.42(-1) | -1.15( 0) | 9.03(-1) | -2.61(-1) | -1.34( 0) |

| $\ell$ | | | E [eV] | | |
|---|---|---|---|---|---|
| | 0.60 | 0.81 | 1.06 | 1.34 | 1.66 |
| 56 | -2.85(-1) | -6.61(-1) | 1.48( 0) | 3.76(-1) | -6.68(-1) |
| 57 | 4.87(-2) | -1.96(-1) | -1.10( 0) | 10.00(-1) | -1.04(-2) |
| 58 | 3.63(-1) | 2.50(-1) | -5.59(-1) | -1.53( 0) | 6.35(-1) |
| 59 | 6.55(-1) | 6.78(-1) | -2.91(-2) | -9.33(-1) | 1.27( 0) |
| 60 | 9.30(-1) | 1.09( 0) | 4.83(-1) | -3.57(-1) | -1.25( 0) |
| 61 | 1.18( 0) | 1.48( 0) | 9.79(-1) | 2.09(-1) | -6.43(-1) |
| 62 | 1.42( 0) | -1.29( 0) | 1.46( 0) | 7.62(-1) | -4.58(-2) |
| 63 | -1.50( 0) | -9.37(-1) | -1.22( 0) | 1.30( 0) | 5.39(-1) |
| 64 | -1.30( 0) | -6.01(-1) | -7.72(-1) | -1.32( 0) | 1.11( 0) |
| 65 | -1.12( 0) | -2.83(-1) | -3.41(-1) | -8.06(-1) | -1.47( 0) |
| 66 | -9.55(-1) | 1.83(-2) | 7.40(-2) | -3.10(-1) | -9.19(-1) |
| 67 | -8.04(-1) | 3.02(-1) | 4.73(-1) | 1.72(-1) | -3.82(-1) |
| 68 | -6.69(-1) | 5.69(-1) | 8.56(-1) | 6.41(-1) | 1.43(-1) |
| 69 | -5.46(-1) | 8.19(-1) | 1.22( 0) | 1.09( 0) | 6.57(-1) |
| 70 | -4.38(-1) | 1.05( 0) | -1.57( 0) | 1.53( 0) | 1.16( 0) |
| 71 | -3.41(-1) | 1.27( 0) | -1.23( 0) | -1.18( 0) | -1.49( 0) |
| 72 | -2.55(-1) | 1.47( 0) | -9.12(-1) | -7.69(-1) | -1.02( 0) |
| 73 | -1.82(-1) | -1.48( 0) | -6.07(-1) | -3.71(-1) | -5.53(-1) |
| 74 | -1.17(-1) | -1.30( 0) | -3.18(-1) | 1.33(-2) | -9.96(-2) |
| 75 | -6.12(-2) | -1.14( 0) | -4.30(-2) | 3.83(-1) | 3.41(-1) |
| 76 | -1.33(-2) | -9.98(-1) | 2.17(-1) | 7.40(-1) | 7.70(-1) |
| 77 | 2.74(-2) | -8.63(-1) | 4.63(-1) | 1.08( 0) | 1.19( 0) |
| 78 | 6.16(-2) | -7.40(-1) | 6.95(-1) | 1.41( 0) | -1.55( 0) |
| 79 | 9.01(-2) | -6.29(-1) | 9.13(-1) | -1.41( 0) | -1.16( 0) |
| 80 | 1.14(-1) | -5.28(-1) | 1.12( 0) | -1.11( 0) | -7.76(-1) |
| 81 | 1.33(-1) | -4.37(-1) | 1.31( 0) | -8.24(-1) | -4.07(-1) |
| 82 | 1.49(-1) | -3.56(-1) | 1.49( 0) | -5.48(-1) | -5.08(-2) |
| 83 | 1.59(-1) | -2.83(-1) | -1.49( 0) | -2.85(-1) | 2.94(-1) |
| 84 | 1.68(-1) | -2.18(-1) | -1.33( 0) | -3.51(-2) | 6.27(-1) |
| 85 | 1.74(-1) | -1.61(-1) | -1.19( 0) | 2.03(-1) | 9.48(-1) |
| 86 | 1.79(-1) | -1.11(-1) | -1.05( 0) | 4.28(-1) | 1.26( 0) |
| 87 | 1.81(-1) | -6.63(-2) | -9.31(-1) | 6.41(-1) | 1.55( 0) |
| 88 | 1.82(-1) | -2.77(-2) | -8.18(-1) | 8.43(-1) | -1.30( 0) |
| 89 | 1.81(-1) | 5.73(-3) | -7.14(-1) | 1.03( 0) | -1.03( 0) |
| 90 | 1.80(-1) | 3.45(-2) | -6.19(-1) | 1.21( 0) | -7.65(-1) |
| 91 | 1.78(-1) | 5.92(-2) | -5.32(-1) | 1.38( 0) | -5.13(-1) |
| 92 | 1.75(-1) | 8.01(-2) | -4.53(-1) | 1.54( 0) | -2.72(-1) |
| 93 | 1.71(-1) | 9.76(-2) | -3.82(-1) | -1.46( 0) | -4.30(-2) |
| 94 | 1.67(-1) | 1.12(-1) | -3.17(-1) | -1.32( 0) | 1.76(-1) |
| 95 | 1.63(-1) | 1.24(-1) | -2.59(-1) | -1.19( 0) | 3.84(-1) |
| 96 | 1.59(-1) | 1.34(-1) | -2.06(-1) | -1.07( 0) | 5.82(-1) |
| 97 | 1.53(-1) | 1.41(-1) | -1.60(-1) | -9.59(-1) | 7.70(-1) |
| 98 | 1.49(-1) | 1.47(-1) | -1.18(-1) | -8.55(-1) | 9.47(-1) |
| 99 | 1.44(-1) | 1.51(-1) | -8.04(-2) | -7.61(-1) | 1.12( 0) |
| 100 | 1.39(-1) | 1.54(-1) | -4.74(-2) | -6.73(-1) | 1.27( 0) |
| 101 | 1.34(-1) | 1.56(-1) | -1.83(-2) | -5.92(-1) | 1.42( 0) |
| 102 | 1.29(-1) | 1.57(-1) | 7.28(-3) | -5.17(-1) | 1.57( 0) |
| 103 | 1.24(-1) | 1.57(-1) | 2.97(-2) | -4.49(-1) | -1.44( 0) |
| 104 | 1.20(-1) | 1.56(-1) | 4.91(-2) | -3.87(-1) | -1.32( 0) |
| 105 | 1.15(-1) | 1.55(-1) | 6.53(-2) | -3.30(-1) | -1.20( 0) |
| 106 | 1.11(-1) | 1.53(-1) | 8.03(-2) | -2.78(-1) | -1.09( 0) |
| 107 | 1.07(-1) | 1.51(-1) | 9.25(-2) | -2.31(-1) | -9.91(-1) |
| 108 | 1.03(-1) | 1.48(-1) | 1.03(-1) | -1.89(-1) | -8.96(-1) |
| 109 | 9.85(-2) | 1.45(-1) | 1.12(-1) | -1.50(-1) | -8.08(-1) |
| 110 | 9.47(-2) | 1.42(-1) | 1.17(-1) | -1.15(-1) | -7.26(-1) |
| 111 | 9.10(-2) | 1.38(-1) | 1.24(-1) | -8.37(-2) | -6.49(-1) |
| 112 | 8.74(-2) | 1.35(-1) | 1.29(-1) | -5.56(-2) | -5.79(-1) |
| 113 | 9.40(-2) | 1.31(-1) | 1.32(-1) | -3.06(-2) | -5.13(-1) |
| 114 | 8.07(-2) | 1.28(-1) | 1.35(-1) | -8.26(-3) | -4.53(-1) |
| 115 | 7.75(-2) | 1.24(-1) | 1.37(-1) | 1.15(-2) | -3.97(-1) |

APPENDIX B. (continued)

| $\ell$ | | | E [eV] | | |
|---|---|---|---|---|---|
| | 0.60 | 0.81 | 1.06 | 1.34 | 1.66 |
| 116 | 7.45(-2) | 1.21(-1) | 1.38(-1) | 2.91(-2) | -3.46(-1) |
| 117 | 7.15(-2) | 1.17(-1) | 1.39(-1) | 4.45(-2) | -2.99(-1) |
| 118 | 6.87(-2) | 1.13(-1) | 1.39(-1) | 5.80(-2) | -2.56(-1) |
| 119 | 6.61(-2) | 1.10(-1) | 1.37(-1) | 6.93(-2) | -2.16(-1) |
| 120 | 6.35(-2) | 1.06(-1) | 1.36(-1) | 8.00(-2) | -1.80(-1) |
| 121 | 6.10(-2) | 1.03(-1) | 1.35(-1) | 8.89(-2) | -1.47(-1) |
| 122 | 5.87(-2) | 9.97(-2) | 1.33(-1) | 9.63(-2) | -1.18(-1) |
| 123 | 5.64(-2) | 9.64(-2) | 1.31(-1) | 1.03(-1) | -9.04(-2) |
| 124 | 5.43(-2) | 9.33(-2) | 1.29(-1) | 1.08(-1) | -6.58(-2) |
| 125 | 5.22(-2) | 9.02(-2) | 1.27(-1) | 1.12(-1) | -4.36(-2) |
| 126 | 5.02(-2) | 8.71(-2) | 1.24(-1) | 1.16(-1) | -2.34(-2) |
| 127 | 4.83(-2) | 8.42(-2) | 1.22(-1) | 1.19(-1) | -5.46(-3) |
| 128 | 4.65(-2) | 8.14(-2) | 1.19(-1) | 1.21(-1) | 1.09(-2) |
| 129 | 4.48(-2) | 7.86(-2) | 1.16(-1) | 1.22(-1) | 2.52(-2) |
| 130 | 4.31(-2) | 7.60(-2) | 1.14(-1) | 1.23(-1) | 3.82(-2) |
| 131 | 4.15(-2) | 7.34(-2) | 1.11(-1) | 1.24(-1) | 4.96(-2) |
| 132 | 4.00(-2) | 7.09(-2) | 1.09(-1) | 1.24(-1) | 5.97(-2) |
| 133 | 3.85(-2) | 6.85(-2) | 1.05(-1) | 1.24(-1) | 6.87(-2) |
| 134 | 3.72(-2) | 6.62(-2) | 1.03(-1) | 1.23(-1) | 7.64(-2) |
| 135 | 3.58(-2) | 6.40(-2) | 9.98(-2) | 1.22(-1) | 8.33(-2) |
| 136 | 3.45(-2) | 6.18(-2) | 9.71(-2) | 1.21(-1) | 8.91(-2) |
| 137 | 3.33(-2) | 5.97(-2) | 9.44(-2) | 1.20(-1) | 9.43(-2) |
| 138 | 3.22(-2) | 5.77(-2) | 9.18(-2) | 1.18(-1) | 9.85(-2) |
| 139 | 3.10(-2) | 5.53(-2) | 8.92(-2) | 1.16(-1) | 1.02(-1) |
| 140 | 2.99(-2) | 5.37(-2) | 8.66(-2) | 1.15(-1) | 1.05(-1) |
| 141 | 2.89(-2) | 5.21(-2) | 8.42(-2) | 1.13(-1) | 1.07(-1) |
| 142 | 2.79(-2) | 5.04(-2) | 8.17(-2) | 1.11(-1) | 1.09(-1) |
| 143 | 2.70(-2) | 4.88(-2) | 7.94(-2) | 1.09(-1) | 1.11(-1) |
| 144 | 2.61(-2) | 4.72(-2) | 7.71(-2) | 1.07(-1) | 1.12(-1) |
| 145 | 2.52(-2) | 4.56(-2) | 7.48(-2) | 1.05(-1) | 1.12(-1) |
| 146 | 2.43(-2) | 4.41(-2) | 7.26(-2) | 1.02(-1) | 1.13(-1) |
| 147 | 2.35(-2) | 4.27(-2) | 7.05(-2) | 1.00(-1) | 1.13(-1) |
| 148 | 2.27(-2) | 4.13(-2) | 6.84(-2) | 9.80(-2) | 1.13(-1) |
| 149 | 2.20(-2) | 4.00(-2) | 6.64(-2) | 9.59(-2) | 1.12(-1) |
| 150 | 2.13(-2) | 3.87(-2) | 6.44(-2) | 9.36(-2) | 1.11(-1) |
| 151 | 2.06(-2) | 3.75(-2) | 6.25(-2) | 9.14(-2) | 1.11(-1) |
| 152 | 1.99(-2) | 3.63(-2) | 6.07(-2) | 8.92(-2) | 1.10(-1) |
| 153 | 1.93(-2) | 3.51(-2) | 5.89(-2) | 8.71(-2) | 1.08(-1) |
| 154 | 1.87(-2) | 3.40(-2) | 5.72(-2) | 8.50(-2) | 1.07(-1) |
| 155 | 1.81(-2) | 3.30(-2) | 5.55(-2) | 8.29(-2) | 1.06(-1) |
| 156 | 1.75(-2) | 3.20(-2) | 5.39(-2) | 8.09(-2) | 1.04(-1) |
| 157 | 1.70(-2) | 3.10(-2) | 5.23(-2) | 7.89(-2) | 1.03(-1) |
| 158 | 1.64(-2) | 3.00(-2) | 5.08(-2) | 7.68(-2) | 1.01(-1) |
| 159 | 1.59(-2) | 2.91(-2) | 4.93(-2) | 7.49(-2) | 9.95(-2) |
| 160 | 1.54(-2) | 2.82(-2) | 4.79(-2) | 7.29(-2) | 9.78(-2) |
| 161 | 1.50(-2) | 2.74(-2) | 4.65(-2) | 7.11(-2) | 9.61(-2) |
| 162 | 1.45(-2) | 2.66(-2) | 4.51(-2) | 6.92(-2) | 9.43(-2) |
| 163 | 1.41(-2) | 2.58(-2) | 4.38(-2) | 6.75(-2) | 9.26(-2) |
| 164 | 1.36(-2) | 2.50(-2) | 4.26(-2) | 6.57(-2) | 9.08(-2) |
| 165 | 1.32(-2) | 2.43(-2) | 4.14(-2) | 6.40(-2) | 8.91(-2) |
| 166 | 1.28(-2) | 2.35(-2) | 4.02(-2) | 6.24(-2) | 8.72(-2) |
| 167 | 1.25(-2) | 2.29(-2) | 3.90(-2) | 6.07(-2) | 8.55(-2) |
| 168 | 1.21(-2) | 2.22(-2) | 3.80(-2) | 5.92(-2) | 8.37(-2) |
| 169 | 1.17(-2) | 2.15(-2) | 3.69(-2) | 5.76(-2) | 8.19(-2) |
| 170 | 1.14(-2) | 2.09(-2) | 3.58(-2) | 5.61(-2) | 8.02(-2) |
| 171 | 1.11(-2) | 2.03(-2) | 3.48(-2) | 5.47(-2) | 7.84(-2) |
| 172 | 1.08(-2) | 1.98(-2) | 3.39(-2) | 5.32(-2) | 7.68(-2) |
| 173 | 1.05(-2) | 1.92(-2) | 3.30(-2) | 5.19(-2) | 7.51(-2) |
| 174 | 1.02(-2) | 1.87(-2) | 3.20(-2) | 5.05(-2) | 7.34(-2) |
| 175 | 9.87(-3) | 1.81(-2) | 3.12(-2) | 4.92(-2) | 7.18(-2) |

APPENDIX B. (continued)

| $\ell$ | E [eV] | | | | |
|---|---|---|---|---|---|
| | 0.60 | 0.81 | 1.06 | 1.34 | 1.66 |
| 176 | 9.59(-3) | 1.76(-2) | 3.03(-2) | 4.80(-2) | 7.01(-2) |
| 177 | 9.32(-3) | 1.71(-2) | 2.95(-2) | 4.67(-2) | 6.86(-2) |
| 178 | 9.06(-3) | 1.67(-2) | 2.87(-2) | 4.55(-2) | 6.70(-2) |
| 179 | 8.82(-3) | 1.62(-2) | 2.79(-2) | 4.43(-2) | 6.55(-2) |
| 180 | 8.57(-3) | 1.58(-2) | 2.72(-2) | 4.32(-2) | 6.41(-2) |
| 181 | 8.34(-3) | 1.54(-2) | 2.65(-2) | 4.21(-2) | 6.25(-2) |
| 182 | 8.11(-3) | 1.49(-2) | 2.57(-2) | 4.10(-2) | 6.12(-2) |
| 183 | 7.69(-3) | 1.45(-2) | 2.51(-2) | 4.00(-2) | 5.97(-2) |
| 184 | 7.63(-3) | 1.42(-2) | 2.44(-2) | 3.90(-2) | 5.83(-2) |
| 185 | 7.43(-3) | 1.38(-2) | 2.38(-2) | 3.80(-2) | 5.70(-2) |
| 186 | 7.27(-3) | 1.34(-2) | 2.32(-2) | 3.71(-2) | 5.57(-2) |
| 187 | 7.08(-3) | 1.31(-2) | 2.26(-2) | 3.61(-2) | 5.44(-2) |
| 188 | 6.90(-3) | 1.27(-2) | 2.20(-2) | 3.52(-2) | 5.31(-2) |
| 189 | 6.71(-3) | 1.24(-2) | 2.14(-2) | 3.43(-2) | 5.19(-2) |
| 190 | 6.54(-3) | 1.21(-2) | 2.09(-2) | 3.35(-2) | 5.08(-2) |
| 191 | 6.37(-3) | 1.18(-2) | 2.04(-2) | 3.27(-2) | 4.95(-2) |
| 192 | 6.20(-3) | 1.15(-2) | 1.98(-2) | 3.19(-2) | 4.85(-2) |
| 193 | 6.05(-3) | 1.12(-2) | 1.93(-2) | 3.11(-2) | 4.73(-2) |
| 194 | 5.89(-3) | 1.09(-2) | 1.89(-2) | 3.03(-2) | 4.63(-2) |
| 195 | 5.74(-3) | 1.06(-2) | 1.84(-2) | 2.96(-2) | 4.52(-2) |
| 196 | 5.60(-3) | 1.03(-2) | 1.79(-2) | 2.89(-2) | 4.41(-2) |
| 197 | 5.45(-3) | 1.01(-2) | 1.75(-2) | 2.82(-2) | 4.32(-2) |
| 198 | 5.32(-3) | 9.84(-3) | 1.71(-2) | 2.75(-2) | 4.21(-2) |
| 199 | 5.19(-3) | 9.57(-3) | 1.67(-2) | 2.69(-2) | 4.12(-2) |
| 200 | 5.05(-3) | 9.37(-3) | 1.62(-2) | 2.62(-2) | 4.03(-2) |
| 201 | 4.93(-3) | 9.13(-3) | 1.59(-2) | 2.56(-2) | 3.94(-2) |
| 202 | 4.81(-3) | 8.91(-3) | 1.55(-2) | 2.50(-2) | 3.85(-2) |
| 203 | 4.69(-3) | 8.70(-3) | 1.51(-2) | 2.44(-2) | 3.76(-2) |
| 204 | 4.57(-3) | 8.49(-3) | 1.48(-2) | 2.39(-2) | 3.68(-2) |
| 205 | 4.47(-3) | 8.28(-3) | 1.44(-2) | 2.33(-2) | 3.60(-2) |
| 206 | 4.36(-3) | 8.09(-3) | 1.41(-2) | 2.28(-2) | 3.52(-2) |
| 207 | 4.25(-3) | 7.89(-3) | 1.37(-2) | 2.22(-2) | 3.44(-2) |
| 208 | 4.15(-3) | 7.71(-3) | 1.34(-2) | 2.18(-2) | 3.36(-2) |
| 209 | 4.05(-3) | 7.53(-3) | 1.31(-2) | 2.13(-2) | 3.29(-2) |
| 210 | 3.95(-3) | 7.34(-3) | 1.28(-2) | 2.07(-2) | 3.22(-2) |
| 211 | 3.86(-3) | 7.18(-3) | 1.25(-2) | 2.03(-2) | 3.15(-2) |
| 212 | 3.77(-3) | 7.01(-3) | 1.22(-2) | 1.98(-2) | 3.08(-2) |
| 213 | 3.68(-3) | 6.84(-3) | 1.19(-2) | 1.94(-2) | 3.01(-2) |
| 214 | 3.60(-3) | 6.70(-3) | 1.17(-2) | 1.90(-2) | 2.95(-2) |
| 215 | 3.51(-3) | 6.54(-3) | 1.14(-2) | 1.85(-2) | 2.89(-2) |
| 216 | 3.43(-3) | 6.38(-3) | 1.11(-2) | 1.82(-2) | 2.82(-2) |
| 217 | 3.35(-3) | 6.25(-3) | 1.09(-2) | 1.77(-2) | 2.77(-2) |
| 218 | 3.27(-3) | 6.10(-3) | 1.07(-2) | 1.73(-2) | 2.70(-2) |
| 219 | 3.19(-3) | 5.96(-3) | 1.04(-2) | 1.70(-2) | 2.65(-2) |
| 220 | 3.12(-3) | 5.84(-3) | 1.02(-2) | 1.66(-2) | 2.59(-2) |
| 221 | 3.05(-3) | 5.70(-3) | 9.97(-3) | 1.63(-2) | 2.54(-2) |
| 222 | 2.98(-3) | 5.57(-3) | 9.74(-3) | 1.59(-2) | 2.49(-2) |
| 223 | 2.92(-3) | 5.46(-3) | 9.55(-3) | 1.55(-2) | 2.43(-2) |
| 224 | 2.85(-3) | 5.33(-3) | 9.33(-3) | 1.53(-2) | 2.39(-2) |
| 225 | 2.79(-3) | 5.21(-3) | 9.13(-3) | 1.49(-2) | 2.34(-2) |
| 226 | 2.72(-3) | 5.11(-3) | 8.95(-3) | 1.46(-2) | 2.29(-2) |
| 227 | 2.67(-3) | 4.99(-3) | 8.74(-3) | 1.43(-2) | 2.25(-2) |
| 228 | 2.60(-3) | 4.89(-3) | 8.56(-3) | 1.40(-2) | 2.19(-2) |
| 229 | 2.55(-3) | 4.78(-3) | 8.39(-3) | 1.37(-2) | 2.15(-2) |
| 230 | 2.49(-3) | 4.67(-3) | 8.19(-3) | 1.34(-2) | 2.11(-2) |
| 231 | 2.44(-3) | 4.57(-3) | 8.03(-3) | 1.31(-2) | 2.06(-2) |
| 232 | 2.39(-3) | 4.48(-3) | 7.87(-3) | 1.29(-2) | 2.03(-2) |
| 233 | 2.33(-3) | 4.39(-3) | 7.69(-3) | 1.26(-2) | 1.99(-2) |
| 234 | 2.29(-3) | 4.29(-3) | 7.55(-3) | 1.24(-2) | 1.94(-2) |
| 235 | 2.23(-3) | 4.20(-3) | 7.38(-3) | 1.21(-2) | 1.91(-2) |

| ℓ | E [eV] | | | | |
|---|---|---|---|---|---|
| | 0.60 | 0.81 | 1.06 | 1.34 | 1.66 |
| 235 | 2.18(-3) | 4.10(-3) | 7.22(-3) | 1.18(-2) | 1.87(-2) |
| 236 | 2.14(-3) | 4.02(-3) | 7.09(-3) | 1.16(-2) | 1.84(-2) |
| 237 | 2.09(-3) | 3.94(-3) | 6.93(-3) | 1.14(-2) | 1.80(-2) |
| 238 | 2.04(-3) | 3.85(-3) | 6.79(-3) | 1.12(-2) | 1.76(-2) |
| 239 | 2.00(-3) | 3.77(-3) | 6.67(-3) | 1.10(-2) | 1.73(-2) |
| 240 | 1.96(-3) | 3.70(-3) | 6.52(-3) | 1.07(-2) | 1.69(-2) |
| 241 | 1.92(-3) | 3.62(-3) | 6.39(-3) | 1.05(-2) | 1.66(-2) |
| 242 | 1.88(-3) | 3.55(-3) | 6.23(-3) | 1.03(-2) | 1.64(-2) |
| 243 | 1.84(-3) | 3.48(-3) | 6.13(-3) | 1.01(-2) | 1.60(-2) |
| 244 | 1.80(-3) | 3.40(-3) | 6.02(-3) | 9.92(-3) | 1.57(-2) |
| 245 | 1.76(-3) | 3.33(-3) | 5.91(-3) | 9.74(-3) | 1.54(-2) |
| 246 | 1.73(-3) | 3.27(-3) | 5.77(-3) | 9.52(-3) | 1.51(-2) |
| 247 | 1.69(-3) | 3.20(-3) | 5.67(-3) | 9.37(-3) | 1.49(-2) |
| 248 | 1.65(-3) | 3.14(-3) | 5.57(-3) | 9.19(-3) | 1.46(-2) |
| 249 | 1.62(-3) | 3.08(-3) | 5.44(-3) | 8.99(-3) | 1.43(-2) |
| 250 | 1.59(-3) | 3.02(-3) | 5.35(-3) | 8.85(-3) | 1.41(-2) |
| 251 | 1.55(-3) | 2.95(-3) | 5.25(-3) | 8.67(-3) | 1.38(-2) |
| 252 | 1.52(-3) | 2.90(-3) | 5.13(-3) | 8.50(-3) | 1.36(-2) |
| 253 | 1.49(-3) | 2.84(-3) | 5.05(-3) | 8.37(-3) | 1.33(-2) |
| 254 | 1.46(-3) | 2.78(-3) | 4.95(-3) | 8.18(-3) | 1.30(-2) |
| 255 | 1.43(-3) | 2.73(-3) | 4.84(-3) | 8.04(-3) | 1.29(-2) |
| 256 | 1.40(-3) | 2.68(-3) | 4.77(-3) | 7.91(-3) | 1.26(-2) |
| 257 | 1.38(-3) | 2.62(-3) | 4.67(-3) | 7.73(-3) | 1.24(-2) |
| 258 | 1.35(-3) | 2.57(-3) | 4.57(-3) | 7.61(-3) | 1.22(-2) |
| 259 | 1.32(-3) | 2.53(-3) | 4.50(-3) | 7.48(-3) | 1.19(-2) |
| 260 | 1.29(-3) | 2.47(-3) | 4.41(-3) | 7.31(-3) | 1.17(-2) |
| 261 | 1.27(-3) | 2.43(-3) | 4.32(-3) | 7.21(-3) | 1.15(-2) |
| 262 | 1.24(-3) | 2.38(-3) | 4.26(-3) | 7.07(-3) | 1.13(-2) |
| 263 | 1.22(-3) | 2.33(-3) | 4.17(-3) | 6.93(-3) | 1.12(-2) |
| 264 | 1.19(-3) | 2.29(-3) | 4.08(-3) | 6.83(-3) | 1.09(-2) |
| 265 | 1.17(-3) | 2.25(-3) | 4.02(-3) | 6.69(-3) | 1.07(-2) |
| 266 | 1.14(-3) | 2.20(-3) | 3.94(-3) | 6.57(-3) | 1.06(-2) |
| 267 | 1.12(-3) | 2.16(-3) | 3.86(-3) | 6.48(-3) | 1.03(-2) |
| 268 | 1.10(-3) | 2.12(-3) | 3.81(-3) | 6.34(-3) | 1.02(-2) |
| 269 | 1.08(-3) | 2.08(-3) | 3.73(-3) | 6.23(-3) | 1.00(-2) |
| 270 | 1.06(-3) | 2.04(-3) | 3.65(-3) | 6.14(-3) | 9.83(-3) |
| 271 | 1.04(-3) | 2.00(-3) | 3.60(-3) | 6.03(-3) | 9.72(-3) |
| 272 | 1.02(-3) | 1.97(-3) | 3.53(-3) | 5.91(-3) | 9.52(-3) |
| 273 | 9.97(-4) | 1.93(-3) | 3.46(-3) | 5.82(-3) | 9.36(-3) |
| 274 | 9.77(-4) | 1.89(-3) | 3.41(-3) | 5.69(-3) | 9.24(-3) |
| 275 | 9.60(-4) | 1.86(-3) | 3.35(-3) | 5.62(-3) | 9.03(-3) |
| 276 | 9.41(-4) | 1.83(-3) | 3.28(-3) | 5.53(-3) | 8.91(-3) |
| 277 | 9.22(-4) | 1.79(-3) | 3.23(-3) | 5.40(-3) | 8.78(-3) |
| 278 | 9.04(-4) | 1.76(-3) | 3.18(-3) | 5.34(-3) | 8.59(-3) |
| 279 | 8.88(-4) | 1.73(-3) | 3.11(-3) | 5.24(-3) | 8.50(-3) |
| 280 | 8.71(-4) | 1.69(-3) | 3.07(-3) | 5.13(-3) | 8.35(-3) |
| 281 | 8.53(-4) | 1.66(-3) | 3.01(-3) | 5.07(-3) | 8.18(-3) |
| 282 | 8.35(-4) | 1.64(-3) | 2.95(-3) | 4.98(-3) | 8.10(-3) |
| 283 | 8.21(-4) | 1.60(-3) | 2.91(-3) | 4.89(-3) | 7.93(-3) |
| 284 | 8.05(-4) | 1.57(-3) | 2.86(-3) | 4.83(-3) | 7.80(-3) |
| 285 | 7.89(-4) | 1.55(-3) | 2.80(-3) | 4.73(-3) | 7.72(-3) |
| 286 | 7.74(-4) | 1.52(-3) | 2.76(-3) | 4.64(-3) | 7.55(-3) |
| 287 | 7.60(-4) | 1.49(-3) | 2.72(-3) | 4.59(-3) | 7.45(-3) |
| 288 | 7.46(-4) | 1.47(-3) | 2.65(-3) | 4.50(-3) | 7.35(-3) |
| 289 | 7.31(-4) | 1.44(-3) | 2.61(-3) | 4.41(-3) | 7.19(-3) |
| 290 | 7.17(-4) | 1.41(-3) | 2.59(-3) | 4.37(-3) | 7.11(-3) |
| 291 | 7.04(-4) | 1.39(-3) | 2.52(-3) | 4.28(-3) | 7.00(-3) |
| 292 | 6.91(-4) | 1.37(-3) | 2.49(-3) | 4.20(-3) | 6.85(-3) |
| 293 | 6.77(-4) | 1.34(-3) | 2.45(-3) | 4.16(-3) | 6.79(-3) |

APPENDIX B. (continued)

| $\ell$ | E [eV] | | | | |
|---|---|---|---|---|---|
| | 0.60 | 0.81 | 1.06 | 1.34 | 1.66 |
| 295 | 6.64(-4) | 1.31(-3) | 2.40(-3) | 4.07(-3) | 6.67(-3) |
| 296 | 6.52(-4) | 1.29(-3) | 2.35(-3) | 4.00(-3) | 6.54(-3) |
| 297 | 6.40(-4) | 1.27(-3) | 2.33(-3) | 3.96(-3) | 6.49(-3) |
| 298 | 6.27(-4) | 1.25(-3) | 2.28(-3) | 3.89(-3) | 6.36(-3) |
| 299 | 6.15(-4) | 1.22(-3) | 2.24(-3) | 3.81(-3) | 6.25(-3) |
| 300 | 6.04(-4) | 1.21(-3) | 2.21(-3) | 3.77(-3) | 6.20(-3) |

[a] The number in parentheses denotes the power of ten by which the entry should be multiplied.

Differential Cross Section $\sigma(\theta)$ in $\text{Å}^2$/sr for

Relative Collision Energies $E \leq 0.41$ eV

| $\theta$ [deg] | E [eV] | | | | |
|---|---|---|---|---|---|
| | .02 | .07 | .15 | .27 | .41 |
| .1 | 3.38( 3)ᵃ | 4.24( 3) | 5.19( 3) | 6.51( 3) | 7.99( 3) |
| .2 | 3.37( 3) | 4.21( 3) | 5.13( 3) | 6.40( 3) | 7.84( 3) |
| .3 | 3.36( 3) | 4.16( 3) | 5.03( 3) | 6.23( 3) | 7.59( 3) |
| .4 | 3.34( 3) | 4.10( 3) | 4.89( 3) | 6.01( 3) | 7.27( 3) |
| .5 | 3.32( 3) | 4.01( 3) | 4.73( 3) | 5.73( 3) | 6.88( 3) |
| .6 | 3.29( 3) | 3.91( 3) | 4.53( 3) | 5.42( 3) | 6.45( 3) |
| .7 | 3.25( 3) | 3.80( 3) | 4.32( 3) | 5.09( 3) | 6.00( 3) |
| .8 | 3.22( 3) | 3.67( 3) | 4.09( 3) | 4.75( 3) | 5.54( 3) |
| .9 | 3.18( 3) | 3.54( 3) | 3.85( 3) | 4.41( 3) | 5.09( 3) |
| 1.0 | 3.13( 3) | 3.39( 3) | 3.61( 3) | 4.07( 3) | 4.66( 3) |
| 1.1 | 3.08( 3) | 3.24( 3) | 3.37( 3) | 3.75( 3) | 4.26( 3) |
| 1.2 | 3.03( 3) | 3.09( 3) | 3.14( 3) | 3.44( 3) | 3.88( 3) |
| 1.3 | 2.97( 3) | 2.94( 3) | 2.91( 3) | 3.16( 3) | 3.54( 3) |
| 1.4 | 2.91( 3) | 2.78( 3) | 2.69( 3) | 2.90( 3) | 3.21( 3) |
| 1.5 | 2.85( 3) | 2.63( 3) | 2.48( 3) | 2.66( 3) | 2.91( 3) |
| 1.6 | 2.79( 3) | 2.48( 3) | 2.29( 3) | 2.44( 3) | 2.63( 3) |
| 1.7 | 2.72( 3) | 2.33( 3) | 2.11( 3) | 2.24( 3) | 2.37( 3) |
| 1.8 | 2.65( 3) | 2.18( 3) | 1.95( 3) | 2.05( 3) | 2.12( 3) |
| 1.9 | 2.58( 3) | 2.04( 3) | 1.79( 3) | 1.88( 3) | 1.88( 3) |
| 2.0 | 2.51( 3) | 1.90( 3) | 1.65( 3) | 1.72( 3) | 1.65( 3) |
| 2.1 | 2.44( 3) | 1.77( 3) | 1.53( 3) | 1.58( 3) | 1.44( 3) |
| 2.2 | 2.36( 3) | 1.65( 3) | 1.41( 3) | 1.44( 3) | 1.24( 3) |
| 2.3 | 2.29( 3) | 1.53( 3) | 1.30( 3) | 1.30( 3) | 1.05( 3) |
| 2.4 | 2.21( 3) | 1.42( 3) | 1.21( 3) | 1.18( 3) | 8.70( 2) |
| 2.5 | 2.14( 3) | 1.32( 3) | 1.12( 3) | 1.06( 3) | 7.10( 2) |
| 2.6 | 2.06( 3) | 1.22( 3) | 1.04( 3) | 9.49( 2) | 5.66( 2) |
| 2.7 | 1.99( 3) | 1.13( 3) | 9.70( 2) | 8.43( 2) | 4.40( 2) |
| 2.8 | 1.92( 3) | 1.04( 3) | 9.03( 2) | 7.42( 2) | 3.30( 2) |
| 2.9 | 1.84( 3) | 9.66( 2) | 8.42( 2) | 6.46( 2) | 2.37( 2) |
| 3.0 | 1.77( 3) | 8.95( 2) | 7.86( 2) | 5.57( 2) | 1.62( 2) |
| 3.1 | 1.70( 3) | 8.29( 2) | 7.33( 2) | 4.73( 2) | 1.02( 2) |
| 3.2 | 1.63( 3) | 7.69( 2) | 6.83( 2) | 3.95( 2) | 5.74( 1) |
| 3.3 | 1.56( 3) | 7.15( 2) | 6.35( 2) | 3.24( 2) | 2.68( 1) |
| 3.4 | 1.49( 3) | 6.65( 2) | 5.90( 2) | 2.60( 2) | 8.90( 0) |
| 3.5 | 1.43( 3) | 6.21( 2) | 5.46( 2) | 2.03( 2) | 1.98( 0) |
| 3.6 | 1.36( 3) | 5.80( 2) | 5.03( 2) | 1.53( 2) | 4.32( 0) |
| 3.7 | 1.30( 3) | 5.44( 2) | 4.62( 2) | 1.11( 2) | 1.40( 1) |
| 3.8 | 1.23( 3) | 5.11( 2) | 4.22( 2) | 7.55( 1) | 2.91( 1) |
| 3.9 | 1.17( 3) | 4.82( 2) | 3.83( 2) | 4.77( 1) | 4.77( 1) |
| 4.0 | 1.12( 3) | 4.56( 2) | 3.46( 2) | 2.68( 1) | 6.79( 1) |
| 4.1 | 1.06( 3) | 4.32( 2) | 3.10( 2) | 1.23( 1) | 8.81( 1) |
| 4.2 | 1.00( 3) | 4.11( 2) | 2.75( 2) | 3.69( 0) | 1.07( 2) |
| 4.3 | 9.51( 2) | 3.92( 2) | 2.42( 2) | 2.49(-1) | 1.23( 2) |
| 4.4 | 9.00( 2) | 3.74( 2) | 2.11( 2) | 1.23( 0) | 1.36( 2) |
| 4.5 | 8.50( 2) | 3.58( 2) | 1.82( 2) | 5.85( 0) | 1.44( 2) |
| 4.6 | 8.02( 2) | 3.43( 2) | 1.54( 2) | 1.33( 1) | 1.49( 2) |
| 4.7 | 7.57( 2) | 3.29( 2) | 1.29( 2) | 2.29( 1) | 1.49( 2) |
| 4.8 | 7.13( 2) | 3.16( 2) | 1.06( 2) | 3.38( 1) | 1.46( 2) |
| 4.9 | 6.71( 2) | 3.04( 2) | 8.56( 1) | 4.54( 1) | 1.40( 2) |
| 5.0 | 6.31( 2) | 2.92( 2) | 6.72( 1) | 5.70( 1) | 1.31( 2) |
| 5.1 | 5.93( 2) | 2.81( 2) | 5.11( 1) | 6.83( 1) | 1.20( 2) |
| 5.2 | 5.56( 2) | 2.69( 2) | 3.74( 1) | 7.86( 1) | 1.08( 2) |
| 5.3 | 5.22( 2) | 2.58( 2) | 2.60( 1) | 8.77( 1) | 9.45( 1) |
| 5.4 | 4.89( 2) | 2.47( 2) | 1.68( 1) | 9.52( 1) | 8.12( 1) |
| 5.5 | 4.58( 2) | 2.36( 2) | 9.81( 0) | 1.01( 2) | 6.83( 1) |
| 5.6 | 4.29( 2) | 2.25( 2) | 4.88( 0) | 1.05( 2) | 5.64( 1) |

APPENDIX C. (continued)

| $\theta$ [deg] | E [eV] | | | | |
|---|---|---|---|---|---|
| | .02 | .07 | .15 | .27 | .41 |
| 5.7 | 4.01( 2) | 2.14( 2) | 1.89( 0) | 1.07( 2) | 4.56( 1) |
| 5.8 | 3.75( 2) | 2.03( 2) | 6.66(-1) | 1.07( 2) | 3.64( 1) |
| 5.9 | 3.51( 2) | 1.92( 2) | 1.03( 0) | 1.05( 2) | 2.89( 1) |
| 6.0 | 3.28( 2) | 1.81( 2) | 2.77( 0) | 1.01( 2) | 2.33( 1) |
| 6.1 | 3.07( 2) | 1.70( 2) | 5.70( 0) | 9.59( 1) | 1.96( 1) |
| 6.2 | 2.87( 2) | 1.59( 2) | 9.60( 0) | 8.96( 1) | 1.77( 1) |
| 6.3 | 2.68( 2) | 1.48( 2) | 1.43( 1) | 8.23( 1) | 1.75( 1) |
| 6.4 | 2.51( 2) | 1.37( 2) | 1.95( 1) | 7.44( 1) | 1.87( 1) |
| 6.5 | 2.35( 2) | 1.26( 2) | 2.50( 1) | 6.61( 1) | 2.11( 1) |
| 6.6 | 2.21( 2) | 1.16( 2) | 3.07( 1) | 5.78( 1) | 2.43( 1) |
| 6.7 | 2.08( 2) | 1.05( 2) | 3.65( 1) | 4.97( 1) | 2.80( 1) |
| 6.8 | 1.95( 2) | 9.53( 1) | 4.20( 1) | 4.21( 1) | 3.19( 1) |
| 6.9 | 1.84( 2) | 8.57( 1) | 4.73( 1) | 3.51( 1) | 3.57( 1) |
| 7.0 | 1.74( 2) | 7.64( 1) | 5.22( 1) | 2.88( 1) | 3.92( 1) |
| 7.1 | 1.65( 2) | 6.76( 1) | 5.66( 1) | 2.34( 1) | 4.20( 1) |
| 7.2 | 1.57( 2) | 5.93( 1) | 6.03( 1) | 1.90( 1) | 4.42( 1) |
| 7.3 | 1.49( 2) | 5.15( 1) | 6.34( 1) | 1.55( 1) | 4.55( 1) |
| 7.4 | 1.43( 2) | 4.42( 1) | 6.58( 1) | 1.30( 1) | 4.61( 1) |
| 7.5 | 1.37( 2) | 3.74( 1) | 6.74( 1) | 1.14( 1) | 4.59( 1) |
| 7.6 | 1.32( 2) | 3.13( 1) | 6.83( 1) | 1.07( 1) | 4.50( 1) |
| 7.7 | 1.27( 2) | 2.58( 1) | 6.84( 1) | 1.07( 1) | 4.35( 1) |
| 7.8 | 1.24( 2) | 2.08( 1) | 6.78( 1) | 1.15( 1) | 4.16( 1) |
| 7.9 | 1.20( 2) | 1.65( 1) | 6.64( 1) | 1.29( 1) | 3.92( 1) |
| 8.0 | 1.17( 2) | 1.27( 1) | 6.45( 1) | 1.48( 1) | 3.65( 1) |
| 8.1 | 1.15( 2) | 9.61( 0) | 6.20( 1) | 1.70( 1) | 3.38( 1) |
| 8.2 | 1.13( 2) | 7.06( 0) | 5.90( 1) | 1.94( 1) | 3.09( 1) |
| 8.3 | 1.11( 2) | 5.07( 0) | 5.56( 1) | 2.19( 1) | 2.82( 1) |
| 8.4 | 1.10( 2) | 3.63( 0) | 5.18( 1) | 2.44( 1) | 2.56( 1) |
| 8.5 | 1.09( 2) | 2.70( 0) | 4.79( 1) | 2.68( 1) | 2.32( 1) |
| 8.6 | 1.09( 2) | 2.26( 0) | 4.38( 1) | 2.89( 1) | 2.11( 1) |
| 8.7 | 1.08( 2) | 2.27( 0) | 3.96( 1) | 3.07( 1) | 1.94( 1) |
| 8.8 | 1.08( 2) | 2.70( 0) | 3.54( 1) | 3.20( 1) | 1.82( 1) |
| 8.9 | 1.08( 2) | 3.51( 0) | 3.13( 1) | 3.30( 1) | 1.73( 1) |
| 9.0 | 1.08( 2) | 4.66( 0) | 2.74( 1) | 3.36( 1) | 1.68( 1) |
| 9.1 | 1.08( 2) | 6.12( 0) | 2.37( 1) | 3.37( 1) | 1.68( 1) |
| 9.2 | 1.08( 2) | 7.83( 0) | 2.02( 1) | 3.34( 1) | 1.70( 1) |
| 9.3 | 1.08( 2) | 9.76( 0) | 1.71( 1) | 3.27( 1) | 1.75( 1) |
| 9.4 | 1.09( 2) | 1.19( 1) | 1.43( 1) | 3.17( 1) | 1.82( 1) |
| 9.5 | 1.09( 2) | 1.41( 1) | 1.18( 1) | 3.04( 1) | 1.90( 1) |
| 9.6 | 1.09( 2) | 1.64( 1) | 9.71( 0) | 2.89( 1) | 1.98( 1) |
| 9.7 | 1.09( 2) | 1.88( 1) | 8.02( 0) | 2.73( 1) | 2.06( 1) |
| 9.8 | 1.10( 2) | 2.12( 1) | 6.73( 0) | 2.55( 1) | 2.12( 1) |
| 9.9 | 1.10( 2) | 2.36( 1) | 5.81( 0) | 2.37( 1) | 2.17( 1) |
| 10.0 | 1.10( 2) | 2.59( 1) | 5.28( 0) | 2.19( 1) | 2.21( 1) |
| 10.2 | 1.09( 2) | 3.02( 1) | 5.23( 0) | 1.84( 1) | 2.22( 1) |
| 10.4 | 1.09( 2) | 3.40( 1) | 6.35( 0) | 1.55( 1) | 2.17( 1) |
| 10.6 | 1.08( 2) | 3.71( 1) | 8.33( 0) | 1.33( 1) | 2.07( 1) |
| 10.8 | 1.06( 2) | 3.94( 1) | 1.08( 1) | 1.19( 1) | 1.93( 1) |
| 11.0 | 1.04( 2) | 4.07( 1) | 1.36( 1) | 1.15( 1) | 1.77( 1) |
| 11.2 | 1.01( 2) | 4.11( 1) | 1.62( 1) | 1.17( 1) | 1.62( 1) |
| 11.4 | 9.79( 1) | 4.07( 1) | 1.86( 1) | 1.25( 1) | 1.48( 1) |
| 11.6 | 9.42( 1) | 3.94( 1) | 2.04( 1) | 1.36( 1) | 1.38( 1) |
| 11.8 | 9.01( 1) | 3.73( 1) | 2.16( 1) | 1.46( 1) | 1.32( 1) |
| 12.0 | 8.56( 1) | 3.46( 1) | 2.22( 1) | 1.55( 1) | 1.31( 1) |
| 12.2 | 8.08( 1) | 3.15( 1) | 2.20( 1) | 1.60( 1) | 1.32( 1) |
| 12.4 | 7.58( 1) | 2.80( 1) | 2.12( 1) | 1.63( 1) | 1.34( 1) |
| 12.6 | 7.05( 1) | 2.43( 1) | 1.99( 1) | 1.62( 1) | 1.36( 1) |
| 12.8 | 6.52( 1) | 2.06( 1) | 1.81( 1) | 1.57( 1) | 1.37( 1) |
| 13.0 | 5.97( 1) | 1.70( 1) | 1.62( 1) | 1.49( 1) | 1.36( 1) |
| 13.2 | 5.43( 1) | 1.36( 1) | 1.42( 1) | 1.39( 1) | 1.33( 1) |

APPENDIX C. (continued)

| θ [deg] | E [eV] | | | | |
|---|---|---|---|---|---|
| | .02 | .07 | .15 | .27 | .41 |
| 13.4 | 4.89( 1) | 1.05( 1) | 1.22( 1) | 1.28( 1) | 1.30( 1) |
| 13.6 | 4.36( 1) | 7.88( 0) | 1.05( 1) | 1.17( 1) | 1.25( 1) |
| 13.8 | 3.85( 1) | 5.67( 0) | 9.04( 0) | 1.08( 1) | 1.20( 1) |
| 14.0 | 3.36( 1) | 3.97( 0) | 7.92( 0) | 1.01( 1) | 1.15( 1) |
| 14.2 | 2.90( 1) | 2.77( 0) | 7.18( 0) | 9.65( 0) | 1.09( 1) |
| 14.4 | 2.47( 1) | 2.08( 0) | 6.81( 0) | 9.41( 0) | 1.05( 1) |
| 14.6 | 2.07( 1) | 1.86( 0) | 6.78( 0) | 9.34( 0) | 1.01( 1) |
| 14.8 | 1.71( 1) | 2.08( 0) | 7.05( 0) | 9.42( 0) | 9.94( 0) |
| 15.0 | 1.39( 1) | 2.66( 0) | 7.54( 0) | 9.55( 0) | 9.85( 0) |
| 15.2 | 1.11( 1) | 3.55( 0) | 8.16( 0) | 9.80( 0) | 9.80( 0) |
| 15.4 | 8.71( 0) | 4.67( 0) | 8.83( 0) | 1.00( 1) | 9.73( 0) |
| 15.6 | 6.72( 0) | 5.94( 0) | 9.49( 0) | 1.01( 1) | 9.62( 0) |
| 15.8 | 5.14( 0) | 7.29( 0) | 1.01( 1) | 1.02( 1) | 9.50( 0) |
| 16.0 | 3.96( 0) | 8.65( 0) | 1.05( 1) | 1.01( 1) | 9.37( 0) |
| 18.0 | 8.67( 0) | 1.29( 1) | 7.41( 0) | 7.30( 0) | 7.55( 0) |
| 20.0 | 2.17( 1) | 4.54( 0) | 6.52( 0) | 6.78( 0) | 6.46( 0) |
| 22.0 | 2.12( 1) | 5.07( 0) | 6.08( 0) | 5.66( 0) | 5.66( 0) |
| 24.0 | 9.74( 0) | 6.90( 0) | 4.91( 0) | 5.04( 0) | 4.91( 0) |
| 26.0 | 1.10( 0) | 4.26( 0) | 4.84( 0) | 4.51( 0) | 4.35( 0) |
| 28.0 | 1.71( 0) | 3.80( 0) | 4.09( 0) | 4.05( 0) | 3.92( 0) |
| 30.0 | 6.62( 0) | 4.52( 0) | 3.91( 0) | 3.70( 0) | 3.54( 0) |
| 32.0 | 8.58( 0) | 3.68( 0) | 3.52( 0) | 3.38( 0) | 3.26( 0) |
| 34.0 | 5.97( 0) | 3.17( 0) | 3.28( 0) | 3.11( 0) | 2.99( 0) |
| 36.0 | 2.45( 0) | 3.37( 0) | 3.06( 0) | 2.85( 0) | 2.75( 0) |
| 38.0 | 1.47( 0) | 3.11( 0) | 2.85( 0) | 2.69( 0) | 2.56( 0) |
| 40.0 | 2.90( 0) | 2.76( 0) | 2.70( 0) | 2.52( 0) | 2.38( 0) |
| 42.0 | 4.35( 0) | 2.74( 0) | 2.53( 0) | 2.37( 0) | 2.25( 0) |
| 44.0 | 4.21( 0) | 2.65( 0) | 2.40( 0) | 2.24( 0) | 2.12( 0) |
| 46.0 | 2.93( 0) | 2.45( 0) | 2.23( 0) | 2.12( 0) | 2.01( 0) |
| 48.0 | 1.96( 0) | 2.36( 0) | 2.18( 0) | 2.02( 0) | 1.91( 0) |
| 50.0 | 2.00( 0) | 2.30( 0) | 2.08( 0) | 1.93( 0) | 1.81( 0) |
| 52.0 | 2.63( 0) | 2.19( 0) | 1.99( 0) | 1.84( 0) | 1.72( 0) |
| 54.0 | 2.98( 0) | 2.10( 0) | 1.92( 0) | 1.76( 0) | 1.65( 0) |
| 56.0 | 2.74( 0) | 2.04( 0) | 1.84( 0) | 1.69( 0) | 1.53( 0) |
| 58.0 | 2.23( 0) | 1.98( 0) | 1.78( 0) | 1.62( 0) | 1.52( 0) |
| 60.0 | 1.92( 0) | 1.91( 0) | 1.72( 0) | 1.57( 0) | 1.47( 0) |
| 65.0 | 2.28( 0) | 1.78( 0) | 1.59( 0) | 1.44( 0) | 1.34( 0) |
| 70.0 | 1.96( 0) | 1.67( 0) | 1.48( 0) | 1.34( 0) | 1.24( 0) |
| 75.0 | 1.88( 0) | 1.57( 0) | 1.39( 0) | 1.25( 0) | 1.16( 0) |
| 80.0 | 1.85( 0) | 1.50( 0) | 1.31( 0) | 1.18( 0) | 1.09( 0) |
| 85.0 | 1.70( 0) | 1.43( 0) | 1.25( 0) | 1.12( 0) | 1.03( 0) |
| 90.0 | 1.72( 0) | 1.37( 0) | 1.19( 0) | 1.06( 0) | 9.81( -1) |
| 95.0 | 1.64( 0) | 1.32( 0) | 1.14( 0) | 1.02( 0) | 9.36( -1) |
| 100.0 | 1.58( 0) | 1.28( 0) | 1.10( 0) | 9.77( -1) | 8.93( -1) |
| 105.0 | 1.56( 0) | 1.24( 0) | 1.07( 0) | 9.44( -1) | 8.61( -1) |
| 110.0 | 1.51( 0) | 1.20( 0) | 1.04( 0) | 9.12( -1) | 8.29( -1) |
| 115.0 | 1.48( 0) | 1.17( 0) | 1.01( 0) | 8.86( -1) | 8.05( -1) |
| 120.0 | 1.46( 0) | 1.15( 0) | 9.82( -1) | 8.62( -1) | 7.80( -1) |
| 125.0 | 1.43( 0) | 1.12( 0) | 9.61( -1) | 8.42( -1) | 7.61( -1) |
| 130.0 | 1.41( 0) | 1.10( 0) | 9.42( -1) | 8.23( -1) | 7.41( -1) |
| 135.0 | 1.39( 0) | 1.09( 0) | 9.26( -1) | 8.07( -1) | 7.26( -1) |
| 140.0 | 1.37( 0) | 1.07( 0) | 9.11( -1) | 7.94( -1) | 7.10( -1) |
| 145.0 | 1.36( 0) | 1.06( 0) | 8.99( -1) | 7.81( -1) | 6.99( -1) |
| 150.0 | 1.35( 0) | 1.05( 0) | 8.89( -1) | 7.71( -1) | 6.88( -1) |

APPENDIX C. (continued)

| $\theta$ [deg] | E [eV] | | | | |
|---|---|---|---|---|---|
| | .41 | .27 | .15 | .07 | .02 |
| 155.0 | 1.33( 0) | 1.04( 0) | 8.80(-1) | 7.63(-1) | 6.78(-1) |
| 160.0 | 1.33( 0) | 1.03( 0) | 8.72(-1) | 7.55(-1) | 6.73(-1) |
| 165.0 | 1.32( 0) | 1.03( 0) | 8.68(-1) | 7.51(-1) | 6.66(-1) |
| 170.0 | 1.32( 0) | 1.02( 0) | 8.65(-1) | 7.50(-1) | 6.58(-1) |
| 175.0 | 1.31( 0) | 1.02( 0) | 8.62(-1) | 7.47(-1) | 6.56(-1) |

[a]The number in parentheses denotes the power of ten by which
the entry should be multiplied.

# APPENDIX D

Differential Cross Section $\sigma(\theta)$ in $\text{Å}^2/\text{sr}$ for

Relative Collision Energies $E \geqslant 0.60$ eV

| $\theta$ [deg] | E [eV] | | | | |
|---|---|---|---|---|---|
| | 0.60 | 0.81 | 1.06 | 1.34 | 1.66 |
| | a | | | | |
| .1 | 1.01( 4) | 1.23( 4) | 1.49( 4) | 1.77( 4) | 2.03( 4) |
| .2 | 9.88( 3) | 1.20( 4) | 1.44( 4) | 1.71( 4) | 2.00( 4) |
| .3 | 9.48( 3) | 1.14( 4) | 1.37( 4) | 1.61( 4) | 1.87( 4) |
| .4 | 8.93( 3) | 1.08( 4) | 1.28( 4) | 1.49( 4) | 1.72( 4) |
| .5 | 8.37( 3) | 9.93( 3) | 1.17( 4) | 1.35( 4) | 1.54( 4) |
| .6 | 7.78( 3) | 9.16( 3) | 1.07( 4) | 1.21( 4) | 1.35( 4) |
| .7 | 7.15( 3) | 8.34( 3) | 9.56( 3) | 1.07( 4) | 1.16( 4) |
| .8 | 6.54( 3) | 7.53( 3) | 8.45( 3) | 9.25( 3) | 9.76( 3) |
| .9 | 5.95( 3) | 6.75( 3) | 7.44( 3) | 7.86( 3) | 7.96( 3) |
| 1.0 | 5.39( 3) | 6.01( 3) | 6.43( 3) | 6.53( 3) | 6.27( 3) |
| 1.1 | 4.85( 3) | 5.29( 3) | 5.45( 3) | 5.26( 3) | 4.72( 3) |
| 1.2 | 4.35( 3) | 4.60( 3) | 4.52( 3) | 4.09( 3) | 3.35( 3) |
| 1.3 | 3.88( 3) | 3.94( 3) | 3.65( 3) | 3.04( 3) | 2.22( 3) |
| 1.4 | 3.43( 3) | 3.32( 3) | 2.85( 3) | 2.14( 3) | 1.34( 3) |
| 1.5 | 3.00( 3) | 2.74( 3) | 2.14( 3) | 1.41( 3) | 7.16( 2) |
| 1.6 | 2.59( 3) | 2.20( 3) | 1.54( 3) | 8.45( 2) | 3.23( 2) |
| 1.7 | 2.20( 3) | 1.71( 3) | 1.04( 3) | 4.50( 2) | 1.25( 2) |
| 1.8 | 1.84( 3) | 1.29( 3) | 6.49( 2) | 2.02( 2) | 7.32( 1) |
| 1.9 | 1.51( 3) | 9.29( 2) | 3.65( 2) | 7.74( 1) | 1.17( 2) |
| 2.0 | 1.21( 3) | 6.32( 2) | 1.76( 2) | 4.67( 1) | 2.09( 2) |
| 2.1 | 9.43( 2) | 3.99( 2) | 6.90( 1) | 8.05( 1) | 3.13( 2) |
| 2.2 | 7.08( 2) | 2.27( 2) | 2.93( 1) | 1.51( 2) | 4.02( 2) |
| 2.3 | 5.08( 2) | 1.10( 2) | 3.98( 1) | 2.34( 2) | 4.53( 2) |
| 2.4 | 3.45( 2) | 4.32( 1) | 8.37( 1) | 3.12( 2) | 4.76( 2) |
| 2.5 | 2.17( 2) | 1.73( 1) | 1.45( 2) | 3.69( 2) | 4.56( 2) |
| 2.6 | 1.22( 2) | 2.34( 1) | 2.10( 2) | 3.99( 2) | 4.07( 2) |
| 2.7 | 5.82( 1) | 5.19( 1) | 2.66( 2) | 4.00( 2) | 3.38( 2) |
| 2.8 | 2.18( 1) | 9.33( 1) | 3.07( 2) | 3.74( 2) | 2.64( 2) |
| 2.9 | 8.24( 0) | 1.39( 2) | 3.28( 2) | 3.29( 2) | 1.95( 2) |
| 3.0 | 1.28( 1) | 1.83( 2) | 3.30( 2) | 2.74( 2) | 1.40( 2) |
| 3.1 | 3.05( 1) | 2.20( 2) | 3.13( 2) | 2.16( 2) | 1.04( 2) |
| 3.2 | 5.69( 1) | 2.45( 2) | 2.82( 2) | 1.63( 2) | 8.79( 1) |
| 3.3 | 8.76( 1) | 2.59( 2) | 2.43( 2) | 1.21( 2) | 8.75( 1) |
| 3.4 | 1.19( 2) | 2.61( 2) | 2.01( 2) | 9.11( 1) | 9.78( 1) |
| 3.5 | 1.48( 2) | 2.51( 2) | 1.59( 2) | 7.43( 1) | 1.13( 2) |
| 3.6 | 1.72( 2) | 2.33( 2) | 1.22( 2) | 6.89( 1) | 1.27( 2) |
| 3.7 | 1.90( 2) | 2.08( 2) | 9.18( 1) | 7.20( 1) | 1.38( 2) |
| 3.8 | 2.01( 2) | 1.79( 2) | 6.99( 1) | 8.08( 1) | 1.42( 2) |
| 3.9 | 2.04( 2) | 1.48( 2) | 5.66( 1) | 9.21( 1) | 1.41( 2) |
| 4.0 | 2.00( 2) | 1.18( 2) | 5.15( 1) | 1.03( 2) | 1.34( 2) |
| 4.1 | 1.90( 2) | 9.21( 1) | 5.32( 1) | 1.13( 2) | 1.23( 2) |
| 4.2 | 1.75( 2) | 7.04( 1) | 6.00( 1) | 1.18( 2) | 1.10( 2) |
| 4.3 | 1.56( 2) | 5.44( 1) | 6.97( 1) | 1.19( 2) | 9.64( 1) |
| 4.4 | 1.35( 2) | 4.42( 1) | 8.01( 1) | 1.15( 2) | 8.33( 1) |
| 4.5 | 1.13( 2) | 3.95( 1) | 8.93( 1) | 1.08( 2) | 7.25( 1) |
| 4.6 | 9.28( 1) | 3.96( 1) | 9.60( 1) | 9.72( 1) | 6.49( 1) |
| 4.7 | | 4.32( 1) | 9.93( 1) | 8.58( 1) | 6.09( 1) |
| 4.8 | | 4.91( 1) | 9.90( 1) | 7.47( 1) | 6.01( 1) |
| 4.9 | | 5.62( 1) | 9.55( 1) | 6.53( 1) | 6.18( 1) |
| 5.0 | | 6.34( 1) | 8.94( 1) | 5.82( 1) | 6.48( 1) |
| 5.1 | | 6.99( 1) | 8.18( 1) | 5.38( 1) | 6.76( 1) |
| 5.2 | | | 7.34( 1) | 5.16( 1) | 6.93( 1) |
| 5.3 | | | 6.52( 1) | 5.13( 1) | 6.94( 1) |
| 5.4 | | | 5.79( 1) | 5.21( 1) | 6.78( 1) |
| 5.5 | | | 5.24( 1) | 5.34( 1) | 6.48( 1) |
| 5.6 | | | | 5.47( 1) | 6.11( 1) |

APPENDIX D. (continued)

| $\theta$ [deg] | E [eV] | | | | |
|---|---|---|---|---|---|
| | 0.60 | 0.81 | 1.06 | 1.34 | 1.66 |
| 5.7 | 4.56( 1) | 7.05( 1) | 4.23( 1) | 5.58( 1) | 5.71( 1) |
| 5.8 | 5.10( 1) | 6.48( 1) | 4.05( 1) | 5.63( 1) | 5.33( 1) |
| 5.9 | 5.57( 1) | 5.85( 1) | 4.02( 1) | 5.61( 1) | 4.99( 1) |
| 6.0 | 5.92( 1) | 5.22( 1) | 4.10( 1) | 5.52( 1) | 4.69( 1) |
| 6.1 | 6.14( 1) | 4.64( 1) | 4.26( 1) | 5.34( 1) | 4.45( 1) |
| 6.2 | 6.22( 1) | 4.13( 1) | 4.45( 1) | 5.09( 1) | 4.26( 1) |
| 6.3 | 6.17( 1) | 3.73( 1) | 4.61( 1) | 4.79( 1) | 4.13( 1) |
| 6.4 | 5.99( 1) | 3.44( 1) | 4.72( 1) | 4.47( 1) | 4.06( 1) |
| 6.5 | 5.72( 1) | 3.26( 1) | 4.76( 1) | 4.17( 1) | 4.04( 1) |
| 6.6 | 5.36( 1) | 3.18( 1) | 4.71( 1) | 3.92( 1) | 4.06( 1) |
| 6.7 | 4.95( 1) | 3.18( 1) | 4.59( 1) | 3.73( 1) | 4.08( 1) |
| 6.8 | 4.51( 1) | 3.24( 1) | 4.42( 1) | 3.61( 1) | 4.08( 1) |
| 6.9 | 4.07( 1) | 3.35( 1) | 4.20( 1) | 3.55( 1) | 4.03( 1) |
| 7.0 | 3.65( 1) | 3.47( 1) | 3.97( 1) | 3.52( 1) | 3.93( 1) |
| 7.1 | 3.27( 1) | 3.59( 1) | 3.74( 1) | 3.51( 1) | 3.80( 1) |
| 7.2 | 2.96( 1) | 3.70( 1) | 3.52( 1) | 3.50( 1) | 3.63( 1) |
| 7.3 | 2.71( 1) | 3.77( 1) | 3.32( 1) | 3.47( 1) | 3.48( 1) |
| 7.4 | 2.54( 1) | 3.80( 1) | 3.15( 1) | 3.43( 1) | 3.34( 1) |
| 7.5 | 2.44( 1) | 3.78( 1) | 3.01( 1) | 3.38( 1) | 3.22( 1) |
| 7.6 | 2.40( 1) | 3.70( 1) | 2.91( 1) | 3.33( 1) | 3.14( 1) |
| 7.7 | 2.42( 1) | 3.58( 1) | 2.85( 1) | 3.26( 1) | 3.06( 1) |
| 7.8 | 2.47( 1) | 3.43( 1) | 2.83( 1) | 3.18( 1) | 2.99( 1) |
| 7.9 | 2.56( 1) | 3.26( 1) | 2.84( 1) | 3.09( 1) | 2.92( 1) |
| 8.0 | 2.65( 1) | 3.08( 1) | 2.86( 1) | 2.98( 1) | 2.85( 1) |
| 8.1 | 2.75( 1) | 2.90( 1) | 2.88( 1) | 2.88( 1) | 2.79( 1) |
| 8.2 | 2.84( 1) | 2.74( 1) | 2.88( 1) | 2.77( 1) | 2.74( 1) |
| 8.3 | 2.91( 1) | 2.60( 1) | 2.67( 1) | 2.67( 1) | 2.70( 1) |
| 8.4 | 2.97( 1) | 2.49( 1) | 2.84( 1) | 2.59( 1) | 2.67( 1) |
| 8.5 | 2.99( 1) | 2.40( 1) | 2.78( 1) | 2.53( 1) | 2.64( 1) |
| 8.6 | 2.98( 1) | 2.33( 1) | 2.71( 1) | 2.50( 1) | 2.60( 1) |
| 8.7 | 2.94( 1) | 2.29( 1) | 2.64( 1) | 2.47( 1) | 2.55( 1) |
| 8.8 | 2.87( 1) | 2.27( 1) | 2.55( 1) | 2.45( 1) | 2.48( 1) |
| 8.9 | 2.78( 1) | 2.26( 1) | 2.47( 1) | 2.43( 1) | 2.41( 1) |
| 9.0 | 2.66( 1) | 2.27( 1) | 2.39( 1) | 2.39( 1) | 2.34( 1) |
| 9.1 | 2.54( 1) | 2.29( 1) | 2.32( 1) | 2.35( 1) | 2.28( 1) |
| 9.2 | 2.41( 1) | 2.31( 1) | 2.24( 1) | 2.30( 1) | 2.24( 1) |
| 9.3 | 2.29( 1) | 2.32( 1) | 2.18( 1) | 2.25( 1) | 2.21( 1) |
| 9.4 | 2.17( 1) | 2.31( 1) | 2.12( 1) | 2.21( 1) | 2.18( 1) |
| 9.5 | 2.06( 1) | 2.30( 1) | 2.08( 1) | 2.17( 1) | 2.14( 1) |
| 9.6 | 1.98( 1) | 2.27( 1) | 2.05( 1) | 2.13( 1) | 2.10( 1) |
| 9.7 | 1.90( 1) | 2.22( 1) | 2.03( 1) | 2.08( 1) | 2.06( 1) |
| 9.8 | 1.85( 1) | 2.17( 1) | 2.02( 1) | 2.04( 1) | 2.01( 1) |
| 9.9 | 1.81( 1) | 2.11( 1) | 2.01( 1) | 1.99( 1) | 1.96( 1) |
| 10.0 | 1.78( 1) | 2.05( 1) | 1.99( 1) | 1.94( 1) | 1.92( 1) |
| 10.2 | 1.77( 1) | 1.93( 1) | 1.95( 1) | 1.86( 1) | 1.87( 1) |
| 10.4 | 1.80( 1) | 1.82( 1) | 1.88( 1) | 1.82( 1) | 1.82( 1) |
| 10.6 | 1.82( 1) | 1.73( 1) | 1.81( 1) | 1.78( 1) | 1.75( 1) |
| 10.8 | 1.83( 1) | 1.67( 1) | 1.74( 1) | 1.73( 1) | 1.68( 1) |
| 11.0 | 1.80( 1) | 1.64( 1) | 1.67( 1) | 1.66( 1) | 1.64( 1) |
| 11.2 | 1.74( 1) | 1.63( 1) | 1.60( 1) | 1.60( 1) | 1.61( 1) |
| 11.4 | 1.67( 1) | 1.60( 1) | 1.55( 1) | 1.55( 1) | 1.55( 1) |
| 11.6 | 1.58( 1) | 1.57( 1) | 1.51( 1) | 1.51( 1) | 1.48( 1) |
| 11.8 | 1.50( 1) | 1.52( 1) | 1.46( 1) | 1.46( 1) | 1.43( 1) |
| 12.0 | 1.42( 1) | 1.48( 1) | 1.45( 1) | 1.41( 1) | 1.40( 1) |
| 12.2 | 1.36( 1) | 1.43( 1) | 1.40( 1) | 1.38( 1) | 1.36( 1) |
| 12.4 | 1.33( 1) | 1.37( 1) | 1.36( 1) | 1.35( 1) | 1.32( 1) |
| 12.6 | 1.30( 1) | 1.32( 1) | 1.32( 1) | 1.31( 1) | 1.29( 1) |
| 12.8 | 1.29( 1) | 1.28( 1) | 1.29( 1) | 1.27( 1) | 1.26( 1) |
| 13.0 | 1.28( 1) | 1.25( 1) | 1.25( 1) | 1.23( 1) | 1.24( 1) |
| 13.2 | 1.26( 1) | 1.22( 1) | 1.21( 1) | 1.20( 1) | 1.20( 1) |

APPENDIX D. (continued)

| $\theta$ [deg] | E [eV] | | | | |
|---|---|---|---|---|---|
| | 0.60 | 0.81 | 1.06 | 1.34 | 1.66 |
| 13.4 | 1.25( 1) | 1.20( 1) | 1.18( 1) | 1.17( 1) | 1.15( 1) |
| 13.6 | 1.22( 1) | 1.17( 1) | 1.16( 1) | 1.14( 1) | 1.11( 1) |
| 13.8 | 1.18( 1) | 1.15( 1) | 1.13( 1) | 1.11( 1) | 1.09( 1) |
| 14.0 | 1.14( 1) | 1.13( 1) | 1.10( 1) | 1.09( 1) | 1.07( 1) |
| 14.2 | 1.10( 1) | 1.10( 1) | 1.07( 1) | 1.07( 1) | 1.04( 1) |
| 14.4 | 1.07( 1) | 1.07( 1) | 1.05( 1) | 1.04( 1) | 1.01( 1) |
| 14.6 | 1.04( 1) | 1.04( 1) | 1.03( 1) | 1.01( 1) | 1.00( 1) |
| 14.8 | 1.01( 1) | 1.01( 1) | 1.01( 1) | 9.73( 0) | 9.85( 0) |
| 15.0 | 9.93( 0) | 9.89( 0) | 9.79( 0) | 9.60( 0) | 9.57( 0) |
| 15.2 | 9.79( 0) | 9.67( 0) | 9.55( 0) | 9.44( 0) | 9.23( 0) |
| 15.4 | 9.66( 0) | 9.46( 0) | 9.36( 0) | 9.23( 0) | 9.00( 0) |
| 15.6 | 9.51( 0) | 9.29( 0) | 9.17( 0) | 9.00( 0) | 8.86( 0) |
| 15.8 | 9.33( 0) | 9.15( 0) | 8.94( 0) | 8.83( 0) | 8.68( 0) |
| 16.0 | 9.14( 0) | 8.99( 0) | 8.73( 0) | 8.69( 0) | 8.46( 0) |
| 18.0 | 7.49( 0) | 7.37( 0) | 7.19( 0) | 7.10( 0) | 6.94( 0) |
| 20.0 | 6.32( 0) | 6.19( 0) | 6.07( 0) | 5.92( 0) | 5.89( 0) |
| 22.0 | 5.44( 0) | 5.32( 0) | 5.21( 0) | 5.06( 0) | 5.07( 0) |
| 24.0 | 4.77( 0) | 4.64( 0) | 4.53( 0) | 4.43( 0) | 4.39( 0) |
| 26.0 | 4.22( 0) | 4.09( 0) | 4.00( 0) | 3.93( 0) | 3.84( 0) |
| 28.0 | 3.77( 0) | 3.66( 0) | 3.58( 0) | 3.51( 0) | 3.43( 0) |
| 30.0 | 3.41( 0) | 3.30( 0) | 3.22( 0) | 3.16( 0) | 3.12( 0) |
| 32.0 | 3.11( 0) | 3.00( 0) | 2.92( 0) | 2.87( 0) | 2.87( 0) |
| 34.0 | 2.85( 0) | 2.75( 0) | 2.67( 0) | 2.64( 0) | 2.64( 0) |
| 36.0 | 2.63( 0) | 2.54( 0) | 2.47( 0) | 2.44( 0) | 2.43( 0) |
| 38.0 | 2.45( 0) | 2.36( 0) | 2.29( 0) | 2.25( 0) | 2.25( 0) |
| 40.0 | 2.28( 0) | 2.20( 0) | 2.13( 0) | 2.10( 0) | 2.10( 0) |
| 42.0 | 2.14( 0) | 2.06( 0) | 2.01( 0) | 1.98( 0) | 1.99( 0) |
| 44.0 | 2.01( 0) | 1.94( 0) | 1.89( 0) | 1.87( 0) | 1.88( 0) |
| 46.0 | 1.90( 0) | 1.83( 0) | 1.78( 0) | 1.76( 0) | 1.75( 0) |
| 48.0 | 1.80( 0) | 1.73( 0) | 1.69( 0) | 1.67( 0) | 1.68( 0) |
| 50.0 | 1.71( 0) | 1.65( 0) | 1.61( 0) | 1.60( 0) | 1.61( 0) |
| 52.0 | 1.63( 0) | 1.57( 0) | 1.53( 0) | 1.52( 0) | 1.54( 0) |
| 54.0 | 1.56( 0) | 1.50( 0) | 1.46( 0) | 1.45( 0) | 1.46( 0) |
| 56.0 | 1.49( 0) | 1.44( 0) | 1.40( 0) | 1.39( 0) | 1.40( 0) |
| 58.0 | 1.44( 0) | 1.38( 0) | 1.35( 0) | 1.34( 0) | 1.34( 0) |
| 60.0 | 1.38( 0) | 1.33( 0) | 1.29( 0) | 1.28( 0) | 1.29( 0) |
| 65.0 | 1.26( 0) | 1.21( 0) | 1.19( 0) | 1.16( 0) | 1.16( 0) |
| 70.0 | 1.17( 0) | 1.12( 0) | 1.08( 0) | 1.07( 0) | 1.05( 0) |
| 75.0 | 1.09( 0) | 1.04( 0) | 1.00( 0) | 9.77(-1) | 9.54(-1) |
| 80.0 | 1.02( 0) | 9.68(-1) | 9.28(-1) | 9.02(-1) | 8.55(-1) |
| 85.0 | 9.58(-1) | 9.07(-1) | 8.66(-1) | 8.30(-1) | 7.71(-1) |
| 90.0 | 9.08(-1) | 8.55(-1) | 8.09(-1) | 7.66(-1) | 6.88(-1) |
| 95.0 | 8.62(-1) | 8.07(-1) | 7.60(-1) | 7.03(-1) | 6.22(-1) |
| 100.0 | 8.23(-1) | 7.66(-1) | 7.11(-1) | 6.50(-1) | 5.58(-1) |
| 105.0 | 7.88(-1) | 7.28(-1) | 6.68(-1) | 6.01(-1) | 5.06(-1) |
| 110.0 | 7.56(-1) | 6.94(-1) | 6.31(-1) | 5.56(-1) | 4.67(-1) |
| 115.0 | 7.28(-1) | 6.63(-1) | 5.96(-1) | 5.18(-1) | 4.32(-1) |
| 120.0 | 7.02(-1) | 6.35(-1) | 5.63(-1) | 4.86(-1) | 4.02(-1) |
| 125.0 | 6.80(-1) | 6.11(-1) | 5.36(-1) | 4.54(-1) | 3.82(-1) |
| 130.0 | 6.60(-1) | 5.88(-1) | 5.10(-1) | 4.31(-1) | 3.63(-1) |
| 135.0 | 6.43(-1) | 5.69(-1) | 4.90(-1) | 4.09(-1) | 3.49(-1) |
| 140.0 | 6.27(-1) | 5.51(-1) | 4.70(-1) | 3.93(-1) | 3.35(-1) |
| 145.0 | 6.13(-1) | 5.36(-1) | 4.54(-1) | 3.78(-1) | 3.27(-1) |
| 150.0 | 6.02(-1) | 5.23(-1) | 4.41(-1) | 3.68(-1) | 3.17(-1) |

APPENDIX D. (continued)

| θ[deg] | E [eV] | | | | |
|---|---|---|---|---|---|
| | 0.60 | 0.81 | 1.06 | 1.34 | 1.66 |
| 155.0 | 5.92(-1) | 5.12(-1) | 4.28(-1) | 3.58(-1) | 3.12(-1) |
| 160.0 | 5.84(-1) | 5.04(-1) | 4.21(-1) | 3.49(-1) | 3.08(-1) |
| 165.0 | 5.78(-1) | 4.97(-1) | 4.14(-1) | 3.45(-1) | 3.03(-1) |
| 170.0 | 5.73(-1) | 4.91(-1) | 4.08(-1) | 3.41(-1) | 3.02(-1) |
| 175.0 | 5.70(-1) | 4.88(-1) | 4.03(-1) | 3.36(-1) | 3.05(-1) |

[a]The number in parentheses denotes the power of ten by
which the entry should be multiplied.

## LABORATORY OPERATIONS

The Laboratory Operations of The Aerospace Corporation is conducting experimental and theoretical investigations necessary for the evaluation and application of scientific advances to new military concepts and systems. Versatility and flexibility have been developed to a high degree by the laboratory personnel in dealing with the many problems encountered in the Nation's rapidly developing space systems. Expertise in the latest scientific developments is vital to the accomplishment of tasks related to these problems. The laboratories that contribute to this research are:

**Aerophysics Laboratory:** Aerodynamics; fluid dynamics; plasmadynamics; chemical kinetics; engineering mechanics; flight dynamics; heat transfer; high-power gas lasers, continuous and pulsed, IR, visible, UV; laser physics; laser resonator optics; laser effects and countermeasures.

**Chemistry and Physics Laboratory:** Atmospheric reactions and optical backgrounds; radiative transfer and atmospheric transmission; thermal and state-specific reaction rates in rocket plumes; chemical thermodynamics and propulsion chemistry; laser isotope separation; chemistry and physics of particles; space environmental and contamination effects on spacecraft materials; lubrication; surface chemistry of insulators and conductors; cathode materials; sensor materials and sensor optics; applied laser spectroscopy; atomic frequency standards; pollution and toxic materials monitoring.

**Electronics Research Laboratory:** Electromagnetic theory and propagation phenomena; microwave and semiconductor devices and integrated circuits; quantum electronics, lasers, and electro-optics; communication sciences, applied electronics, superconducting and electronic device physics; millimeter-wave and far-infrared technology.

**Materials Sciences Laboratory:** Development of new materials; composite materials; graphite and ceramics; polymeric materials; weapons effects and hardened materials; materials for electronic devices; dimensionally stable materials; chemical and structural analyses; stress corrosion; fatigue of metals.

**Space Sciences Laboratory:** Atmospheric and ionospheric physics, radiation from the atmosphere, density and composition of the atmosphere, aurorae and airglow; magnetospheric physics, cosmic rays, generation and propagation of plasma waves in the magnetosphere; solar physics, x-ray astronomy; the effects of nuclear explosions, magnetic storms, and solar activity on the earth's atmosphere, ionosphere, and magnetosphere; the effects of optical, electromagnetic, and particulate radiations in space on space systems.

• • •

# END

## DATE
## FILMED

# 7-81

# DTIC